

Vibratory cone penetration test to investigate cyclic soil behavior in-situ

Kumulative Dissertation

zur Erlangung des Doktorgrades der Naturwissenschaften

(Dr. rer. nat.)

am Fachbereich 5, Geowissenschaften der



vorgelegt von

Dina Al-Sammarraie

Bremen

Januar 2020

Gutachter: Prof. Dr. Tobias Mörz (Universität Bremen)
Prof. Dr. Nina Stark (Virginia Tech.)

Betreuer: Prof. Dr. Tobias Mörz (Universität Bremen)
Dr. Stefan Kreiter (Universität Bremen)
Dr. Max O. Kluger (Universität Bremen)

Erste Version eingereicht am: 22. Januar 2020

Kolloquium gehalten am: 11. März 2020

Versicherung an Eides Statt

gem. § 5 Abs. 5 der Promotionsordnung vom 18.06.2018

Ich, Dina Al-Sammarraie, wohnhaft in der Fahrenheit Str. 19, 28359 Bremen, versichere an Eides Statt durch meine Unterschrift, dass ich die vorliegende Dissertation selbständig und ohne fremde Hilfe angefertigt und alle Stellen, die ich wörtlich dem Sinne nach aus Veröffentlichungen entnommen habe, als solche kenntlich gemacht habe, mich auch keiner anderen als der angegebenen Literatur oder sonstiger Hilfsmittel bedient habe und die zu Prüfungszwecken beigelegte elektronische Version (PDF) der Dissertation mit der abgegebenen gedruckten Version identisch ist.

Ich versichere an Eides Statt, dass ich die vorgenannten Angaben nach bestem Wissen und Gewissen gemacht habe und dass die Angaben der Wahrheit entsprechen und ich nichts verschwiegen habe

Die Strafbarkeit einer falschen eidesstattlichen Versicherung ist mir bekannt, namentlich die Strafandrohung gemäß § 156 StGB bis zu drei Jahren Freiheitsstrafe oder Geldstrafe bei vorsätzlicher Begehung der Tat bzw. gemäß § 161 Abs. 1 StGB bis zu einem Jahr Freiheitsstrafe oder Geldstrafe bei fahrlässiger Begehung.

Bremen, 22.01.2020

Acknowledgements

I acknowledge the Federal Ministry for Economic Affairs and Energy (BMWi), project: Vibro Drucksondierungen (Vibro-CPTu), FKZ: 0325906, and the MARUM Center for Marine Environmental Science at the University of Bremen for funding this Ph.D. position.

I want to thank my supervisor Tobias Mörz as well as my advisors Stefan Kreiter and Max Oke Kluger for their never ending support during my Ph.D. project. Your guidance during experimental work and your knowledge and patience during countless discussions provided the basis for a successful completion of my thesis. I further thank Dr. Nina Stark for her interest in the doctoral thesis. Thank you for taking time to read and grade the thesis.

Furthermore, I want to acknowledge the invaluable contributions of my co-authors Stefan Kreiter, Tobias Mörz, Max Oke Kluger, Majid Goodarzi, Florian Stähler, and Benjamin Ossig. I thank Wolfgang Schunn, Marc Huhndorf, and Joann Schmid for their help and assistance in engineering issues.

Last but not least, I would like to thank my family and friends for supporting me during this Ph.D. project.

Abstract:

Climate change increased the need of using renewable energy as replacement for fossil fuel. This led to a fast growth of the offshore wind energy sector, especially in Germany where offshore wind energy turbines are built in great numbers in the North Sea. Piles are usually used as foundations for these turbines. In recent years, new projects planned to install these piles with the vibratory pile driving technique which installs piles with axial vibrations. One of the main challenges with vibratory pile driving is the choice of the vibrator that should have a sufficient weight and energy to drive the pile to the designed depth. The selection of the vibrator usually depends on predictions from drivability analyses that use parameters obtained from the conventional in-situ soil investigation methods such as cone penetration test CPT as an input for the analysis. CPT is a cone that is pushed into the ground at constant speed while sensors in the cone measure the cone resistance, sleeve friction, and pore water pressure. The static soil behavior obtained from these conventional CPTs differs from the cyclic soil behavior exhibited during vibratory pile driving.

In this research, vibratory cone penetration test VCPT is introduced to improve the geotechnical in-situ methods for evaluating the cyclic soil behavior during vibratory pile driving. The new device controls displacement amplitudes in real time and it penetrates the ground while inducing vertical cyclic strains. The cyclic motion of VCPT resembles the motion of the piles during vibratory driving, therefore it could be used to investigate the cyclic soil behavior and degradation during vibratory pile driving. Major obstacles with any in-situ soil investigation method are the inherent variations in soil properties which could affect the results obtained from in-situ tests. Performing a number of tests in small spacings increases the statistical significance and reduces the effect of soil variations on test results. Still, there is no consensus on how to define the minimum spacing between testing zones and no consensus on the effect of disturbance caused by in situ tests.

This doctoral thesis has divided the in-situ soil investigations into three studies:

In the first study, static cone penetration tests were used to develop a procedure to characterize the in-situ properties of soil and to investigate the minimum spacing between tests without the effect of soil disturbance. A systematic grid of 33 CPTs was performed in the field by sequentially and successively refining the grid spacing between CPTs, starting with a spacing of 119 cone diameters down to a grid spacing of 7 cone diameters. It was found that the cone resistance is affected by previous CPT measurements below a spacing threshold of 24 cone diameters in medium-dense sands. Silt and clay layers showed no reduction in the cone

resistance for our minimum grid spacing of 7 cone diameters. The study also showed that the spacing between the tests and natural variations in soil properties are deciding factors for the number of CPTs needed in the field for a sufficient statistical significance.

In the second study, VCPT was used to investigate the cyclic behavior of the soil. The device proved to generate constant amplitudes until the final depth of penetration. Two sand layers reacted to the applied cyclic loads by showing high reduction in the resistance. It was also found that even a distance of 50 cm does not guarantee a good correlation between CPT and VCPT. Therefore, two or more pairs of CPT and VCPT should be conducted in order to minimize misinterpretations of the data which are caused by small scale geological structures such as the presence of inclined layers, cross bedding, or other heterogeneities.

In the third study, nine static CPTs and VCPTs were performed in a systematic grid. The vibratory CPTs were performed at a constant frequency of 20 Hz and at three different amplitudes of 3, 5, and 7 mm. It was found that the degradation of soil resistance to vibratory cone penetration increased with increasing cyclic displacement amplitudes. This degradation was not accompanied by any increase in pore water pressure. Cyclic cone resistance-displacement hysteresis loops indicated the formation of a cavity between the cone and soil during the upward movement of the cone. Furthermore, a distinct difference between the loading and the unloading stiffness during the vibratory penetration was observed. The results demonstrated that there is no unique relation between static and vibratory cone resistance, therefore, current practices that estimate the degradation in soil resistance due to vibratory pile driving from the static cone resistance are probably not sufficient.

The results obtained from the three studies showed that the current civil engineering approaches that assess the cyclic soil behavior during vibratory pile driving from static cone resistance are not sufficient because there is no unique relation between static and vibratory cone resistance. VCPT could be used to assess the cyclic soil behavior, however, several tests should be performed in order to have statistical significance to consider the effect of the variation in soil properties.

Zusammenfassung

Der Klimawandel hat den Bedarf an erneuerbaren Energien als Ersatz für fossile Brennstoffe erhöht. Dies führte insbesondere in Deutschland zu einem schnellen Wachstum der Offshore-Windenergiebranche, wobei zunehmend Offshore-Windenergieanlagen in der Nordsee gebaut wurden. Beim Bau dieser Turbinen werden üblicherweise Pfahlgründungen verwendet. In den letzten Jahren planen mehr und mehr Projekte, die Pfähle mit Vibrationsrammung zu installieren. Eine der Hauptherausforderungen bei der Vibrationsrammung ist die Wahl der passenden Vibrationsramme. Die Vibrationsramme muss über ausreichend Gewicht und Vibrationsenergie verfügen, um den Pfahl auf die vorgesehene Tiefe zu bringen. Die Auswahl der Vibrationsramme hängt von der Rammbarkeitsanalyse ab, bei denen Parameter verwendet werden, die mit herkömmlichen In-situ-Bodenuntersuchungsmethoden, wie der Drucksondierung (engl. CPT), ermittelt wurden. Bei der Drucksondierung wird eine kegelförmige Sonde mit konstanter Geschwindigkeit in den Boden gedrückt und dabei der Spitzendruck, die Mantelreibung und der Porenwasserdruck gemessen. Das Bodenverhalten bei dieser konventionellen Drucksondierung unterscheidet sich vom zyklischen Bodenverhalten bei der Vibrationsrammung.

In dieser Arbeit wird die vibrierende Drucksondierung, im folgenden mit der englischen Abkürzung VCPT genannt, vorgestellt, um die geotechnischen In-situ-Methoden zur Bewertung des zyklischen Bodenverhaltens für die Vibrationsrammung zu erweitern und zu verbessern. Das neue Gerät steuert die Wegamplitude in Echtzeit und dringt in den Boden ein, wobei vertikale zyklische Belastungen induziert werden. Die zyklische Bewegung der VCPT ähnelt der Bewegung von Pfählen während der Vibrationsrammung und ist deswegen geeignet das zyklische Bodenverhalten und die Verringerung des Rammwiderstands während des Vibrationsrammens von Pfählen zu untersuchen. Ein großes Problem bei allen In-situ-Bodenuntersuchungsmethoden sind kleinräumliche Schwankungen der Bodeneigenschaften, die sich auf die Anwendung der Ergebnisse von In-situ-Tests auswirken. Die Durchführung einer Anzahl von Tests in kleinen Abständen erhöht die statistische Signifikanz der Ergebnisse und verringert die Auswirkung von kleinräumlichen Schwankungen. Es gibt jedoch keinen Konsens darüber, wie groß der Mindestabstand zwischen den Sondierpunkten sein muss, und es ist unklar wie sich die Störungen im Boden durch vorherige Sondierungen auf die folgenden In-situ-Tests auswirken.

Diese Doktorarbeit ist in drei Studien unterteilt:

In der ersten Studie wurden quasi statische Drucksondierungen durchgeführt, um den Mindestabstand für Sondierungen ohne den Einfluss von Bodenstörungen zu untersuchen. Darüber hinaus wurden die in-situ-Eigenschaften des Bodens statistisch charakterisiert. Ein systematisches Raster von 33 Drucksondierungen wurde so durchgeführt, dass der Abstand zu vorhergehenden Sondierungen in der Nachbarschaft, angegeben in der relativen Längeneinheit D für den Sondendruckmesser, von $119 D$ systematisch bis $7 D$ reduziert wurde. Es wurde festgestellt, dass der Spitzendruck durch vorhergehende Sondierungen in der Nachbarschaft unterhalb der Schwelle von $24 D$ in mitteldichten Sanden beeinflusst wird. Schluff- und Tonschichten zeigten beim kleinsten gemessenen Abstand von $7 D$ keine Abnahme des Spitzendrucks. Der Abstand zwischen den Tests und die natürliche räumliche Schwankung der Bodeneigenschaften ist der ausschlaggebende Faktor für die Anzahl der Drucksondierungen, die für eine gewünschte statistische Signifikanz benötigt werden.

In der zweiten Studie wurde mit VCPT das zyklische Verhalten des Bodens untersucht. Das Gerät erzeugte nachweislich konstante Amplituden bis zur endgültigen Eindringtiefe. Zwei Sandschichten reagierten auf die aufgebrachten zyklischen Lasten mit einer Verringerung des Eindringwiderstands. Es wurde auch festgestellt, dass selbst ein Abstand von 50 cm keine gute Korrelation zwischen normalen Drucksondierungen und VCPT garantiert. Daher sollten zwei oder mehr Paare von Drucksondierungen und Vibro-CPTu durchgeführt werden, um Fehlinterpretationen der Daten zu minimieren, die durch geologische Strukturen und natürliche räumliche Schwankungen im kleinen Maßstab verursacht werden, wie beispielsweise das Vorhandensein von geneigten Schichten, Schrägschichtungen, Kreuzschichtungen oder anderen Heterogenitäten.

In der dritten Studie wurden neun statische Drucksondierungen und fünfzehn vibrierende Drucksondierungen (VCPT) in einem systematischen Raster durchgeführt. Die VCPTs wurden bei einer konstanten Frequenz von 20 Hz und mit drei verschiedenen Amplituden von 3 , 5 und 7 mm durchgeführt. Es wurde festgestellt, dass die Verringerung des Eindringwiderstands gegen VCPT mit zunehmenden Amplituden der zyklischen Wegamplitude zunahm. Diese Verringerung ging nicht mit einem Anstieg des Porenwasserdrucks einher. Zyklische Hystereseschleifen aus Kegelwiderstand und -verschiebung zeigten einen Kontaktverlust zwischen Boden und Sonde während der Aufwärtsbewegung des Kegels. Darüber hinaus wurde ein deutlicher Unterschied zwischen der Belastungs- und der Entlastungsteifigkeit während der vibrierenden Eindringung gemessen. Die Ergebnisse zeigen, dass es keine eindeutige

Beziehung zwischen dem Widerstand gegen quasistatische Eindringung und dem Widerstand gegen vibrierende Eindringung gibt. Daher ist die derzeitige Praxis, den Widerstand gegen Vibrationsrammung aus quasistatischen Drucksondierungen zu bestimmen aus prinzipiellen physikalischen Gründen stark fehlerbehaftet.

Die in den drei Studien erzielten Ergebnisse zeigten, dass die aktuellen ingenieurtechnischen Ansätze, die das zyklische Bodenverhalten beim Rammen und den Widerstand gegen Vibrationsrammung anhand von quasistatischen Drucksondierungen bewerten, nicht ausreichen, weil es keine eindeutige Beziehung zwischen quasistatischem und vibrierendem Eindringwiderstand gibt. VCPT ist eine neue und vielversprechende Methode zur Beurteilung des zyklischen Bodenverhaltens bei der Vibrationsrammung. Es sollten jedoch mehrere Sondierungen durchgeführt werden, um statistisch signifikante Ergebnisse zu erhalten und den Effekt der lokalen Variation der Bodeneigenschaften zu berücksichtigen.

Table of contents

Versicherung an Eides Statt	<i>ii</i>
Acknowledgements	<i>iii</i>
Abstract	<i>iv</i>
Zusammenfassung	<i>vi</i>
Table of contents	<i>ix</i>
List of figures	<i>xii</i>
List of tables	<i>xvi</i>
Nomenclature	<i>xvii</i>

CHAPTER 1: 1

1. Introduction	1
1.1 Vibratory pile driving	1
1.2 Assessment of site variability	4
1.3 Static cone penetration test CPT.	6
1.4 Vibratory cone penetration tests	8
1.5 Motivation and research hypotheses	11
1.6 Study area	12
1.6.1 Bremen	12
1.6.2. Cuxhaven	14
1.7 Vibro Crawler	15
1.8 VCPT device	16
1.9 Thesis background	17
1.9.1 Framework	17
1.9.2 Author contributions	17

CHAPTER 2: Effect of closely spaced CPTs on cone resistance 19

2. Abstract.....	19
2.1. Introduction	19
2.2. Materials and Methods.....	22
2.2.1 Geological and geotechnical setting.....	22
2.2.2 Experimental layout	24

2.2.3 Penetration paths of the CPTs	26
2.2.4 Evaluation of CPT datasets	28
2.2.4.1 CPT correlation	28
2.2.4.2 Parameters for assessing the effect of CPT spacing on cone resistance	29
2.2.4.3 Parameters for assessing the effect of number of CPTs and CPT spacing on confidence interval.....	31
2.3. Results	33
2.4. Discussion.....	39
2.4.1 Spacing threshold	39
2.4.2 Confidence Interval	40
2.5. Conclusions.....	41
CHAPTER 3: New vibratory cone penetration device for in-situ measurement of cyclic softening	42
3. Abstract	42
3.1. Introduction	42
3.2. Methodology	44
3.2.1. Vibro Crawler	44
3.2.2. Test scheme	45
3.2.2.1. Reduction ratio	46
3.2.3. In-situ displacement	46
3.3. Results	47
3.3.1 Vibro cone performance.....	47
3.3.2. Vibro-CPTu results	48
3.4. Discussion	51
3.4.1. Vibro cone.....	51
3.4.2. Field tests.....	52
3.5. Conclusion.....	53
CHAPTER 4: Vibratory cone penetration test A new experimental approach to investigate in situ cyclic soil behavior	54
4. Abstract	54
4.1. Introduction	55
4.2. Materials and Methods	56
4.2.1 VCPT device	56

4.2.2 Geological and geotechnical setting	58
4.2.3 Experimental layout	59
4.2.4 Evaluation of SCPT and VCPTs datasets.....	62
4.2.4.1 Correlation	62
4.2.4.2 Cyclic behaviour analysis	65
4.2.4.3 Statistics	69
4.3. Results	72
4.4. Discussion	79
4.5. Conclusions	82
CHAPTER 5 :	84
5. Conclusion	84
CHAPTER 6:	86
6. References cited	86
CHAPTER 7:	90
7. Appendix	90
7.1 Figures	90
7.2 Abstracts of Co-Author papers	96
7.2.1 A small volume calibration chamber for cone penetration tests under simulated field conditions.....	96
7.2.2 Liquefaction resistance by static and vibratory cone penetration tests.....	97

List of figures

Fig. 1.1. An example of liquefaction in medium dense Cuxhaven sand under 150 kPa confining stress showing in a) the pore water pressure ratio and the axial strain; b) the cyclic stress-strain behavior.	2
Fig. 1.2. An example of liquefaction in dense Cuxhaven sand under 150 kPa confining stress showing in a) the pore water pressure ratio and the axial strain; b) the cyclic stress-strain behavior.	3
Fig. 1.3 Description of the four phases of the slow vibratory-motion of the pile-toe force.	4
Fig.1.4. Dune bedforms forming planar cross-beddings and trough cross-beddings.	5
Fig. 1.5. Normal distribution curve showing the confidence interval and the characteristic value.	6
Fig. 1.6. Influence zone of CPT and the disturbed soil zone.	7
Fig. 1.7. Vibratory cone penetration test showing the results of static and vibratory cone resistance after Sasaki and Koga (1982).	9
Fig. 1.8. The vertical cyclic motion of VCPT.	9
Fig. 1.9. Example of cone resistance – displacement hysteresis loops showing in a) three cycles; b) loading and unloading stiffness for the second cycle.	11
Fig. 1.10. Map indicating the location of test areas: 1) Bremen; 2) Cuxhaven. The coordinate system used to create the maps was UTM zone N32.	13
Fig. 1.11. Stratigraphy and soil properties of test field (a) core; (b) grain size distribution; (c) soil behavior types represented by SBT; (d) friction ratio; (e) corrected tip resistance; (f) relative density derived after Baldi et al. (1986).	13
Fig. 1.12. Stratigraphy and soil properties of test site (a) core; (b) grain size distribution (Geo-Engineering, 2014); (c) bulk unit weight (Geo-Engineering, 2014); (d) soil behavior types (SBT); (e) friction ratio; (f) corrected tip resistance; and (g) relative density derived after Baldi et al. (1986).	15
Fig. 1.13. The vibro crawler system.	16
Fig. 1.14. The vibratory cone penetration test system.	17
Fig.2.1. Geological map of Germany – Bremen, indicating the location of the test field (NIBIS, 2014).	23

Fig. 2.2. Maps, using UTM zone N32, of a) the layout of test points; section x – x where the inclination of the rod is shown in Fig. 5; b) the location of the core; c) close up for CPTs of set A6– A8.	23
Fig. 2.3. Stratigraphy and soil properties of test field (a) core; (b) grain size distribution; (c) soil behavior types represented by SBT; (d) friction ratio; (e) corrected tip resistance; (f) relative density derived after Baldi et al. (1986).	24
Fig. 2.4. Penetration path projections a) top view, b) side view section x-x. The symbols represent the starting point of the CPT.	27
Fig. 2.5. Frequency distribution of the depth-dependent spacing of the neighboring CPTs of set A3 – 8.	28
Fig. 2.6. Flow chart describing the mathematical calculations used to evaluate the CPT datasets.	29
Fig.2.7. Representative cone resistance datasets for CPTs of set A see Table 2.2.	34
Fig.2.8. Absolute and relative spacing influence in the representative cone resistance datasets.	35
Fig.2.9. Average absolute spacing influence with respect to soil behavior types, the vertical line representing the threshold spacing, the standard deviation is given as color shading.	36
Fig.2.10. Average relative spacing influence with respect to soil behavior types, the vertical line.	36
Fig. 2.11. Confidence interval of each mean cone resistance for CPTs of set B (Tab. 2.2).	37
Fig. 2.12. The average confidence interval for various number of averaged CPTs with respect to soil behavior type.	38
Fig. 2.13. The relative confidence interval for various number of averaged CPTs with respect to soil behavior type.	38
Fig. 3.1. Vibro crawler system.	44
Fig.3.2. Grain size distribution of soil.	45
Fig. 3.3. Map of test field using UTM zone 32. The dotted line is the correlation section shown in figure 9.	46
Fig. 3.4. Displacement for the three Vibro-CPTu runs.	46

Fig. 3.5. Raw acceleration of the first three cycles in gray and refined acceleration for 100 x 100 stacked data points in red for depth of 2-2.4 m for location P1.	47
Fig. 3.6. Amplitude of vibration at different depths derived from the displacement and acceleration sensors for P1.	48
Fig. 3.7. Velocity of vibration at different depths derived from the displacement and acceleration sensors for P1.	48
Fig. 3.8. Soil behavior type after Lunne et al. (1997).	49
Fig. 3.9. Correlation of soil behavior types SBTs after Lunne et al. (1997). Patterns of SBTs are for visualization purposes only.	49
Fig. 3.10. Soil behavior type SBT after Lunne et al. (1997), Cone resistance q_c and reduction ratio RR over depth for location P1.	50
Fig. 3.11. Soil behavior type SBT after Lunne et al. (1997), Cone resistance q_c and reduction ratio RR over depth for location P2.	50
Fig. 3.12. Soil behavior type SBT after Lunne et al. (1997), Cone resistance q_c and reduction ratio RR over depth for location P3.	51
Fig. 4.1. Vibratory cone penetration test device.	57
Fig. 4.2. Geological map of Cuxhaven, North Germany, indicating the location of the test site (NIBIS, 2014).	58
Fig. 4.3. Maps of the layout of test points and the location of the core. The coordinate system used to create the maps was UTM zone N32.	59
Fig. 4.4. Stratigraphy and soil properties of test site (a) core; (b) grain size distribution (Geo-Engineering, 2014); (c) bulk unit weight (Geo-Engineering, 2014); (d) soil behavior types (SBT); (e) friction ratio; (f) corrected tip resistance; and (g) relative density derived after Baldi et al. (1986).	60
Fig. 4.5. Procedure of SCPT and VCPT data processing. See text for further explanations.	63
Fig. 4.6. Stacking and stiffness calculation procedure for test V4 depth of 7 m: (a) Stacked and neighboring cone resistance triple cycles; (b) stacking process of the triple cycles; (c) stacked and neighboring acceleration triple cycles; (d) cyclic displacement obtained from acceleration sensor and from displacement sensor, respectively; (e) example of stacked cone resistance – displacement hysteresis loops; (f) procedure to determine loading stiffness, unloading stiffness, and upward displacement with cavitation.	67

Fig. 4.7. Cone resistance, sleeve friction, and pore water pressure of SCPT and peak VCPT of different VCPT amplitudes.	73
Fig. 4.8. Degradation factors of representative cone resistance and sleeve friction for different VCPT amplitudes.	74
Fig. 4.9. Representative peak vibratory cone resistances for different soil units plotted against the displacement amplitudes.	75
Fig. 4.10. Loading and unloading stiffnesses and the upward displacement with cavitation plotted along the depth of penetration.	76
Fig. 4.11. Representative cyclic cone resistance – displacement behavior for the three applied VCPT amplitudes at depths of (a) 2.1 m; (b) 4.7 m; (c) 10 m; and (d) 11.6 m. See text for further explanation.	77
Fig. 4.12. Normalized confidence interval for: (b) cone resistance; (c) loading stiffness; (d) unloading stiffness; and the confidence interval for the cone resistance cycles at depth of 2.2 m for VCPT amplitudes: (e) 3 mm; (f) 5 mm; and (g) 7mm.	79
Fig. 7.1.1. Correlated and shifted cone resistance datasets of SCPTs S1 – S7. The SCPT S8 is the reference dataset.	92-91
Fig. 7.1.2 Static and vibratory peak cone resistance for the three VCPT amplitudes. The shading represents the confidence interval.	91
Fig. 7.1.3. Static and vibratory peak sleeve friction for the three VCPT amplitudes. The shading represents the confidence interval.	92
Fig. 7.1.4. Static and vibratory peak pore water pressure for the three VCPT amplitudes. The shading represents the confidence interval.	92
Fig. 7.1.5. Degradation factory of cone resistance for the three VCPT amplitudes. The shading represents the confidence interval.	93
Fig. 7.1.6. Degradation factory of sleeve friction for the three VCPT amplitudes. The shading represents the confidence interval.	93
Fig. 7.1.7. Loading stiffness for the three VCPT amplitudes. The shading represents the confidence interval.	94
Fig. 7.1.8. Unloading stiffness for the three VCPT amplitudes. The shading represents the confidence interval.	94
Fig. 7.1.9. Upward displacement with cavitation for the three VCPT amplitudes. The shading represents the confidence interval.	95

List of tables

Table 1.1. Contributions and development of the VCPT method.	10
Table 2.1. Cone specification.	25
Table 2.2. Location of test points and their respective sets; Set A to investigate the spacing influence on CPTs; Set B to investigate the effect of a number of CPTs on confidence intervals. Distance to the nearest neighbour and the number of nearest neighbours of CPTs.	25
Table 3.1. Test scheme of Vibro-CPTu and static CPTu, where f = frequency; and ε_A = displacement amplitude.	45
Table 3.2. Maximum reduction ratio values.	51
Table 4.1. Specifications of the cone used in the present study.	57
Table 4.2. Location of test points and parameters considered for VCPT.	61
Table 4.3. Datasets measured from SCPT and VCPT.	64
Table 4.4. Individual and representative datasets for SCPT and VCPT.	68
Table 4.5. Mean values of normalized confidence intervals of cone resistance and loading and unloading stiffnesses for the different VCPT amplitudes.	78

Nomenclature

βf_s	Degradation factor of representative sleeve friction
βq_c	Degradation factor of representative cone resistance
$\sigma \beta f_s$	Standard deviation of degradation factor of representative sleeve friction
$\sigma \beta q_c$	Standard deviation of degradation factor of representative cone resistance
$\sigma d_{cav,r}$	Standard deviation of representative upward displacement with cavitation
$\sigma E_{loading,r}$	Standard deviation of representative loading stiffness
$\sigma E_{unloading,r}$	Standard deviation of representative unloading stiffness
$\sigma f_{s,r}$	Standard deviation of representative sleeve friction
$\sigma q_{c,r}$	Standard deviation representative cone resistance
σu_r	Standard deviation of representative pore water pressure
$\sigma v f_{s,p,r}$	Standard deviation of representative peak vibratory sleeve friction
$\sigma v q_{c,p,r}$	Standard deviation of representative peak vibratory cone resistance
$\sigma v q_{c,cy,r}$	Standard deviation of representative cone resistance cycles
$\sigma v u_{p,r}$	Standard deviation of representative peak vibratory pore water pressure
σX_r	Standard deviation of the representative datasets
$CI \beta f_s$	Confidence interval of degradation factor of representative sleeve friction
$CI \beta q_c$	Confidence interval of degradation factor of representative cone resistance
$CI d_{cav,r}$	Confidence interval of representative upward displacement of cavitation
$CI E_{loading,r}$	Confidence interval of representative loading stiffness
$CI E_{unloading,r}$	Confidence interval of representative unloading stiffness
$CI f_{s,r}$	Confidence interval of representative sleeve friction
$CI q_{c,r}$	Confidence interval of representative cone resistance
$CI u_r$	Confidence interval of representative pore water pressure
$CI v f_{s,p,r}$	Confidence interval of representative peak vibratory sleeve friction
$CI v q_{c,p,r}$	Confidence interval of representative peak vibratory cone resistance
$CI v q_{c,cy,r}$	Confidence interval of representative cone resistance cycles
$CI v u_{p,r}$	Confidence interval of representative peak vibratory pore water pressure
$CI X_r$	Confidence interval for the representative datasets
$CI X_{r,norm}$	Normalized confidence interval for the representative datasets
a	Acceleration

a_{st}	Stacked acceleration
d_{amp}	Displacement amplitude
$d_{cav,r}$	Representative upward displacement with cavitation
d_{cy}	Cyclic displacement
$E_{loading,r}$	Representative loading stiffness
$E_{unloading,r}$	Representative unloading stiffness
$f_{s,r}$	Representative sleeve friction
$q_{c,r}$	Representative cone resistance
u_r	Representative pore water pressure
f_s	Sleeve friction
q_c	Cone resistance
u	Pore water pressure
$vf_{s,p,r}$	Representative peak vibratory sleeve friction
$vf_{s,p}$	Peak vibratory sleeve friction
$vq_{c,p,r}$	Representative peak vibratory cone resistance
$vq_{c,p}$	Peak vibratory cone resistance
$vq_{c,cy}$	Cone resistance cycles
$vq_{c,cy,r}$	Representative cone resistance cycles
$vq_{c,cy,st}$	Stacked cone resistance cycles
vu_p	Peak vibratory pore water pressure
X_i	Individual dataset
X_r	Representative dataset
δSI	Absolute spacing influence
δSI_{SBT}	Average absolute spacing influence for soil behavior type
ρSI	Relative spacing influence
ρSI_{SBT}	Average relative spacing influence for soil behavior type
σ	Standard deviation
$\sigma \delta SI$	Standard deviation of absolute spacing influence
$\sigma \delta SI_{SBT}$	Standard deviation of average absolute spacing influence
$\sigma \rho SI$	Standard deviation of relative spacing influence
$\sigma \rho SI_{SBT}$	Standard deviation of average relative spacing influence
$\sigma q_{c,\mu}$	Standard deviation of mean cone resistance

$\sigma_{q_{c,r}}$	Standard deviation of representative cone resistance
CI_{μ}	Confidence interval of mean cone resistance
$CI_{\mu,SBT}$	Average confidence interval for soil behavior type
CI_r	Confidence interval of representative cone resistance
$CI_{r,SBT}$	Average confidence interval for soil behavior type
D_{50}	50% pass particle size
D_r	Relative density
F_r	Friction ratio
i	Subscript represents one specific CPT of a set
m	Set number
n	Total number of CPTs in a set
q_c	Cone resistance
$q_{c,\mu}$	Mean cone resistance
$q_{c,r}$	Representative cone resistance
q_t	Corrected total cone resistance
SBT	Soil behavior type
t	Student coefficient
Q_t	Normalized cone resistance
B_q	Pore pressure ratio

CHAPTER 1

1. Introduction:

1.1 Vibratory pile driving:

The demand for renewable sources of energy as replacement for fossil fuel is continuously increasing because of the climate change. Wind energy is one of those resources and it experiences a fast growth in the offshore sector where offshore wind energy turbines are built in the North Sea. Monopiles are mostly used as foundations for these structures. These monopiles are installed in the ground using the vibratory pile driving technique as a replacement to impact pile driving. The vibratory pile driving technique installs piles with axial vibrations, therefore it produces less noise and damage to the piles during driving, has less installation time, and allows for easier pile handling compared to impact pile driving (O'Neill and Vipulanandan, 1989, Whenham and Holeyman, 2012, Holeyman and Whenham, 2017b). One of the main challenges with the vibratory pile driving technique is the choice of the vibrator that should have the sufficient weight and energy to install the pile to the designed depth. The selection of the vibrator usually depends on drivability analysis which is based on soil-pile interaction models that use parameters obtained from the conventional in-situ soil investigation methods such as static cone penetration test CPT as input (Jonker, 1987, Wong et al., 1992, van Baars, 2004, Viking, 2006, Holeyman and Whenham, 2017a, Lee et al., 2012). The resistance of conventional models are multiplied by degradation factors in order to account for the induced dynamic mobility of soil and the increase in pore water pressure during vibratory pile driving (Wong et al., 1992). The degradation factors are in the best case based on analysis of test piles that have been installed by vibratory pile driving technique. In cases where the installation of test piles is not practical, degradation factors for vibratory pile driving are very uncertain (Jonker, 1987). In such cases, a soil-pile interaction model is likely unable to predict degradation in the soil resistance along the pile shaft and pile toe (Jonker, 1987, Holeyman and Whenham, 2017b).

The degradation in the soil resistance during vibratory pile installation has been attributed to liquefaction (Nogami et al., 1997, Rodger and Littlejohn, 1980). Soil liquefaction is generally described as the loss in shear strength of a soil caused by the increase in pore water pressure during cyclic loading (Seed and Idriss, 1971). The assessment of liquefaction resistance is mostly done by performing laboratory tests on reconstituted or undisturbed soil samples. One

of the first studies determined the liquefaction resistance and thus the soil cyclic resistance by performing undrained cyclic triaxial tests on sand samples (Seed and Lee, 1966). A cumulative increase in pore water pressure with the cyclic loading was observed. The increase in pore water pressure continued till it reached a value equal to the confining stress and therefore zero effective stress (Eq. 1.1):

$$\sigma' = \sigma - u \tag{1.1}$$

Where σ' is the effective stress; σ is the confining stress; and u is the pore water pressure. Fig.1.1(a) shows an example of liquefaction where the pore water pressure ratio Ru continues to increase with increasing cyclic loading till it reaches 100% (Eq.1.2):

$$Ru = \frac{u}{\sigma} * 100 \tag{1.2}$$

When Ru is equal to 100% large strains develop with further cyclic loading, this process is called liquefaction (Fig. 1.1(b)).

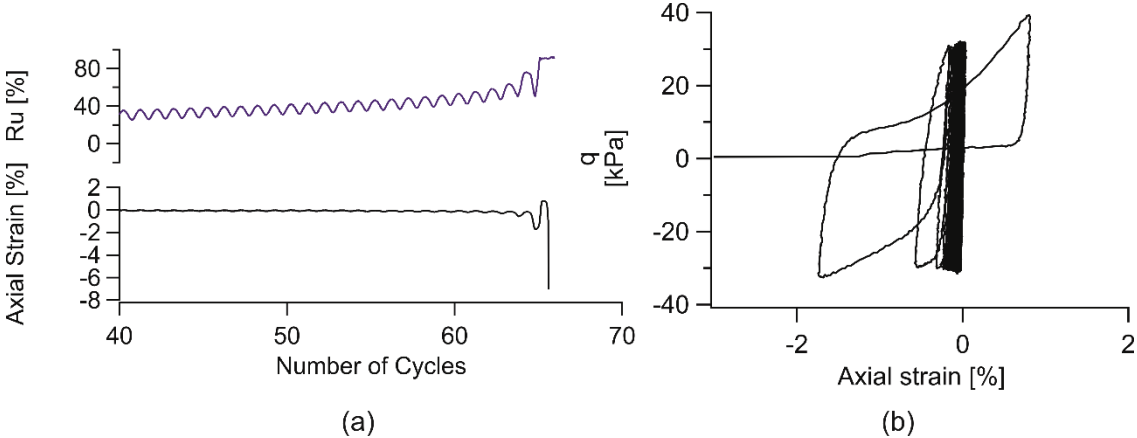


Fig. 1.1. An example of liquefaction in medium dense Cuxhaven Sand under 150 kPa confining stress, for a test performed in this study, showing in a) the pore water pressure ratio and the axial strain; b) the cyclic stress-strain behavior.

During undrained cyclic triaxial tests of dense sand, which is the soil density in the North Sea where vibratory piles are to be driven, the pore water pressure increases at small strains until momentary points of zero effective stress are reached. After that, with further strain the strength of the soil increases and the pore water pressure decreases; this process is named cyclic mobility (Poulos et al., 1985, Casto, 1975). An example of the cyclic mobility is shown in Fig. 1.2. The increase in the pore water pressure ratio with small strain increments is shown in Fig. 1.2 (a), this increase reaches a value of 90% only momentarily before it decreases again with the

increasing axial strain, this decrease indicates dilative behavior of the soil. The cyclic stress-strain behavior is shown in Fig. 1.2(b). Some studies related the phenomena of “cyclic mobility” to the degradation in the cyclic soil resistance during vibratory pile driving (Rao, 1993, Bonita, 2000).

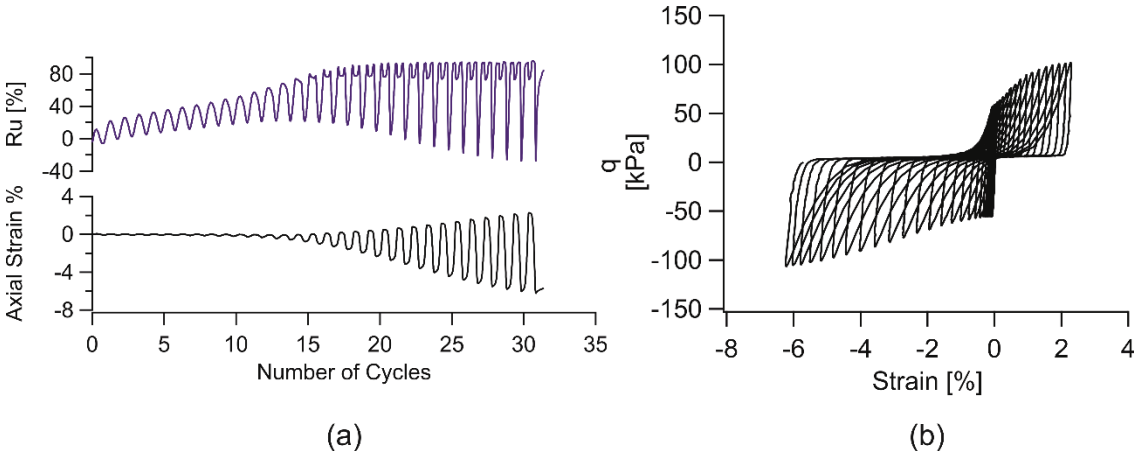


Fig. 1.2. An example of liquefaction in very dense Cuxhaven Sand under 150 kPa confining stress, for a test performed in this study, showing in a) the pore water pressure ratio and the axial strain; b) the cyclic stress-strain behavior.

The cyclic motion and soil degradation during vibratory pile driving has been described by the Karlsruhe model for slow vibratory pile driving (Dierssens, 1994). The schematic plot of this cyclic behaviour is shown in Fig. 1.3, where four phases are illustrated. For the first phase 1-2, the pile is in contact with soil. When the pile moves upward the contact is lost which results in reduction in the stress at the toe. When cyclic amplitude is large enough the pile completely loses contact with soil, and a cavity will form between the pile and the soil, this is the second phase 2-3. During this phase, the stress at the toe will be equal to zero. At phase 3-4, the pile moves downward without contacting the soil which results in that the stress at the toe remains at zero. At phase 4-1, the pile penetrates the soil that has changed properties due to the remoulding process that occurred during the previous cycle, and the stress at the toe starts to increase. This increase in stress depends on the degree of remoulding experienced during the previous cycle.

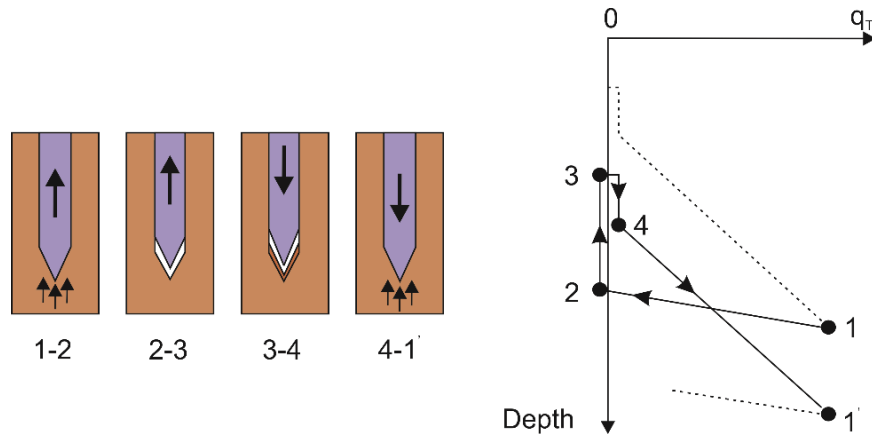


Fig. 1.3 Description of the four phases of the slow vibratory-motion of the pile-toe force.

Until now, the current in-situ soil investigation methods are unable to resemble and assess this complex cyclic soil behavior.

Furthermore, the inherent variations in soil properties affect the comparison of results obtained from any new in-situ soil investigation method with existing methods that are used to assess the cyclic soil behavior during vibratory pile driving. Therefore, the assessment of soil variability of the site is of great importance.

1.2 Assessment of site variability

Geotechnical in-situ and laboratory tests are used to determine the soil profile and to define the geotechnical properties of the soil in the field. The number of the laboratory and in-situ tests performed depend on the level of safety required for the structure, the variability of the soil in the field, the project budget, and time (Salgado et al., 2015). When limited number of tests are performed, there will be a certain level of uncertainty associated with the soil properties obtained from in-situ field tests and laboratory tests. These uncertainties are related to the inherent variations in soil properties which vary due to the sedimentation regime and diagenetic history of the site (Nichols, 2009, Phoon and Kulhawy, 1999). Examples of variation in soil properties caused by physical processes occurring in depositional environments are shown in Fig. 1.4.

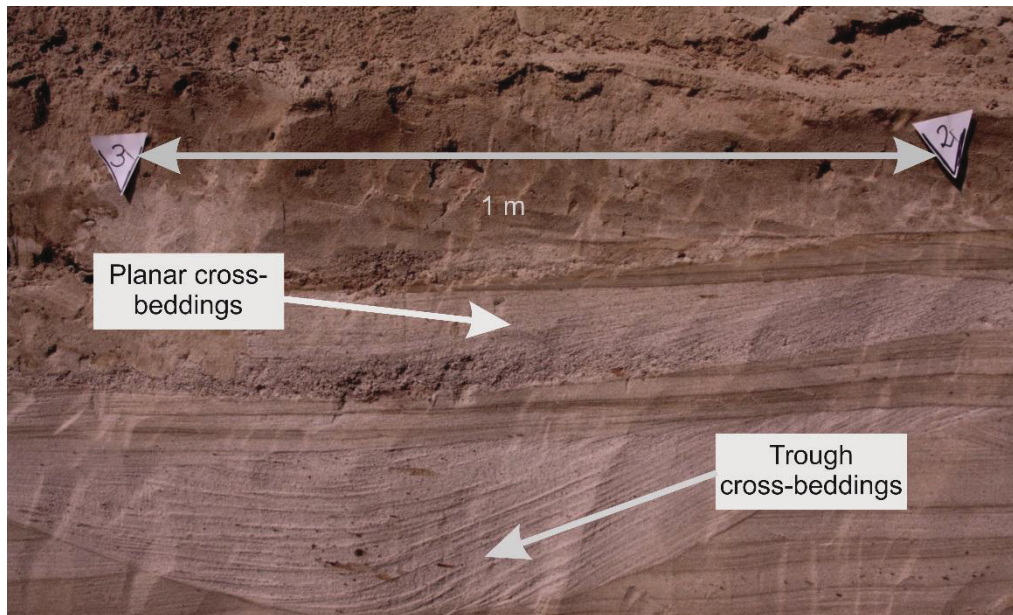


Fig.1.4. Dune bedforms forming planar cross-beddings and trough cross-beddings.

The variations in soil properties increase with increased spacing between the locations of the in-situ tests which lead to a decrease of the correlation between them, thus increasing the uncertainty in test results (Salgado et al., 2015). Therefore, a reduction in spacing improves the correlation between different in-situ soil investigation methods, such as the correlations between CPT and standard penetration test SPT, dilatometer test DMT, or vibratory VCPT (Al-Sammarraie et al., 2018, Lingwanda et al., 2015). Closely spaced and well correlated tests also lead to a better characterization of soil properties, thus reduce the uncertainty in tests results and allow to calculate significant ratios between different methods.

The uncertainty in tests results could be assessed by the confidence interval which represents the lower and upper limit of the mean of tests results, and the narrower the confidence interval, the more precise the estimation (Snedecor and Cochran, 1989). Furthermore, in order to achieve a certain level of safety for structures, design codes start to address these uncertainties by providing guidelines for selecting characteristic values which are mainly for material strength resistances and stiffness. The Eurocode limit state method for geotechnical design requires the determination of characteristic values for soil properties (Bond et al., 2013). The characteristic value of a soil parameter is selected so that the probability for a more unfavourable value must not exceed 5% (Laufer, 2013a). Statistically, the characteristic value is related to finding the 5% fractile of a distribution, therefore it represents the lower bound of the 95% confidence interval which is used for probabilistic geotechnical designs (Fig.1.5) (Bond et al., 2013).

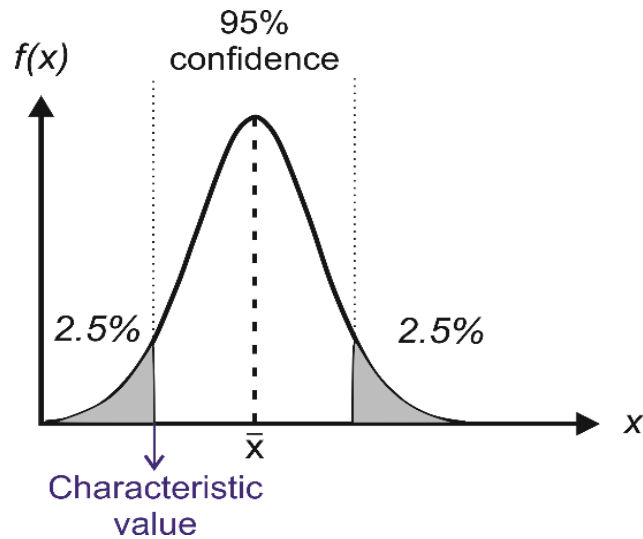


Fig. 1.5. Normal distribution curve showing the confidence interval and the characteristic value.

The characteristic value of soil parameters obtained from the in-situ soil investigation methods such as CPT, is calculated in the literature using Eq. 1.3 (Bond et al., 2013, Orr, 2000, Laufer, 2013b):

$$\text{characteristic value} = X_{mean} - t \cdot \frac{\sigma X_{mean}}{\sqrt{n}}, \quad (1.3)$$

Where X_{mean} is the mean value of the soil parameter; σX_{mean} is the standard deviation of the mean; t is the student coefficient determined from a 95% confidence level and a number of tests; n equals to the number of tests.

1.3 Static cone penetration test CPT.

The cone penetration test is an in-situ soil investigation method where a probe is pushed into the ground at a constant speed of 2 cm/s while measuring continuously the cone resistance q_c , sleeve friction f_s , and pore water pressure u . During site investigation the cone penetration test has three main applications (Lunne et al., 1997):

- 1- Determining stratigraphy and identifying materials
- 2- Estimating mechanical soil parameters
- 3- Providing data for direct geotechnical design.

When performing CPT, the soil around the cone will deform and may either compact or dilate (White and Bolton, 2004). After removing the probe, the hole formed by the CPT may collapse and loosen the soil to various degrees (Gupta and Zaman, 1999, Aadnoy, 1991). The zone that is permanently disturbed soil, after performing a CPT and removing the rod, is referred to as disturbed soil zone of CPT (Fig. 1.6). This zone differs from the influence zone of a CPT which is defined as the physical volume of soil around the cone that influences the measurement of cone resistance during penetration of CPT (Boulanger et al., 2016, Lunne et al., 1997). The size of the influence zone has been investigated in the literature by comparing the results from the cone resistance dataset with undisturbed natural soil layers. It was concluded that the size of the influence zone increases with increasing the diameter of the cone and it varies from 2 to 3 cone diameters for soft soils and from 10 to 20 cone diameters for stiff soils (Lunne et al., 1997, Boulanger et al., 2016). CPTs performed at close spacings lead to reduce – as explained above – the effect of inherent variations of soil properties and to improve the correlations between the tests. However, the influence zone of a CPT may overlap with the disturbed soil zone of previous CPTs when the spacing between the CPTs is smaller than a minimum acceptable value (Fig. 1.6). In such cases, existing empirical correlations between CPT datasets and derived parameters, such as relative density or soil behaviour types, would also be affected. Therefore it is important to consider the effect of the disturbed soil zone of a CPT when deciding on the spacing between the tests (Rogers, 2006, Boulanger et al., 2016).

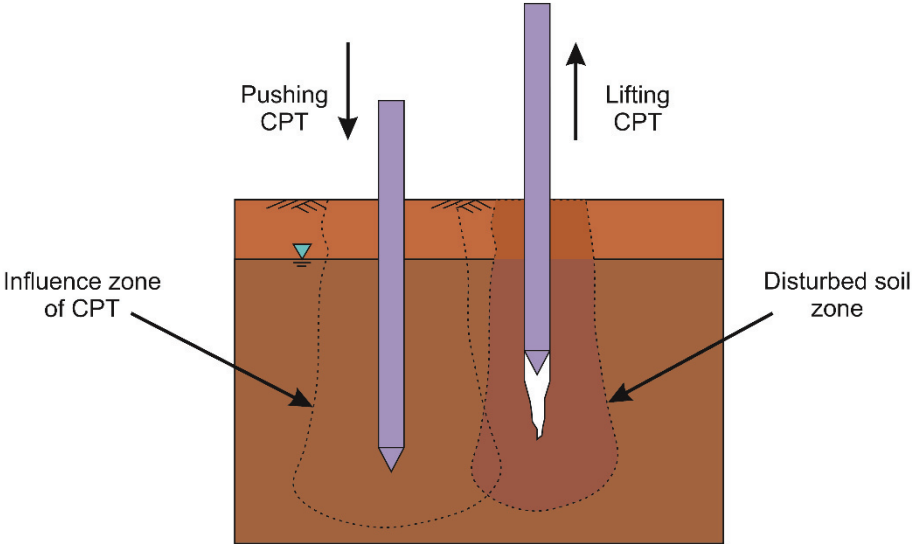


Fig. 1.6. Influence zone of CPT and the disturbed soil zone.

For CPT cones with areas of 10 cm², the British Standard recommends 1 m and the German Standard recommends 2 m minimum spacing (BS 1377-9, 1990, DIN EN ISO 22476-1, 2012). The rationale for these recommendations is not provided in these standards; however, it is likely related to the possible overlap of the CPTs penetration paths when a CPT penetration path deviates from the vertical path with increasing depth. The standard recommendations do not consider the effect of different soil types, therefore they may be too considerate, because the size of the influence zone of CPT depends on the stiffness and strength of the soil which is highly variable for different soil types (Lunne et al., 1997, Boulanger et al., 2016).

1.4 Vibratory cone penetration tests

The vibratory cone penetration test (VCPT) is an in-situ soil investigation method which induces cyclic loads while penetrating the soil (Sasaki and Koga, 1982). VCPT was first introduced as an experimental method to assess the liquefaction potential in earthquake prone areas in Japan (Sasaki and Koga, 1982, Tokimatsu, 1988). This first VCPT utilized horizontal down-hole vibrators, without a control of stress or strain, to apply the cyclic loads. The authors compared the cone resistance obtained from the static and vibratory CPT and observed reduction in the vibratory cone resistance (Fig. 1.7). The authors proposed a reduction ratio RR as an index for soil liquefaction resistance:

$$RR = 1 - \left(\frac{vq_c}{q_c} \right) \quad (1.4)$$

Where RR is the reduction ratio; vq_c is the vibratory cone resistance; q_c is the static cone resistance. This reduction ratio depends on both the density and the effective stress in the soil (Sasaki and Koga, 1982, Tokimatsu, 1988).

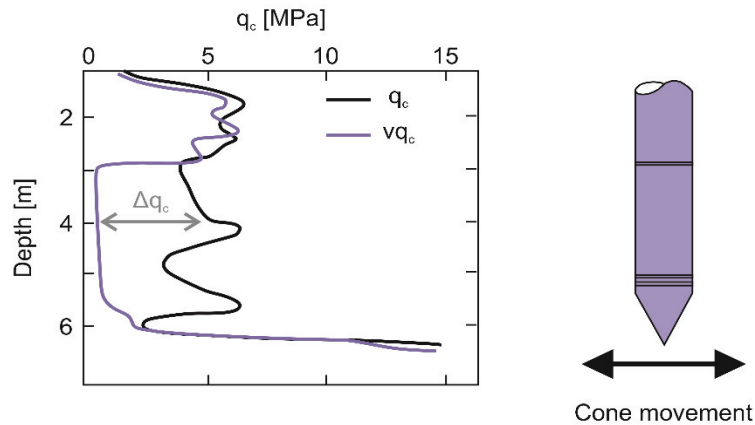


Fig. 1.7. Vibratory cone penetration test showing the results of static and vibratory cone resistance after Sasaki and Koga (1982).

The reduction in cone resistance due to vibratory CPT could also be expressed by the degradation factor β which is commonly used to estimate cyclic soil resistance during vibratory pile driving (Eq. 1.5)

$$\beta = \frac{vq_c}{q_c} \quad (1.5)$$

More recent studies used VCPT that penetrates the ground while applying vertical cyclic strains (Fig. 1.8). Vertical down-hole vibrators were utilized to apply the cyclic loads (Wise et al., 1999, Mayne, 2000, McGillivray et al., 2000). No reduction was observed between static and vibratory cone resistances (Wise et al., 1999, Mayne, 2000, McGillivray et al., 2000). Studies related to VCPT are summarized in Tab. 1.1 where it shows the type of applied cyclic loads and the results.

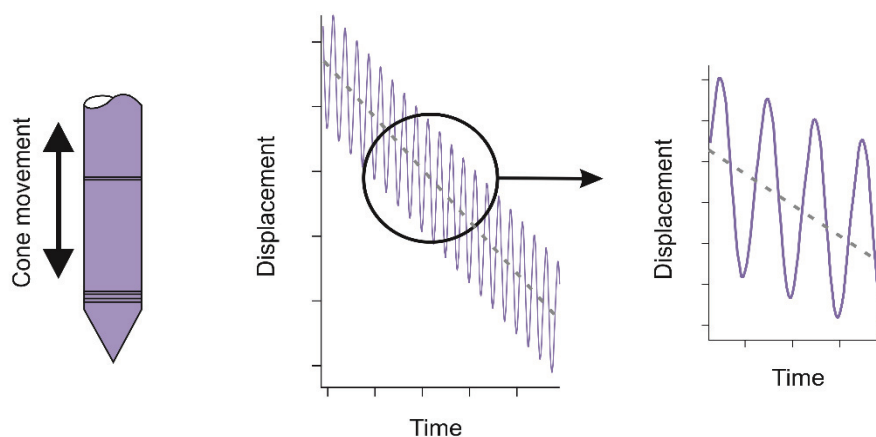


Fig. 1.8. The vertical cyclic motion of VCPT.

Table 1.1. Contributions and development of the VCPT method.

Country	Author(s)	Details	Results
Japan	Sasaki and Koga (1982)	- Down-hole horizontal vibrations at 200 Hz - horizontal centrifugal force	- Reduction in vq_c - No measurement of pore water pressure was available
Canada	(Moore, 1987)	- Vertical up-hole vibration at 75 Hz frequency - Applied vertical force	- No reduction in vq_c - No increase in pore water pressure
Italy	Mitchell (1988)	- Down-hole horizontal vibration at 200 Hz	- Qualitative interpretation of vq_c - No increase in pore water pressure.
USA	Wise et al. (1999) McGillivray et al. (2000)	- Downhole vertical-impulses by pneumatic solenoids (5 Hz)	- No reduction in the vq_c results - High increase in pore water pressure
USA	(Bonita, 2000)	- Chamber tests using pneumatic VCPT.	- Reduction in vq_c - Pore water pressure increased at distance from the test.
Germany	Jorat et al. (2015)	- Up-hole vertical vibrations - Displacement controlled	- Reduction in vq_c - No increase in pore water pressure
Germany	Kluger et al. (2016)	- Up-hole vertical vibrations - Displacement controlled	- Small reduction in vq_c in some layers. - No increase in pore water pressure

All previous studies (Tab.1.1) suffered from the lack of knowledge about the variations of displacement amplitude with depth and material. This lack of knowledge leads to uncertainties in the interpretation of the effect of VCPT on the cone resistance.

The vertical cyclic motion of VCPT resembles the cyclic motion during vibratory pile driving. Therefore, VCPT could be used to investigate the cyclic soil behavior during vibratory pile driving. When sensors with high sampling rate are utilized in the VCPT, the cone resistance and the displacement data is recorded. Therefore, the cyclic cone resistance-displacement behavior could be observed for every cycle Fig. (1.9(a)).

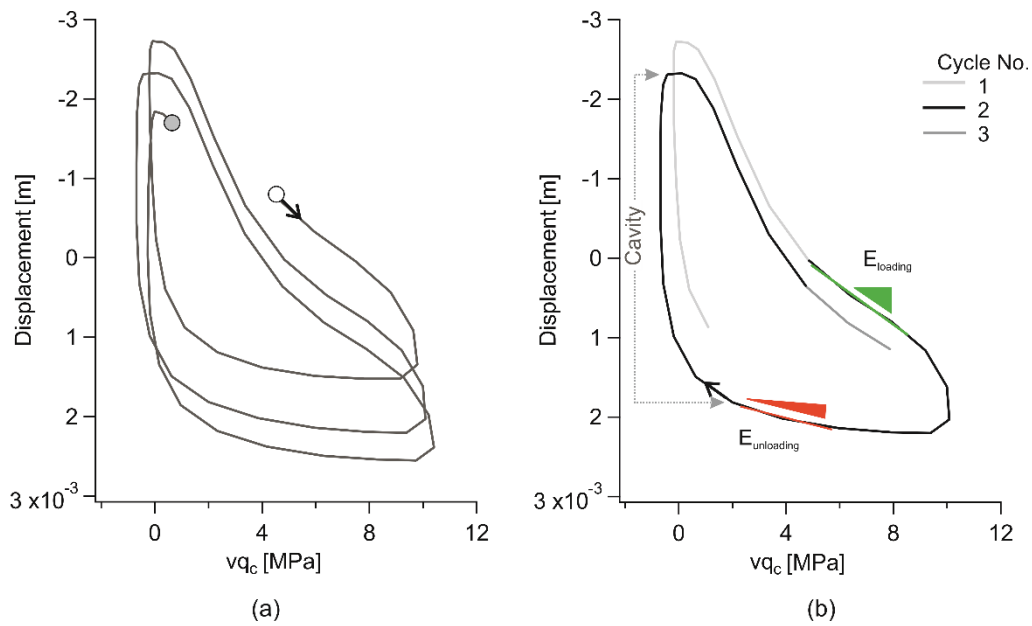


Fig. 1.9. Example of cone resistance – displacement hysteresis loops show in (a) three cycles; (b) loading and unloading stiffness for the second cycle.

When the cone resistance-displacement hysteresis loop is available, it becomes possible to evaluate important cyclic soil parameters such as the stiffness which represent the slope of the linear loading and unloading part of each individual cycle (Fig. 1.9(b)) (Wong et al., 1992, Lee et al., 2012). Furthermore, the VCPT could be used to investigate liquefaction, cyclic mobility, or the phenomenon of cavitation which could be responsible for the degradation of the cyclic soil resistance during vibratory pile driving. This is because the induced pore water pressure during cyclic motion of VCPT is measured using pressure sensor on the cone. Until now, however, the ability of the VCPT to assess the cyclic soil behavior during vibratory pile driving is not investigated.

1.5 Motivation and research hypotheses

Three major knowledge gaps about investigations of cyclic soil behavior in-situ have been identified, which form the basis motivation for this doctoral thesis. The first gap is related to the minimum spacing between two adjacent CPTs. Until now, there is no knowledge regarding this minimum spacing which ensures no effect of the disturbed soil zone on cone resistance and how the number of CPTs and their spacing reduce the effect of inherent variation in soil properties and improve the characterization of cone resistance.

The second gap is related to uncertainties in the in-situ cyclic soil resistance obtained from the early VCPT devices due to the changes of cyclic amplitude with depth of penetration.

The third gap is related to the lack of knowledge of the influence of displacement amplitudes on the degradation of cone resistance, the stiffness during loading and unloading cycles, and on the cavitation.

Based on the knowledge gaps, the following three research hypotheses are formulated. They are studied in chapters 2 - 4 and addressed in the concluding chapter 5 of this doctoral thesis:

1. Decreasing the spacing between CPTs locations and increasing the number of tests give a sufficient confidence interval and improve the characterization of cone resistance, if the distance falls not below minimum acceptable distance.
2. VCPT could be used to investigate the cyclic soil behavior in-situ until the final depth of penetration.
2. Degradation in cyclic soil resistance and stiffness increase with cyclic displacement amplitudes.

1.6 Study area

1.6.1 Bremen

The first study site where CPTs were performed is located in Bremen, Northern Germany (Fig. 1.10(a)). From a sediment core, in vicinity to the study site, stratigraphic age is determined following Ortlam and Schnier (1980) and grain size distribution was analysed by dry sieving (DIN EN ISO 14688-1, 2003). In the sediment core five Holocene units are identified (Fig. 1.11). Unit 1 consists of heterogeneous anthropogenic infill material and is underlain by Unit 2, a 3-m-thick layer of fluvial fine- to medium-grained sands. In Unit 3, the sand is interbedded with clay and silt layers of probably fluvial origin. Unit 4 is a 60-cm-thick sand layer, underlain by Unit 5 which is composed of interlayered silt-sand deposits that form the base of the Holocene sediments. Soil behaviour types were determined from CPT and range from 4 to 7 (Robertson, 2009). The sand layers of Unit 2 and 4 have relative densities between medium to dense following Baldi et al. (1986)'s CPT correlation (Fig. 1.11(f)).

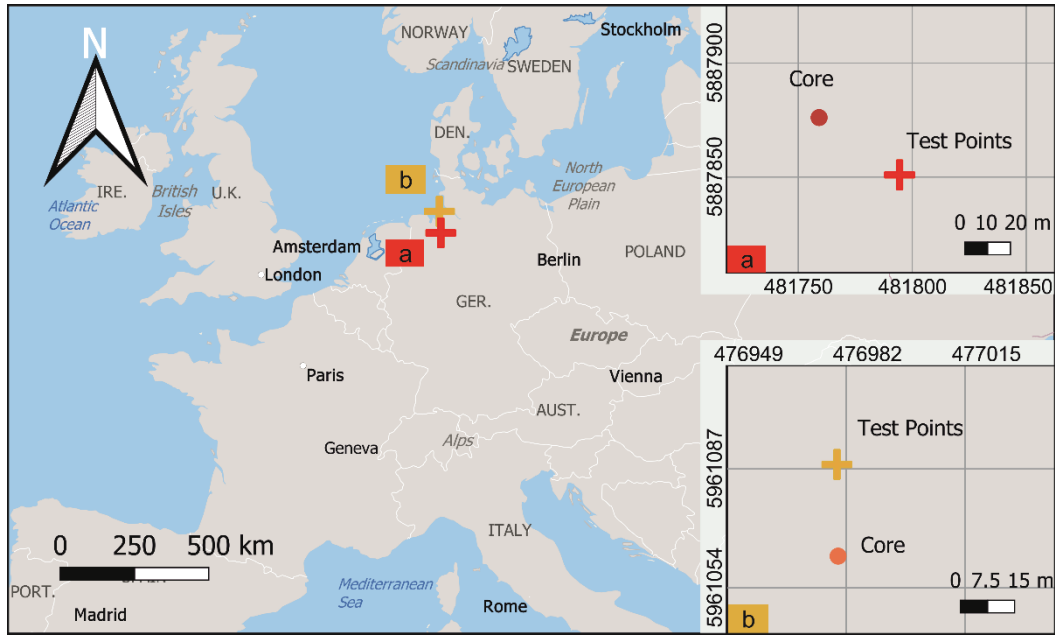


Fig. 1.10. Map indicating test areas locations: a) Bremen; b) Cuxhaven. The coordinate system used to create the maps was UTM zone N32.

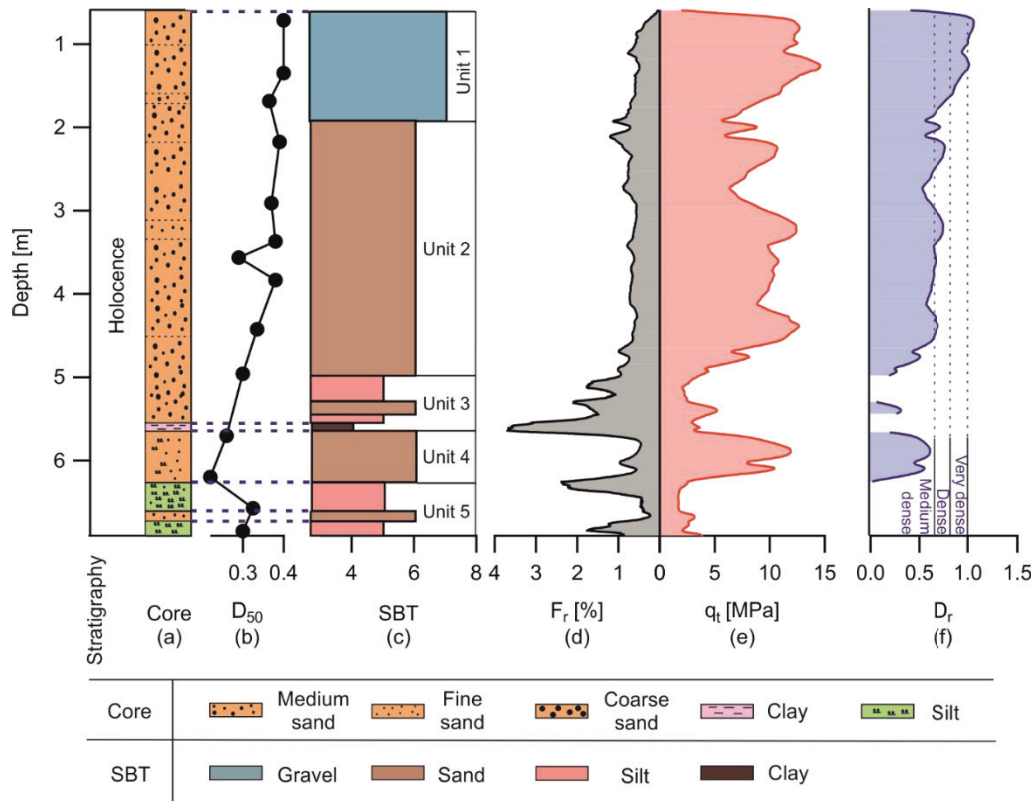


Fig. 1.11. Stratigraphy and soil properties of test field (a) core; (b) grain size distribution; (c) soil behavior types represented by SBT; (d) friction ratio; (e) corrected tip resistance; (f) relative density derived after Baldi et al. (1986).

1.6.2. Cuxhaven

The second study site is located in Cuxhaven, Northern Germany (Fig. 1.10(b)). Three glacial periods, Elsterian, Saalian, and Weichselian, formed the test field being located in the “Altenwalder Geest” moraine (Sindowski, 1965, Ehlers et al., 1984, Goodarzi et al., 2019, Ehlers, 1990). A drill core from the vicinity of the test field was used to determine stratigraphic units and physical properties of the upper twelve meters of the sand deposits. The stratigraphic characterization followed (Sindowski, 1965, Ehlers et al., 1984, Geo-Engineering, 2014) (Fig. 1.12), grain size analyses were carried out according to DIN 18123 (2011), and the unit weight was provided from Geo-Engineering (2014).

The deposits are of Pleistocene age and were subdivided into a 4-m-thick middle Saalian unit (U1 and U2) and an underlying 7-m-thick older Saalian unit (U3–U5) (Fig. 1.12). The first two units (U1 and U2) consist of fine- to medium-grained glacio-fluviatile sands that were probably deposited in a sandur environment. The third unit (U3), is a 60-cm-thick till layer, composed of grains from clay to gravel size. The till layer was probably formed during the Drenthe II ice advance (Hepp pers. comm. 2020). The till layer is underlain by U4 and U5 which are composed of compacted heterogenic stratified sand deposits. The sand layers of U4 and U5 exhibit discontinuous thicknesses due to deposition and erosion in a proximal glacio-fluviatile environment (Ehlers et al., 1984, Quinteros et al., 2018, Ehlers, 1990). The soil behavior types were calculated following Robertson (2009). Most of the sand deposits are soil behavior type 6 (sand like). Only the till layer (U3) is soil behavior type 3 and 4 (clay-like, silt-like). The sand deposits have relative densities between dense to very dense following the CPT correlation of Baldi et al. (1986).

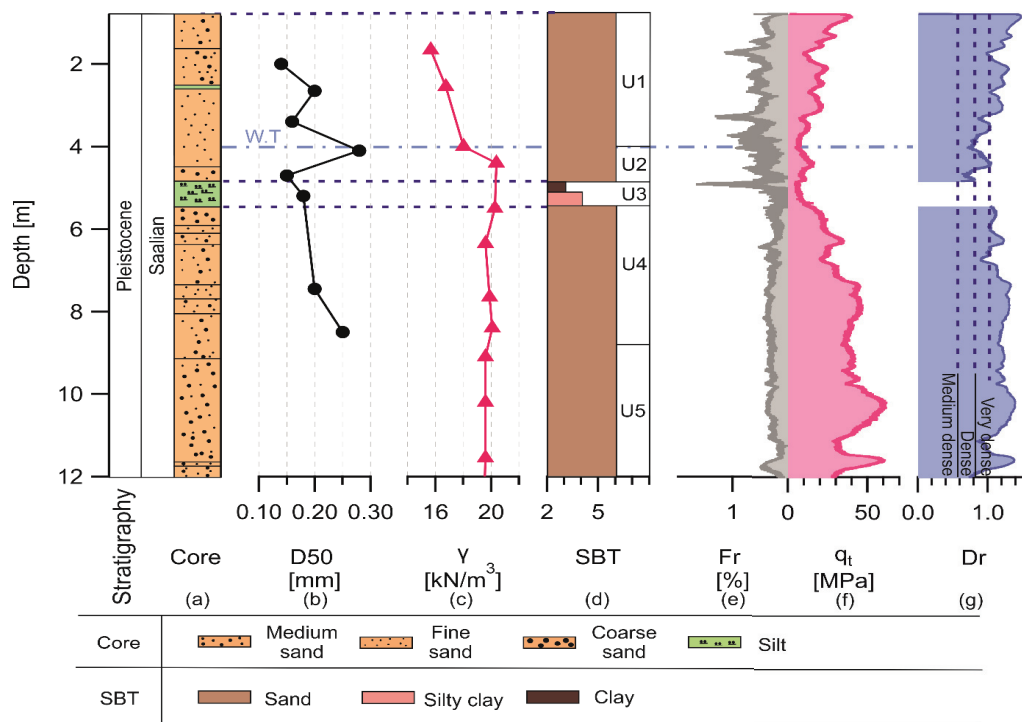


Fig. 1.12. Stratigraphy and soil properties of test site (a) core; (b) grain size distribution (Geo-Engineering, 2014); (c) bulk unit weight (Geo-Engineering, 2014); (d) soil behavior types (SBT); (e) friction ratio; (f) corrected tip resistance; and (g) relative density derived after Baldi et al. (1986).

1.7 Vibro Crawler

The vibro crawler has a highspeed hydraulic system controlled in real time with 5 kHz (Fig. 1.13). The cone is equipped with an inertial system consisting of a 3-axis gyroscope and 3-axis accelerometer sensor working with 500 Hz. The presented tests were displacement controlled by a distance sensor at the hydraulic cylinder.

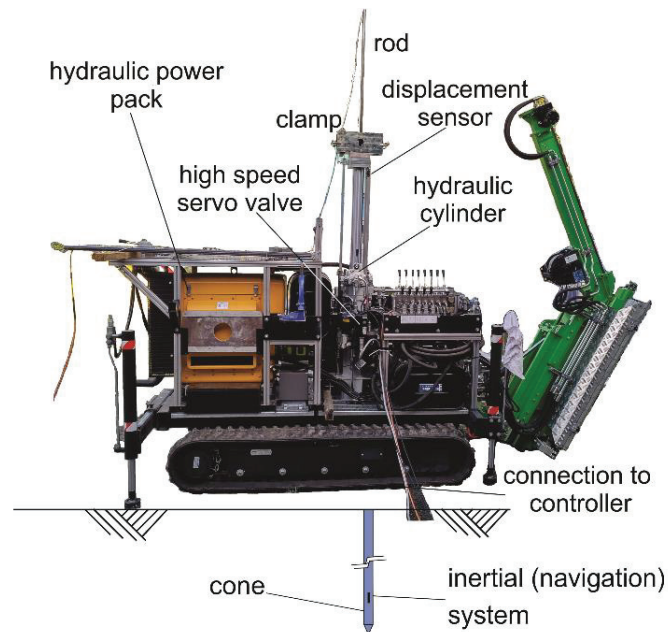


Fig. 1.13. The vibro crawler system.

1.8 VCPT device

The VCPT device consists of two separate units: a hydraulic power unit and a VCPT unit (right sketch in Fig. 1.14). The hydraulic power unit provided a flow capacity of 300 l/min at a pressure of 200 bar which was required to supply the VCPT unit. The CPT unit was built on a metal frame and consisted, among others, of a 100 kN hydraulic cylinder, a clamp, a valve unit, a displacement sensor, and a real time controller (left sketch in Fig. 1.14). The hydraulic cylinder was operated by the valve unit which consisted of three parallelly connected control valves. The control valves received their control signals from the real time controller with a cycle frequency of 5 kHz.

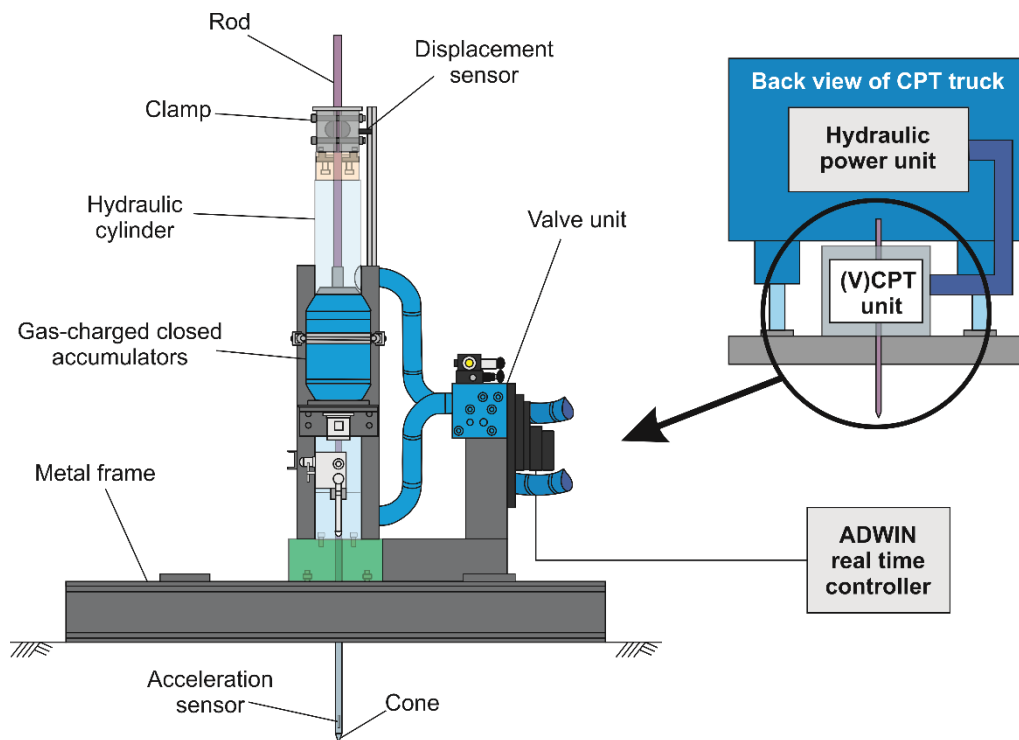


Fig. 1.14. The vibratory cone penetration test system.

1.9 Thesis background

1.9.1 Framework

All in-situ tests were performed within the framework of the project “Vibro Drucksondierungen” (FKZ: 0325906 A). The project was financially supported by the Federal Ministry for Economic Affairs and Energy (BMWi) and the MARUM - Center for Marine Environmental Sciences, University of Bremen.

1.9.2 Author contributions

D. Al-Sammarraie conceived the research hypotheses together with her supervisors, organized the test scheme, and performed the 45 in-situ static cone penetration tests and 18 vibratory cone penetration tests. Engineers, J. Schmid, M. Huhndorf, and W. Schunn helped with practical field work and the handling of the device. D. Al-Sammarraie analyzed the data and wrote three manuscripts, as a first author, together with the co-authors. The manuscripts are:

Manuscript 1. Effect of closely spaced CPTs on cone resistance.

Authors: D. Al-Sammarraie, S. Kreiter, F.T. Stähler, M. Goodarzi, T. Mörz

Status: Accepted 2020 in Géotechnique

Manuscript 2. New vibratory cone penetration device for in-situ measurement of cyclic softening.

Authors D. Al-Sammarraie, S. Kreiter, F.T. Stähler, M. Goodarzi, T. Mörz

Status: Published 2018 in Hicks, Pisanò & Peuchen (eds.) Cone penetration testing 2018, CRCPress/Balkema, pp. 591 – 597 ISBN: 978-0-429-50598-0 (eBook)

Manuscript 3. Vibratory cone penetration test A new experimental approach to investigate in situ cyclic soil behavior.

Authors: D. Al-Sammarraie, S. Kreiter, M.O. Kluger, M. Goodarzi, T. Mörz

Status: Submitted 2020 to Géotechnique

These three manuscripts are reprinted in this thesis in Chapter 2-4:

Chapter 2 investigates the minimum spacing between CPTs that ensures that there is no effect of the disturbed soil zone of previous soundings on cone resistance, and investigates the effect of spacing and number of CPTs on characterization of cone resistance.

Chapter 3 introduces the new VCPT device which is able to measure the cyclic displacement amplitude until the final depth of penetration.

Chapter 4 reports how the VCPT was used to investigate the degradation in the cyclic soil resistance and in the loading and unloading stiffness with increasing cyclic displacement amplitudes.

CHAPTER 2

Effect of closely spaced CPTs on cone resistance

D. Al-Sammarraie, S. Kreiter, F.T. Stähler, M. Goodarzi, T. Mörz

MARUM-Center for Marine Environmental Sciences, University of Bremen, Bremen, Germany

Accepted 2020 in *Géotechnique*

2. Abstract

Geotechnical methods, such as cone penetration tests (CPT), standard penetration tests (SPT), and seismic cone penetration tests (sCPT), are widely used to characterize the in-situ properties of soil. In studies where more than one in situ method in close spacing is used, it is important for geotechnical engineers to balance between soil heterogeneity and the artefacts of disturbed testing zones. The same applies if a detailed information about the subsoil is required and one in situ method is used in close spacing. There is no consensus on how to define the minimum spacing between testing zones and no study on the effect of disturbance caused by in situ tests. In this study, 33 CPTs were performed in natural sediments of Northern Germany and spacing threshold was defined at which cone resistance is affected by soil disturbance from previously performed CPTs. The CPTs were performed sequentially by successively refining the grid spacing, starting with a spacing of 119 cone diameters between CPTs, to a fine grid spacing of 7 cone diameters. The cone resistance is affected by previous CPT measurements below a spacing threshold of 24 cone diameters in medium-dense sands. Silt and clay layers showed no reduction in the cone resistance for our minimum grid spacing of 7 cone diameters.

2.1. Introduction

The cone penetration test (CPT) is a widely-used geotechnical method to characterize the in-situ properties of soil. Its advantages over drilling and sampling include simplicity, repeatability and continuous data recording (Robertson, 2009). During the test, a cone penetrates the ground vertically at constant speed, while sensors in the cone continuously measure the cone resistance, sleeve friction, and induced pore water pressure. These sensor data measured along the depth are hereafter referred to as CPT datasets. The natural variability of soil properties and the engineering safety requirements determines the number and distribution of CPTs performed in

the field (Bond et al., 2013, Orr, 2000). With increasing horizontal spacing between test sites (hereafter simply referred to as ‘spacing’), soil properties vary due to the sedimentation regime and diagenetic history of the site (Nichols, 2009, Phoon and Kulhawy, 1999). Therefore, the ability to correlate between CPT datasets decreases as the spacing between CPTs increases (Phoon and Kulhawy, 1999, Salgado et al., 2015, Lingwanda et al., 2017). CPTs performed at small spacing reduce the effect of soil variability on CPT datasets. Therefore, a reduction in spacing improves the correlation between different in-situ soil investigation methods, such as the correlations between CPT and SPT, DMT, or vibratory CPT (Al-Sammarraie et al., 2018, Lingwanda et al., 2015). Good correlations are important when combinations of certain soil parameters from different in-situ soil investigation methods are required, for example combination of small strain properties, like G_0 from DMT, and large strain properties, like the strength from CPT. A reduction in spacing further helps to investigate changes in soil properties, which could occur over smaller length scales, due to engineering interventions such as piling or foundation improvement methods (van der Stoel, 2001).

Closely spaced and well correlated tests also lead to better estimation of the characteristic cone resistance in a vertically variable soil. The characteristic cone resistance is defined statistically as the cone resistance that falls in the 5%-fractile, it is suggested by the Eurocode for probabilistic design, and it depends on number of tests, nature of soil structure, and variability in CPT datasets (Bond et al., 2013, Frank et al., 2004). The cone resistance dataset from a single CPT is commonly used to calculate the characteristic cone resistance for specifically selected vertical soil units (Bond et al., 2013, Orr, 2000, Laufer, 2013a). However, these selected soil units are assumed to have homogeneous soil properties within the selected depth interval, therefore, there is no consideration for the vertical variability in soil properties. Obtaining only a single characteristic value for a specific soil unit does not allow the evaluation of the results of in-situ soil investigation devices and soil improvement methods, because no characterization of varying soil properties will be possible within smaller depth intervals.

During the CPT, the soil adjacent to the cone undergoes large deformation that may either compact or dilate the surrounding soil (White and Bolton, 2004). After removing the probe, the hole formed by the CPT either remains open or collapses, depending on soil properties, stress state, and groundwater table (Gupta and Zaman, 1999, Aadnoy, 1991). The collapse causes the soil around the hole to soften to various degrees. As a result, every CPT leaves a zone of permanently disturbed soil with properties possibly very different from the original in-situ state, this zone is hereafter referred to as disturbed soil zone of CPT.

The physical volume of soil around the cone that influences the measurement of cone resistance during penetration is called the influence zone of CPT (Boulanger et al., 2016, Lunne et al., 1997). The size of the influence zone increases with cone diameter and it further depends on the stiffness and strength of the soil. The influence zone may vary from 2 to 3 cone diameters for soft soils and from 10 to 20 cone diameters for stiff soils (Lunne et al., 1997, Boulanger et al., 2016). However, these factors of cone diameters are developed from comparing cone resistance datasets with the undisturbed natural soil layers (Rogers, 2006, Boulanger et al., 2016). Till now, there is no study that takes the disturbed soil zone of CPT into account. In CPT calibration chambers there is another parameter related to the influence zone: the minimum chamber-to-cone diameter ratio which is defined to avoid effects of the chamber's boundary on the test results. It ranges from 100 for very dense sand to 33 for loose sand (Ahmadi and Robertson, 2008). One approach to replicate field conditions with smaller chamber-to-cone diameter ratios in the chamber is to use controlled stiffness boundaries (Hsu and Huang, 1998, Stähler et al., 2018, Yu and Mitchell, 1998). The geometry of calibration chamber tests and closely spaced CPTs in the field are not equivalent, because the effect of chamber's circular boundary on test results differs from effect of the disturbed soil zone of previously performed CPT in the field.

For closely spaced CPTs, the influence zone of a CPT may overlap with the disturb soil zone of previous CPTs. In such cases, existing empirical correlations between CPT datasets and derived parameters, such as relative density or soil behaviour types, would be affected too.

As a consequence, in projects where small spacings between CPTs are required, there is a need to consider the minimum spacing between CPTs without effect on CPT datasets. There are different recommendations for the minimum spacing between CPTs without effect on CPT datasets. For CPT cones with areas of 10 cm^2 , the British Standard recommends 1 m and the German Standard recommends 2 m minimum spacing (BS 1377-9, 1990, DIN EN ISO 22476-1, 2012). The rationale for these recommendations is not provided in these standards, and because they do not consider different soil types, they may be inadequate, since the size of the influence zone of CPT depends on the stiffness and strength of the soil which is highly variable for different soil types (Lunne et al., 1997, Boulanger et al., 2016).

In this study, 33 CPTs were performed in natural sediments of Northern Germany and a new threshold spacing is defined at which cone resistance is affected by soil disturbance from previously performed CPTs. We focused on the following questions:

- What is the minimum spacing between two adjacent CPTs, without any effect of the disturbed soil zone on cone resistance?
- How do different soil behaviour types affect this minimum spacing?
- How does the CPT spacing and the number of CPTs effect the characterization of cone resistance in the field?

To answer these questions, the CPTs were performed sequentially in a successively refined grid, starting with a grid spacing of 119 cone diameters between CPTs to a fine grid spacing of 7 cone diameters.

2.2. Materials and Methods

2.2.1 Geological and geotechnical setting

The study site where CPTs were performed is located in Bremen, Northern Germany (Fig. 2.1). From a sediment core, in vicinity to the study site (Fig. 2.2(b)), stratigraphic age is determined following Ortlam and Schnier (1980) and grain size distribution was analysed by dry sieving (DIN EN ISO 14688-1, 2003). In the sediment core, five Holocene units are identified (Fig. 2.3). Unit 1 consists of heterogeneous anthropogenic infill material and is underlain by Unit 2, a 3-m-thick layer of fluvial fine- to medium-grained sands. In Unit 3 the sand is interbedded with clay and silt layers of probably fluvial origin. Unit 4 is a 60-cm-thick sand layer, underlain by Unit 5, which is composed of interlayered silt-sand deposits that form the base of the Holocene sediments. The central CPT (S8 in Fig. 2.2) exhibits soil behaviour types ranging from 4 to 7 (Robertson, 2009). The sand layers of Unit 2 and 4 have relative densities between medium to dense following Baldi et al. (1986)'s CPT correlation (Fig. 2.3(f)).

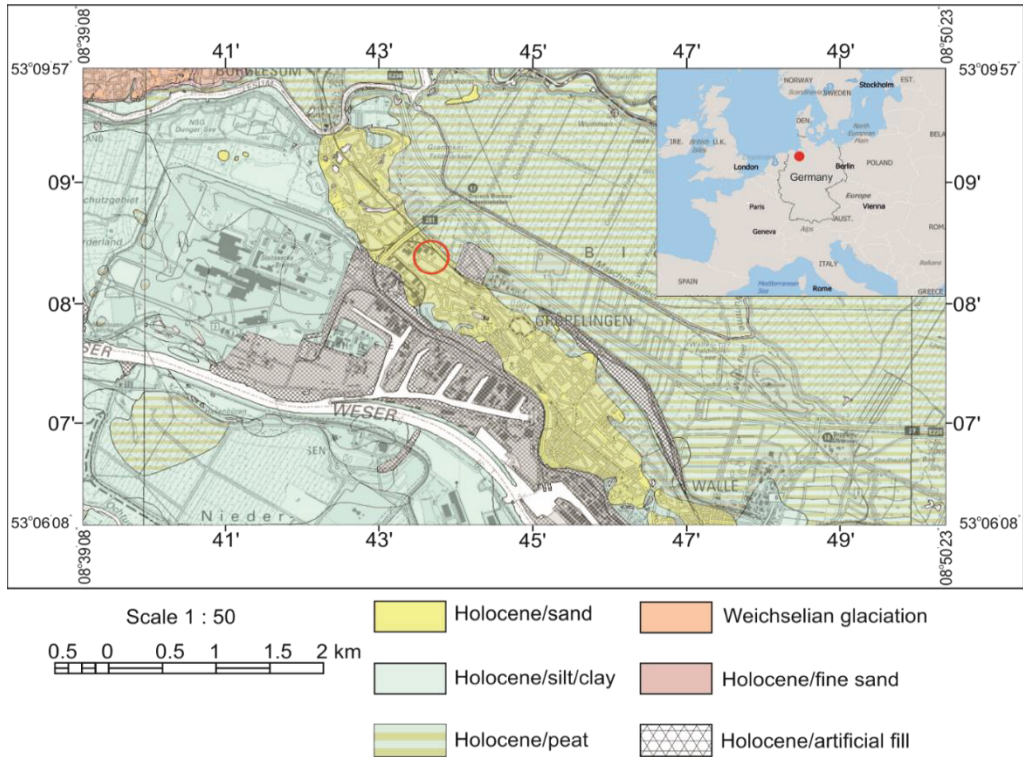


Fig.2.1. Geological map of Germany – Bremen, indicating the location of the test field (NIBIS, 2014).

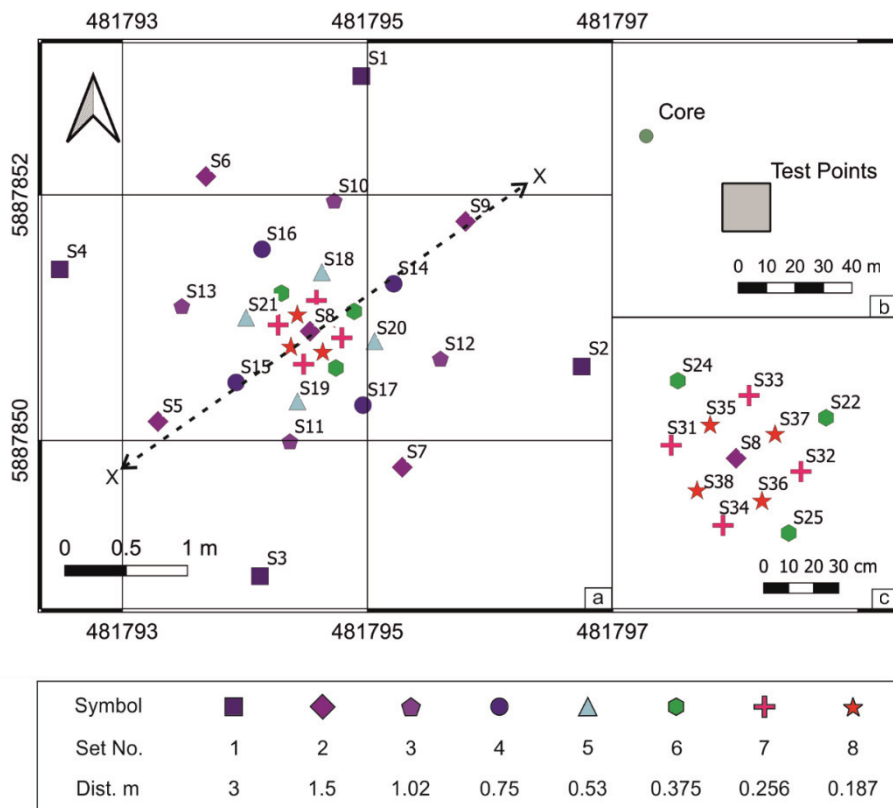


Fig. 2.2. Maps, using UTM zone N32, of a) the layout of test points; section $x - x$, where the inclination of the rod is shown in Fig. 5; b) the location of the core; c) close up for CPTs of set A6– A8.

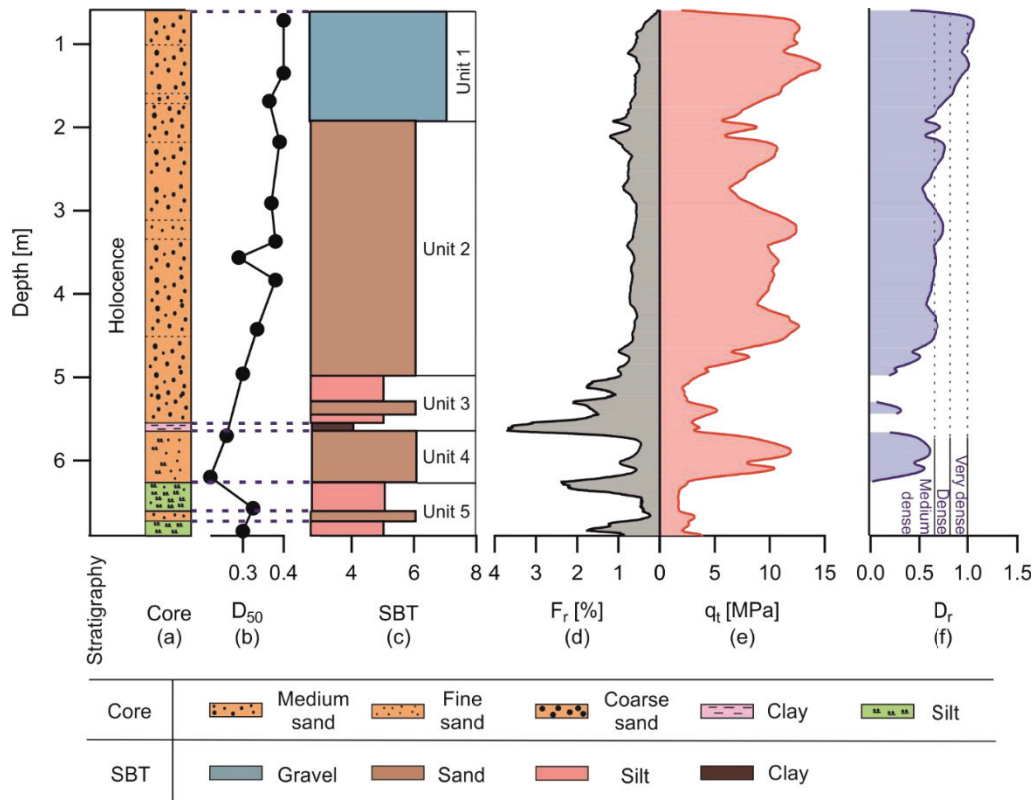


Fig. 2.3. Stratigraphy and soil properties of test field (a) core; (b) grain size distribution; (c) soil behavior types represented by SBT; (d) friction ratio; (e) corrected tip resistance; (f) relative density derived after Baldi et al. (1986).

2.2.2 Experimental layout

33 CPTs were performed within a square, using a CPT cone with an area of 5 cm² (Tab.2.1). The CPTs were grouped into eight sets of various spacings, ranging from 119 to 7 cone diameters (Tab.2.2, Fig. 2.2). The spacing between CPTs of the outermost set A1 was chosen to be 3 m (equivalent to 119 cone diameters), which is presumed to be large enough to avoid any overlapping between the influence zone of CPT and the disturbed soil zone of previous CPTs (BS 1377-9, 1990, DIN EN ISO 22476-1, 2012). The CPTs of the eight sets were performed by sequentially refining the CPT spacing from set A1 to A8. The term ‘CPT spacing’, as indicated in Tab 2.2, is hereafter defined as the minimum spacing between CPTs of a set to CPTs of a previous set. The detailed layout of the test points is visualized in Fig. 2.2. The number of CPT neighbours in Tab. 2.2 represents the number of closest CPTs from previous sets that surround each individual CPT of a current set, except for S8 where the CPT neighbours are from the same set (set A2). This test layout was chosen to provide both (1) equal spacing between each individual CPT and its closest CPT neighbours from the previous set as well as (2) sufficient data for statistical analysis.

The CPT locations were determined by DGPS with a horizontal resolution of ± 2 cm. A theodolite with an accuracy of ± 0.3 cm was used to ensure a common height reference at the start and the end of each CPT.

Table 2.1. Cone specification

Cone diameter [cm]	Cone area [cm ²]	Resolution [Hz]			
		Cone	Sleeve	Pressure	Acceleration
2.52	5	125	125	125	500

Table 2.2. Location of test points and their respective sets; Set A to investigate the spacing influence on CPTs; Set B to investigate the effect of number of CPTs on confidence intervals. Distance to the nearest neighbour and the number of nearest neighbours of CPTs.

Test No.	Date	UTM WGS84		Set A	Set B						CPT spacing		No. of neighbouring CPTs	
		X	Y		1	2	3	4	5	6	m	Spacing /Dia		
S1	14.05.18	481794.949	5887852.968	1			X	X	X	X	3	119	-	
S2	14.05.18	481796.7465	5887850.602						X	X	3	119	-	
S3	14.05.18	481794.122	5887848.893				X	X	X	X	3	119	-	
S4	14.05.18	481792.489	5887851.393						X	X	3	119	-	
S5	15.05.18	481793.29	5887850.154	2				X	X	X	1.5	60	2	
S6	15.05.18	481793.6816	5887852.15			X				X	1.5	60	2	
S7	15.05.18	481795.2832	5887849.781			X				X	1.5	60	2	
S8	15.05.18	481794.5308	5887850.889			X		X	X	X	1.5	60	3*	
S9	15.05.18	481795.7998	5887851.784					X	X	X	1.5	60	2	
S10	02.07.18	481794.7273	5887851.947	3				X	X	X	1.06	42	4	
S11	02.07.18	481794.3665	5887849.986			X				X	X	1.06	42	4
S12	02.07.18	481795.5944	5887850.66			X				X	X	1.06	42	4
S13	02.07.18	481793.485	5887851.088					X	X	X	1.06	42	4	
S14	02.07.18	481795.2134	5887851.276	4		X	X	X	X	X	0.75	30	4	
S15	02.07.18	481793.9279	5887850.472				X			X	0.75	30	4	
S16	03.07.18	481794.1395	5887851.557			X	X	X	X	X	0.75	30	4	
S17	03.07.18	481794.9625	5887850.287				X			X	0.75	30	4	

Test No.	Date	UTM WGS84		Set A	Set B						CPT spacing		No. of neighbouring CPTs	
		X	Y		1	2	3	4	5	6	m	Spacing/Dia		
S18	03.07.18	481794.6271	5887851.37	5							0.53	20	4	
S19	03.07.18	481794.4284	5887850.318									0.53	20	4
S20	03.07.18	481795.0569	5887850.809									0.53	20	4
S21	03.07.18	481794.0093	5887851									0.53	20	4
S22	04.07.18	481794.8911	5887851.051	6							0.375	15	4	
S23	04.07.18	-	-									-	-	-
S24	04.07.18	481794.2976	5887851.199									0.375	15	4
S25	04.07.18	481794.7416	5887850.59									0.375	15	4
S26	04.07.18	481794.7908	5887850.836	7							0.265	10	4	
S27	10.07.18	481794.2709	5887850.941									0.265	10	3
S28	10.07.18	481794.5831	5887851.14									0.265	10	4
S29	18.07.18	481794.4786	5887850.621									0.265	10	3
S30	18.07.18	481794.427	5887851.021	8							0.187	7	4	
S31	20.08.18	481794.6347	5887850.717									0.187	7	4
S32	20.08.18	481794.687	5887850.984									0.187	7	4
S33	20.08.18	481794.3747	5887850.759									0.187	7	3

*For S8 we considered the number of neighbours of set A2 and not the previous set A1.

2.2.3 Penetration paths of the CPTs

The penetration paths of all CPTs were estimated from the orientation of the CPT cone, which is derived from a three-dimensional acceleration sensor in the cone. The cone and rods were marked at the outside and oriented in the same direction at the start of each push. Rotation of the rod around the vertical axis was prevented by a clamp and any torsion in the rod was neglected. The results from the acceleration sensor were first smoothed using moving average for 24×10^3 data points and then used to derive the directional unit vectors for each depth increment. The Cartesian coordinates for the penetration paths of each CPT were then obtained by adding the directional unit vectors for each depth increment to the location of the CPT at the soil surface. The penetration paths of sets A5 to A8 are projected to x-y and x-depth space (Fig. 2.4). The projections of the CPT paths show that no overlapping between any of the CPTs at the same depth occurred (Fig. 2.4).

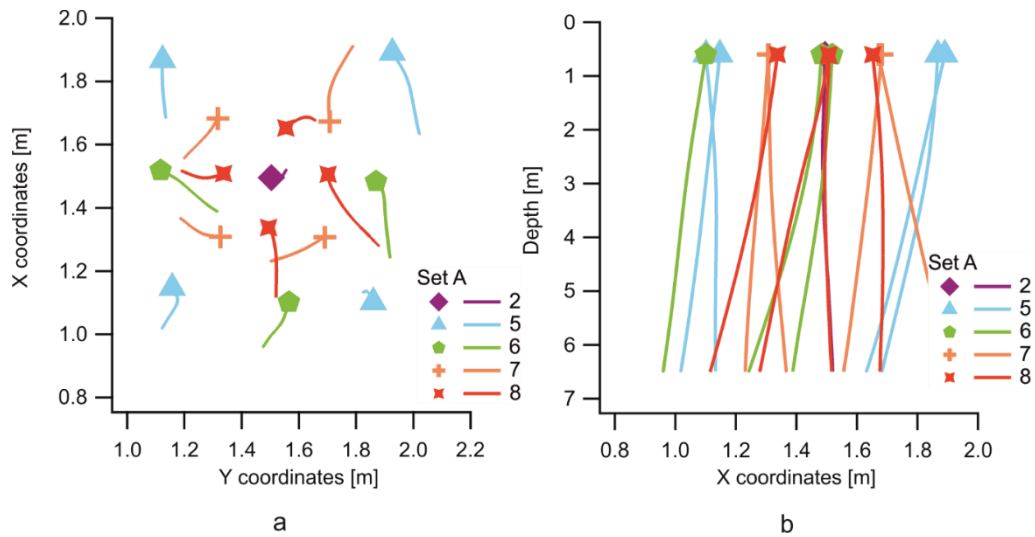


Fig. 2.4. Penetration path projections a) top view, b) side view section x-x. The symbols represent the starting point of the CPT.

For every CPT from sets A3 to A8, the depth-dependent spacing to the closest CPT neighbours of the previous set is calculated. Each CPT from sets A3 to A8 have 3 to 4 CPT neighbours from previous sets (Tab. 2.2). Therefore, 12 to 16 datasets of the depth-dependent spacing are obtained for each CPT set. The depth-dependent spacing measurements from each set are used to produce frequency distribution diagrams (Fig. 2.5). The CPT spacing of sets A3 to A8 lie within the standard deviation of the mean value of depth-dependent spacing, derived from the frequency distributions (Fig.2.5).

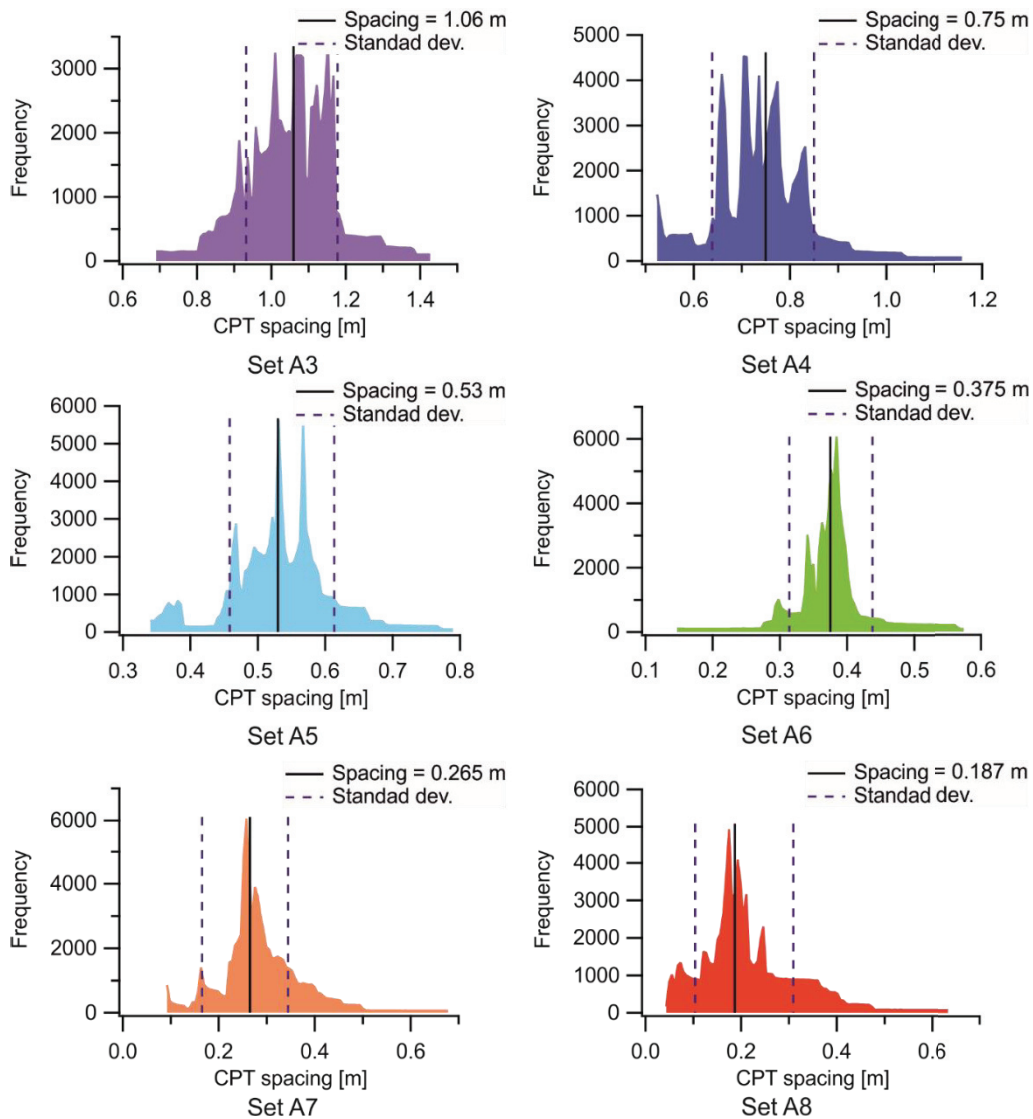


Fig. 2.5. Frequency distribution of the depth-dependent spacing of the neighboring CPTs of set A3 – 8.

2.2.4 Evaluation of CPT datasets

2.2.4.1 CPT correlation

The local changes in depth of specific soil layers at small spacings, led us to establish correlations between cone resistance datasets of all CPTs in the field and to shift these datasets to a common depth. The central CPT S8 was chosen to be the 'reference dataset' for all other CPTs. The correlation process consisted of: (1) smoothing cone resistance datasets of all CPTs using moving average for 13 data points (2) inferring stratigraphic units from the cone resistance dataset of the reference CPT and calculating soil behaviour types and relative density; (3) selecting correlated tie points, which were based on distinctive stratigraphic boundaries

found throughout the study area, and through local minima in the cone resistance datasets; (4) shifting the depths of tie points of all CPTs to the depth of the reference CPT dataset using linear interpolation which led to stretching and shortening of depth increments, and (5) resampling the CPT datasets to a vertical resolution of 0.5 mm. The correlated CPTs with original and shifted depths are displayed in appendix (Fig. 7.1.1). The average depth shift is 5 ± 4.6 cm and the maximum depth shift is 25 cm.

2.2.4.2 Parameters for assessing the effect of CPT spacing on cone resistance

The correlation and shifting of CPT datasets resulted in 33 cone resistance values for each depth increment. These 33 cone resistance values are associated with spacings between 119 and 7 cone diameters (Sets A1 to A8). Statistical parameters of the CPT datasets were calculated to quantify the effect of spacing on cone resistance. The calculation procedure for these parameters is schematized in the right branch of Fig. 2.6. Numbers in circles indicate steps of the calculation procedure, which will be referred to in the following section.

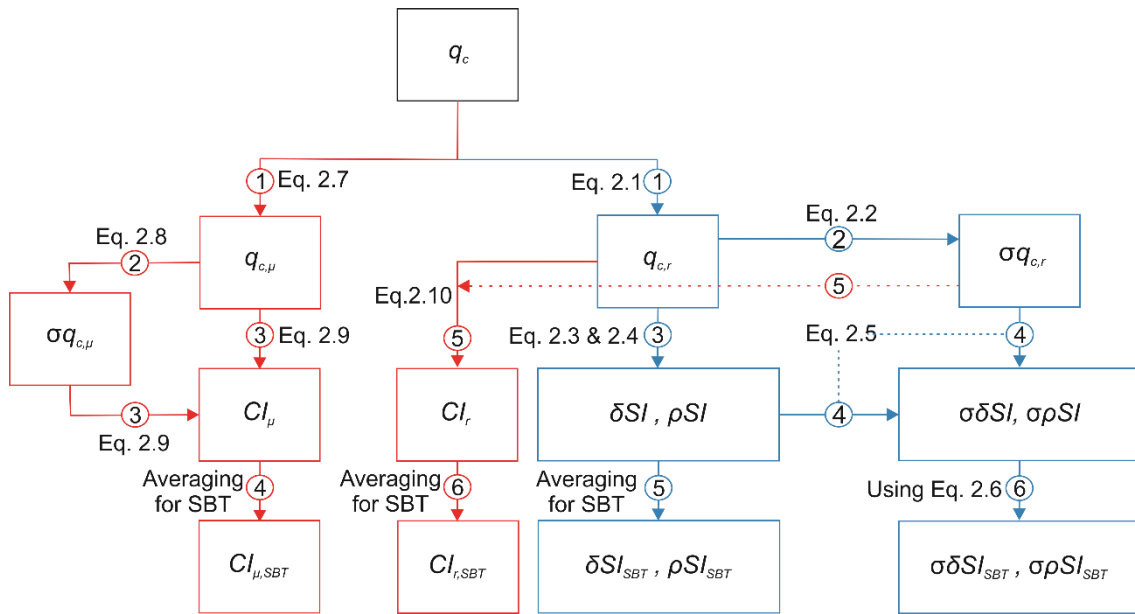


Fig. 2.6. Flow chart describes the mathematical calculations used to evaluate the CPT datasets.

In step 1, the cone resistance datasets were averaged within set A1 to A8. This yielded one representative cone resistance dataset for each spacing.

$$q_{c,r} = \frac{\sum_{i=1}^n q_{c_i}}{n}, \quad (2.1)$$

Where $q_{c,r}$ is the representative cone resistance of set A_m ($1 \leq m \leq 8$); q_{c_i} is an individual cone resistance dataset in set A_m (with $1 \leq i \leq n$). n is the total number of CPTs in set A_m .

In step 2, the standard deviations of the representative cone resistance datasets $\sigma q_{c,r}$ were calculated.

$$\sigma q_{c,r} = \sqrt{\frac{\sum_{i=1}^n (q_{c_i} - q_{c,r})^2}{n-1}}. \quad (2.2)$$

In step 3, all representative cone resistance datasets (A1 to A8) were normalized with respect to set A1, in order to investigate if and how the disturbed soil zone of previously performed CPTs affects the cone resistance of a current CPT. Set A1 with the largest spacing is taken as the undisturbed reference and the change in representative cone resistance was quantified by the absolute and relative change of the representative cone resistance.

$$\delta SI = q_{c,r_1} - q_{c,r}, \quad (2.3)$$

$$\rho SI = \frac{q_{c,r}}{q_{c,r_1}}, \quad (2.4)$$

Where δSI is the absolute change and ρSI is the relative change of the representative cone resistance; q_{c,r_1} is the representative cone resistance dataset of set A1; and $q_{c,r}$ is the representative cone resistance dataset of set A_m , for $1 \leq m \leq 8$.

In step 4, the standard deviation of the absolute and relative change was calculated using the propagation of uncertainty rule (Taylor, 1982, Morgan and Henrion, 1990).

$$\sigma \delta SI \text{ or } \sigma \rho SI = \sum \frac{\partial f(q_{c,r}, q_{c,r_1})}{\partial q_{c,r_1}} * (\sigma q_{c,r_1})^2 + \sum \frac{\partial f(q_{c,r}, q_{c,r_1})}{\partial q_{c,r}} * (\sigma q_{c,r})^2, \quad (2.5)$$

Where $\sigma\delta SI$ is the standard deviation of the absolute change; $\sigma\rho SI$ is the standard deviation of the relative change; $\frac{\partial f(q_{c,r}, q_{c,r_1})}{\partial q_{c,r_1}}$ is the derivative of Equation 2.3 or 2.4 with regards to q_{c,r_1} ; $\sigma q_{c,r_1}$ is the standard deviation of q_{c,r_1} ; $\frac{\partial f(q_{c,r}, q_{c,r_1})}{\partial q_{c,r}}$ is the derivative of Equation 2.3 or 2.4 with respect to $q_{c,r}$; and $\sigma q_{c,r}$ is the standard deviation of $q_{c,r}$.

In steps 5 and 6, the effect of soil behavior types on changes in cone resistance was studied. Therefore, the datasets of absolute and relative change were averaged for the three soil behaviour types sand, silt, and clay, observed in our study. This yielded averaged values of the absolute, δSI_{SBT} , and relative, ρSI_{SBT} , change for each soil behaviour type and for each spacing (Sets A1 to A8), respectively. The standard deviation for each average absolute and relative change is calculated using the root mean square rule.

$$\sigma\delta SI_{SBT} \text{ or } \sigma\rho SI_{SBT} = \sqrt{\frac{1}{n}(\sigma SI_1^2 + \sigma SI_2^2 + \dots + \sigma SI_n^2)}, \quad (2.6)$$

Where $\sigma\delta SI_{SBT}$ is the standard deviation for the average absolute change for each soil behaviour type; $\sigma\rho SI_{SBT}$ is the standard deviation for the average relative change for each soil behaviour type; σSI_n is the standard deviation for a relative or absolute change; and n is the number of data points.

2.2.4.3 Parameters for assessing the effect of number of CPTs and CPT spacing on confidence interval.

To answer the question concerning the effect of various number of CPTs on the characterization of cone resistance in the field, the 95% confidence interval and thus the characteristic cone resistance was calculated. The confidence interval represents the lower and upper limit of the mean, and the narrower the confidence interval, the more precise the estimation (Snedecor and Cochran, 1989) The lower bound of the 95% confidence interval is the characteristic value which is used for probabilistic geotechnical designs (Bond et al., 2013). The 33 cone resistance datasets that resulted from the correlation of CPTs were regrouped into six sets named B - set B1 to B6 (Tab. 2.2) – all not affected by the disturbed zone of previous CPTs. These sets have varying number of CPTs from 3 inset B1 to 17 inset B6. The calculation procedure for obtaining statistical parameters for the effect of number of CPTs on the confidence interval of cone

resistance is schematized in the left branch of Fig. 2.6. Numbers in circles indicate steps of the calculation procedure which will be referred to in the following section.

In step 1 The mean was calculated for each of set B1 to B6.

$$q_{c,\mu} = \frac{\sum_i^n q_{c_i}}{n}, \quad (2.7)$$

Where $q_{c,\mu}$ is the mean cone resistance of set Bm ($1 \leq m \leq 6$); q_{c_i} is an individual cone resistance dataset in set Bm. (with $1 \leq i \leq n$) n is the total number of CPTs in set Bm. Afterwards in step 2, the standard deviation $\sigma q_{c,\mu}$ of the mean cone resistance was calculated.

$$\sigma q_{c,\mu} = \sqrt{\frac{\sum_{i=1}^n (q_{c_i} - q_{c,\mu})^2}{n-1}}, \quad (2.8)$$

In step 3, the confidence interval datasets were then calculated from mean and standard deviations of each cone resistance dataset of set B.

$$CI_{\mu} = q_{c,\mu} \pm t \cdot \frac{\sigma q_{c,\mu}}{\sqrt{n}}, \quad (2.9)$$

Where CI_{μ} is the confidence interval of set Bm ($1 \leq m \leq 6$); $q_{c,\mu}$ is the mean cone resistance dataset from set Bm; t is the Student's Coefficient; $\sigma q_{c,\mu}$ is the standard deviation for the mean cone resistance of set Bm.; n is the total number of CPTs in set Bm.

In step 4, the influence of soil behaviour types on confidence intervals was studied. Therefore, the confidence interval datasets for each of set B1 to B6 were averaged with respect to the three soil behavior types, sand, silt, and clay.

In step 5, the effect of CPT spacing on the confidence interval was studied. Therefore, the confidence intervals were calculated from representative cone resistance datasets and the standard deviation of sets A1 – A4. In order to have the confidence interval calculated for same number of CPTs in each of set A1 – A4, test S9 was excluded from set A2 in this step. These sets are chosen since there is no influence of previous CPTs on cone resistance.

$$CI_r = q_{c,r} \pm t \cdot \frac{\sigma q_{c,r}}{\sqrt{n}}, \quad (2.10)$$

Where CI_r is the confidence interval dataset of set Am ($1 \leq m \leq 4$); $q_{c,r}$ is the representative cone resistance dataset from set Am ; t is the Student's Coefficient; $\sigma q_{c,r}$ is the standard deviation for the representative cone resistance of set Am .; n is the total number of CPTs in set Am .

In step 6, the influence of soil behaviour types on confidence intervals was studied. Therefore, the confidence interval datasets for each of set A1 to A4 were averaged for the three soil behavior types, sand, silt, and clay.

2.3. Results

The representative cone resistances for all sets exhibit the same qualitative pattern and are therefore suitable for comparison (Fig. 2.7, appendix Fig. 7.1.1). Since the soil layers of Unit 1 consist of heterogeneous anthropogenic infill materials, the results from this unit will not be considered, hereafter. For soil behaviour types silt and clay (Units 3 and 5), the representative cone resistances are not influenced by the range of spacings considered in this study. Silt and clay layers exhibit generally low cone resistances with low variability. A significant reduction in representative cone resistance is observed for soil behaviour type sand (Units 2 and 4), for which the reduction in representative cone resistance increases as the CPT spacing decreases from set A5 to A8.

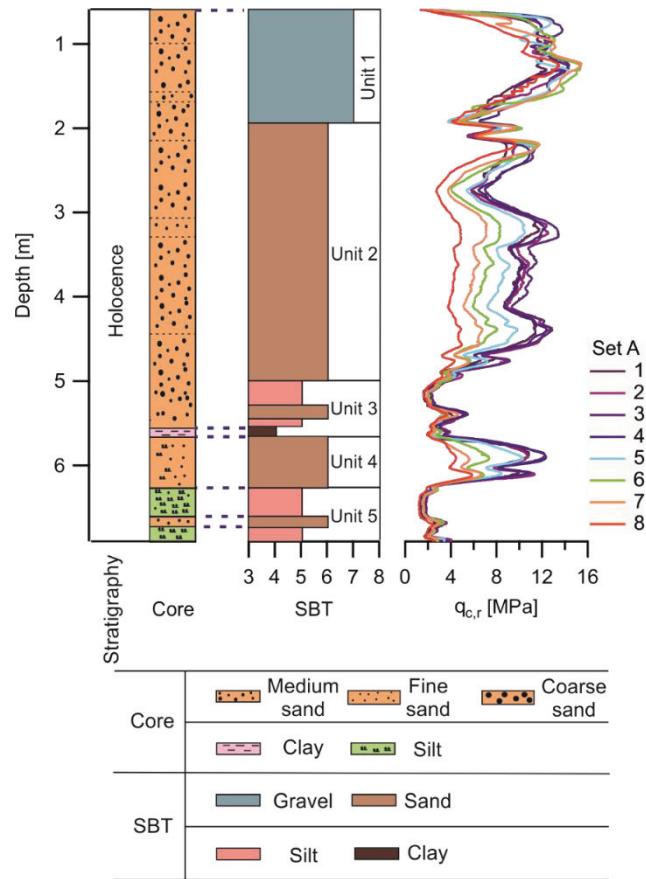


Fig.2.7. Representative cone resistance datasets for CPTs of set A see Table 2.2.

The reduction in representative cone resistance is further analysed in terms of absolute and relative change of representative cone resistance with CPT spacing (Fig. 2.8). The largest relative spacing influence is 75% - corresponding to an absolute spacing influence of more than 5 MPa – and is observed in sand with the closest CPT spacing: set A8, red dashed line in Fig. 2.8. This pronounced spacing influence is not observed for silt and clay layers. On the contrary, in clay and silt, negative absolute spacing influences and relative spacing influences above unity are observed, respectively, which indicates an increase in representative cone resistance towards smaller spacings. The highest increase in representative cone resistance was observed in a clay layer at 5.5 m depth, blue dashed line in Fig. 2.8.

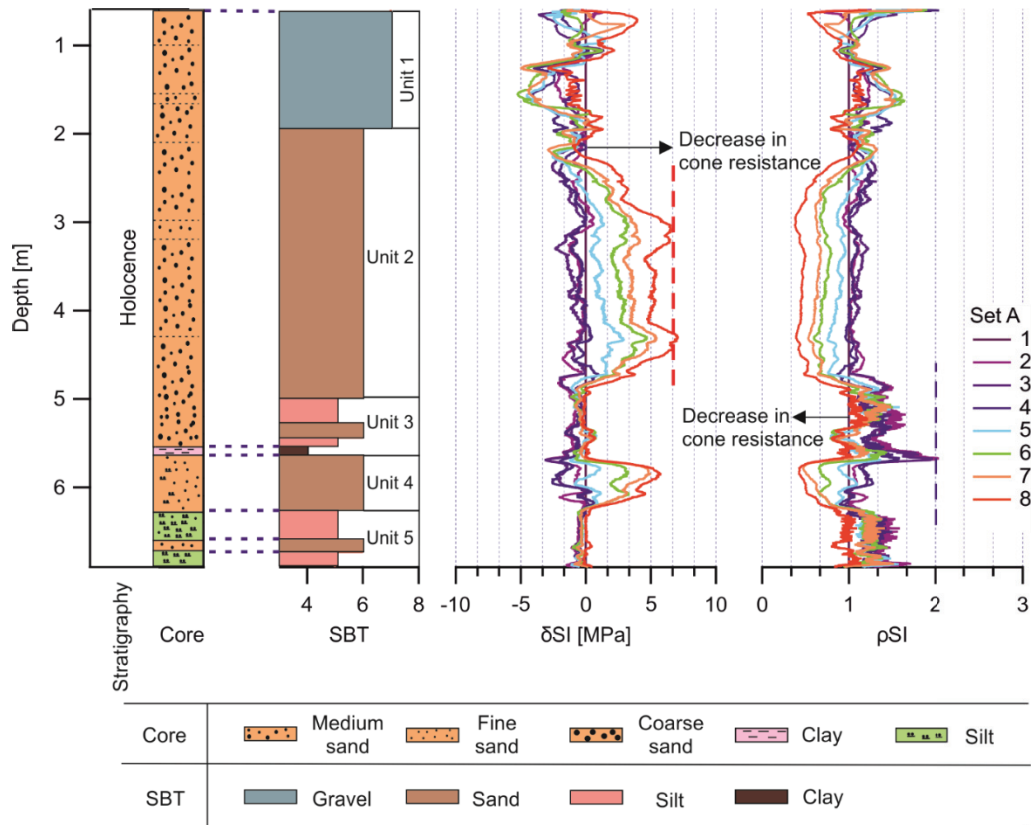


Fig.2.8. Absolute and relative spacing influence in the representative cone resistance datasets.

The effect of soil behavior types on the average spacing influence is shown in Fig. 2.9 and 2.10 where the dashed horizontal lines depict the spacing influence at which no change in the representative cone resistance takes place. At a spacing of 24 cone diameters, the average spacing influence for sand exceeds the no change line. Therefore, a spacing threshold of 24 cone diameters is chosen, below which a reduction in the representative cone resistance occurs in medium dense sand. The error bar of sand crosses the no change line at a spacing of 17 cone diameters, therefore, the spacing threshold could also be argued to be 17 cone diameters (Fig. 2.9 and 2.10). However, as a conservative estimate for unaffected cone resistance we use 24 cone diameters as the spacing threshold.

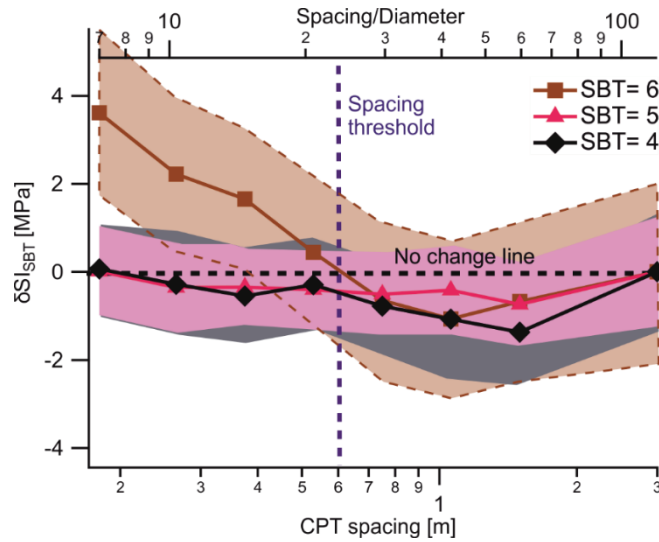


Fig.2.9. Average absolute spacing influence with respect to soil behavior types, the vertical line represents the threshold spacing, the standard deviation is given as colour shading.

For silt and clay, no spacing threshold was observed until the minimum spacing of 7 cone diameters tested in this study. For spacings between 24 and 60 cone diameters, there is an increase in the representative cone resistance for silt and clay which is most prominent for clay. However, the no change line of the representative cone resistance stays within the standard deviation of the observed change.

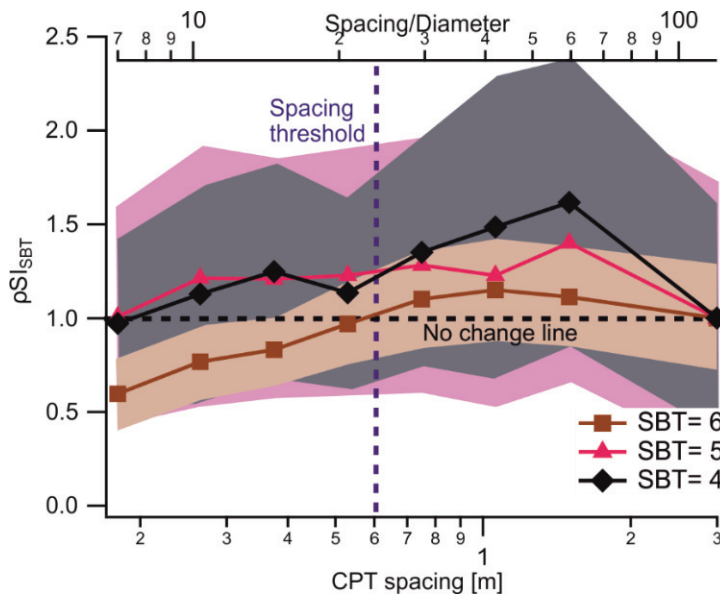


Fig.2.10. Average relative spacing influence with respect to soil behavior types, the vertical line represents the threshold spacing, the standard deviation is given as colour shading.

The confidence interval datasets, which resulted from averaging various numbers of CPTs, show the widest confidence interval for the lowest number CPTs used for averaging (set B1, Tab. 2.2, Fig. 2.11). The confidence interval becomes narrower with increasing the number of CPTs used for averaging, with the narrowest confidence interval for set B6 which consists of 17 CPTs (Fig. 2.11). The effect of averaging various number of CPTs on the confidence interval was further analysed with regard to the soil behaviour types (Fig. 2.12). An increase in average confidence interval was observed when the number of CPTs decreased for all soil behaviour types. For the same number of CPTs the average confidence interval exhibited higher values for soil behaviour type sand than for silt and clay which mean higher uncertainty for sand. When one of the cone resistance datasets has some exceptionally high local changes it may sometimes increase the uncertainty and the confidence interval as it is observed for the silt.

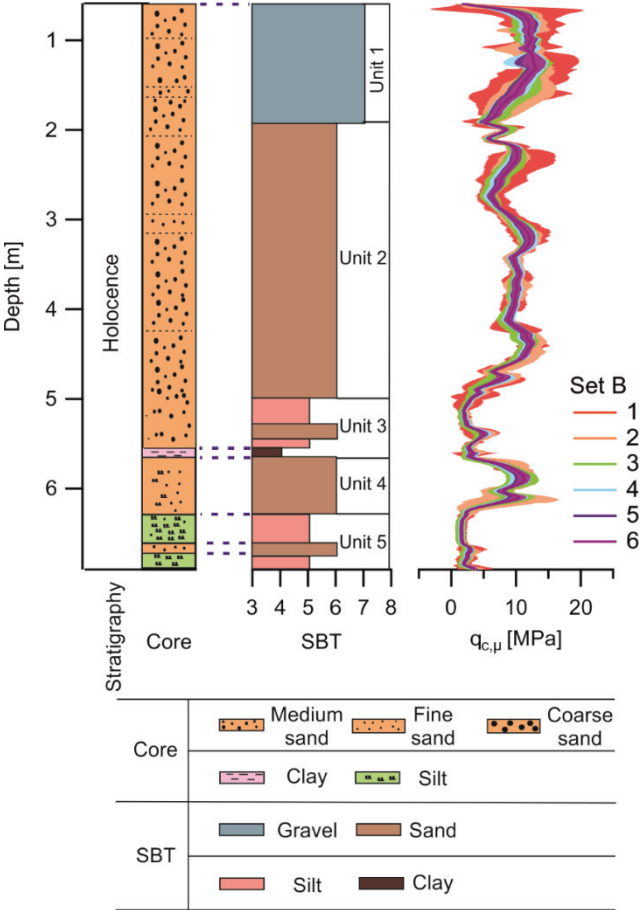


Fig. 2.11. Confidence interval of each mean cone resistance for CPTs of set B (Tab. 2.2).

The effect of soil behaviour types on the average confidence intervals for the same number of CPTs, but at different CPT spacing, is investigated (Fig. 2.13). For all soil behaviour types the average confidence interval decrease with decreasing the CPT spacing. At the same spacing the average confidence interval is higher for sand than for silt and clay. At spacing of 1 m the average confidence interval increases significantly for clay having a value higher than the value at spacing of 3 m.

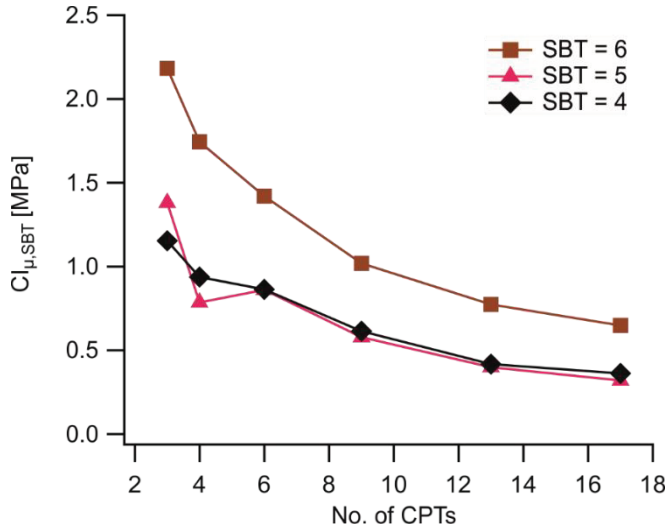


Fig. 2.12. The average confidence interval for various number of averaged CPTs with respect to soil behavior type.

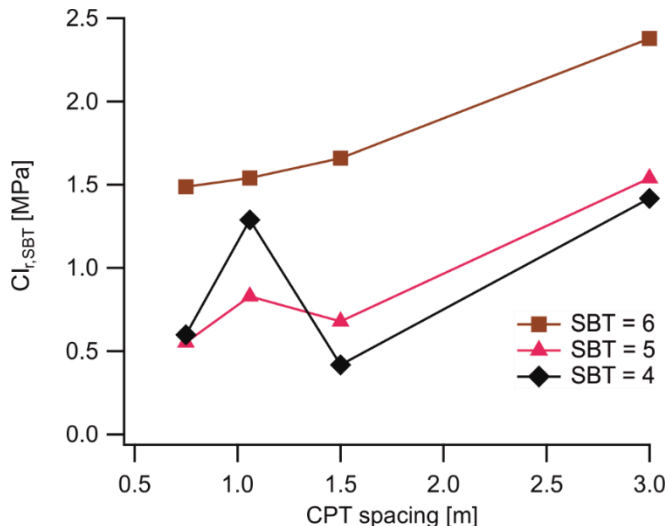


Fig. 2.13. The relative confidence interval for various CPT spacing with respect to soil behavior type.

2.4. Discussion

2.4.1 Spacing threshold

The spacing threshold of 24 cone diameters observed in medium dense sand in this study is smaller than the minimum spacing recommended by the British and German standards (BS 1377-9, 1990, DIN EN ISO 22476-1, 2012), which are 28 and 56 cone diameters, respectively. The spacings recommended by the standards are likely chosen to avoid problems that may arise from the tilting of the CPT rods with increasing penetration depth. As the penetration depth of a CPT increases, increasing tilt may cause the penetration path to cross the path of adjacent CPTs, intersect with the disturbed soil of adjacent CPTs, or causes an overlap between influence zone of a CPT and the disturbed soil zone of adjacent CPTs. In this study, the variation in the depth-dependent spacing between CPTs due to the tilting of rods is smaller than the spacing threshold. Therefore, there is no significant effect of tilting on the spacing threshold (Fig. 2.5).

Below the spacing threshold, a reduction in the cone resistance takes place in sand, which suggests weakening in the disturbed soil zone of previous CPTs. The weakening in the disturbed soil zone may occur during penetration of CPT, because medium dense sands under low effective stresses usually have a negative state parameter, which leads to a dilative and less stiff behaviour of sand in the disturbed soil zone around the cone (Been and Jefferies, 1985). Grain crushing during penetration of CPT could also lead to weakening however the size of the grain crushed zone is small and only affects the region very close to the interface of sand and cone (Yasufuku and Hyde, 1995, White and Bolton, 2004). Additional weakening in the disturbed soil zone probably occurs after removing the probe and the collapse of the CPT hole due to changes in the degree of fabric's anisotropy (Sze and Yang, 2013, Yimsiri and Soga, 2010) and due to loosening in the sand layer. On the other hand, the radial compression around the cone during penetration could cause strengthening in the disturbed soil zone (White&Bolton, 2004, Paniagua et al., 2013). However, the reduction observed in the cone resistance suggests that the amount and the size of weakening in the disturbed soil zone for the sand at our site is larger than the strengthening.

In our study, no change in cone resistance at 7 cone diameters is observed for silt and clay, which indicates that the size or the degree of weakening of the disturbed soil zone is smaller

for silt and clay than for sand. The lack of weakening could be related to the lower propensity for hole collapse in silt and clay than in sand. The propensity for hole collapse is increased in soils with low cohesion and high angle of friction like sand (Gupta and Zaman, 1999, Aadnoy, 1991, Labiouse and Vietor, 2014, Shu and Ma, 2015). The lack of cohesion between sand grains allows them to collapse toward the hole after removing the CPT rods (Hashemi et al., 2014), resulting in a larger and weaker disturbed soil zone. Paniagua et al. (2013) found that in non-plastic unsaturated silt under low overburden pressure a compacted soil zone is formed near the cone surrounded by a dilative zone; the size of these zones combined is equal to 3 cone diameters. A spacing of 3 cone diameters is smaller than the smallest spacing of 7 cone diameters considered in this study, above which no reduction in the cone resistance is observed. A spacing of 3 cone diameters does not represent a safe CPT spacing in silts and clays, since it is not only the size of the disturbed soil zone that effects the safe CPT spacing, but also the influence zone of CPT. The influence zone of CPTs could be larger than 3 cone diameters, therefore an overlap with the disturbed soil zone could occur at larger spacings.

At spacings of 24 to 60 cone diameters, a small increase in the representative cone resistance was observed for all soil behaviour types (Fig. 2.9 and 2.10). This increase could be related to strengthening in the disturbed soil zone of CPT. However, this conclusion is very unlikely, since larger increases are observed for silt and clay than for sand, whereas the disturbed soil zone is smaller in silt and clay. Additionally, the “no change line” is within the error bars for all soil behaviour types for spacings higher than 17 cone diameters. Therefore, this increase is probably related to natural variability of soil properties in the soil layers (Al-Sammarraie et al., 2018, NGI, 2014)

2.4.2 Confidence Interval

It has been stated that the confidence intervals of cone resistance increase with higher variations in soil properties (Bond et al., 2013, Frank et al., 2004). Sand deposits are naturally more variable than silt and clay layers, due to the sedimentary processes during deposition with higher flow velocities (Nichols, 2009) and this matches well with the observation that the average confidence interval for sand is higher than for silt and clay (Fig. 2.12 and 2.13). The smaller average confidence interval for close CPT spacing prove that the correlation of the soil properties decreases with increasing spacing between CPTs (Fig. 2.13). The study is also a practical example of how much certainty can be gained by additional measurements, and this

certainty directly affects the quality of possible relations and correlation with other in-situ datasets.

2.5. Conclusions

A systematically refined grid of cone penetration tests was performed in the field in order to investigate the effect of closely spaced CPTs on cone resistance. A new spacing threshold was defined at which cone resistance starts to be affected by previously performed CPTs. It was found that:

- 1- There is a spacing threshold equal to 24 cone diameters at which a reduction in cone resistance occurs in medium dense sand.
- 2- The observed reduction is related to weakening in the disturbed soil zone of previous CPTs, due to dilative behaviour of soil, changes in the degree of fabric's anisotropy, or to loosening in the sand layer.
- 3- A spacing threshold in silt and clay was not observed in our study, and is probably below 7 cone diameters.
- 4- Increasing the number of CPT datasets leads to a narrower confidence interval and helps to obtain depth-dependent characteristic values of cone resistance.
- 5- CPT spacing and natural variations in soil properties are deciding factors for the number of CPTs in the field to give a sufficient confidence interval.

Acknowledgements

This project was funded by the German Federal Ministry for Economic Affairs and Energy (BMWi), project: Vibro Drucksondierungen, FKZ: 0325906. We thank Marc Huhndorf, Joann Schmid, Wolfgang Schunn, Lukasz Socko, and Thorge Schulz for invaluable technical assistance during field work and construction of the Vibro- CPTu. Matt Ikari is acknowledged for revision of the manuscript.

CHAPTER 3

New vibratory cone penetration device for in-situ measurement of cyclic softening

D. Al-Sammarraie, S. Kreiter, F.T. Stähler, M. Goodarzi, T. Mörz

MARUM-Center for Marine Environmental Sciences, University of Bremen, Bremen, Germany

Published 2018 in Hicks, Pisanò & Peuchen (eds.) Cone penetration testing 2018, CRC Press/Balkema, pp. 591 – 597

ISBN: 978-0-429-50598-0 (eBook)

3. ABSTRACT

A new type of vibratory cone penetration device has been developed to improve the geotechnical in-situ methods for evaluating the dynamic and cyclic properties of the soil. The new device controls displacement amplitudes in real time and is designed to test various cyclic loads that cover different configurations of vibratory pile installation and different magnitudes of earthquakes. Some soil layers reacted strongly to the induced cyclic loads with high reduction ratios RR of the cone resistance, while other layers did not react to cyclic loading. It was also found that even a distance of 50 cm does not guarantee a good correlation between CPT and Vibro-CPTu. Therefore, two or more pairs of CPTs and Vibro-CPTu should be conducted at close distances in order to minimize misinterpretations of the data, which are caused by small scale geological structures, such as the presence of inclined layers, cross bedding, or other heterogeneities.

3.1. Introduction

In recent years there has been an increased interest in using vibratory driving as a method for pile installation, especially for offshore structures where the wellbeing of the sea mammals is of great concern. The method reduces noise and damage to the piles during driving as well as permits fast pile installation (O'Neill et al., 1990). Vibratory pile installation generates vertical

vibrations that impose cyclic loads in the ground which may cause the soil to liquefy (Nagomi et al., 1997). Liquefaction is the loss of soil strength due to an increase in pore water pressure and the resulting loss of shear strength during cyclic loading (Seed & Idriss, 1971). Fluidization is a type of liquefaction where the soil changes from its normal state to a quasi-fluid state under ongoing cyclic loading (Bernhard, 1967). Fluidization is related to the displacement amplitude and frequency of vibration, and it may occur during vibro piling (Rodger & Littlejohn, 1980). The prediction of the soil behavior during vibratory pile installation is uncertain and depends on empirical or combined theoretical and semi-empirical approaches (Nagomi et al., 1997). Nevertheless, there have been some attempts to directly evaluate the soil dynamic behavior and the liquefaction resistance in-situ by utilizing a special type of cone penetration test, the piezovibrocone or Vibro-CPTu, that mechanically induces cyclic loads in the soil while penetrating it (Sasaki & Koga, 1982, Shibata & Teparaksa, 1988). Sasaki and Koga (1982) proposed the reduction ratio RR as an index for soil liquefaction resistance:

$$RR = 1 - \left(\frac{vq_c}{q_c} \right) \quad (3.1)$$

where vq_c is vibratory cone resistance; and q_c is static cone resistance (Sasaki & Koga, 1982). Early Vibro-CPTu devices used horizontal down-hole vibrators without a control of stress or strain (Sasaki & Koga, 1982, Shibata & Teparaksa, 1988, Tokimatsu et al., 1988, Mitchell et al. 1988). However, the applied horizontal loads sometimes led to a gap at the cone-soil interface leading to debatable results. To overcome this gapping problem, vertical down-hole vibrators were used in more recent studies (Wise et al., 1999, McGillivray et al., 2000, Mayne, 2000). The only constant parameter of these vibrators is the energy. However, the variation of the displacement amplitudes with depth and material was not determined. Other recent studies by Jorat et al., (2015) and Kluger et al., (2016) employed the use of distance-controlled method to apply up-hole vertical cyclic loads. Since the cyclic motion of the rod was hydraulically driven up-hole, the actual cyclic movement of the cone may vary with depth. Uncertainties in the applied amplitude lead to uncertainties in the interpretation of the effect of Vibro-CPTu on the cone resistance. For this reason, a new vibro cone system has been developed. The main advantage of the new system is the 500 Hz acceleration measurements in the cone which allow to determine the displacements in-situ. This study presents the first tests of the real time controlled Vibro-CPTu concept. In this paper, we compare the results of three pairs of static

CPTu and Vibro-CPTu tests, performed with two different vertical vibration amplitudes and two different frequencies. The reduction ratios for the cone resistances are calculated, and the values for the actual penetration velocity and amplitudes are presented at different penetration depths.

3.2. Methodology

3.2.1. Vibro Crawler

The vibro crawler has a high-speed hydraulic system controlled in real time with 5 kHz (Fig. 3.1). The controller is compatible with bigger CPT frames - currently under construction. The cone is equipped with an inertial (navigation) system consisting of a 3-axis gyroscope and 3-axis accelerometer sensor working with 500 Hz. The presented tests were displacement controlled by a distance sensor at the hydraulic cylinder. The acceleration data was for this first study only recorded for post processing.

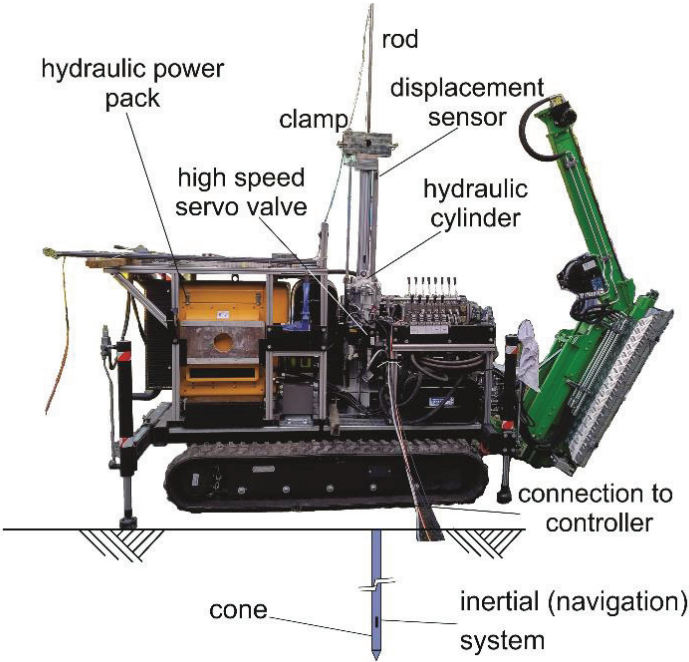


Fig. 3.1. Vibro crawler system.

3.2.2. Test scheme

The test area is located in Bremen, Germany where the soil is mainly composed of dense sands with medium to coarse grains (Fig. 3.2).

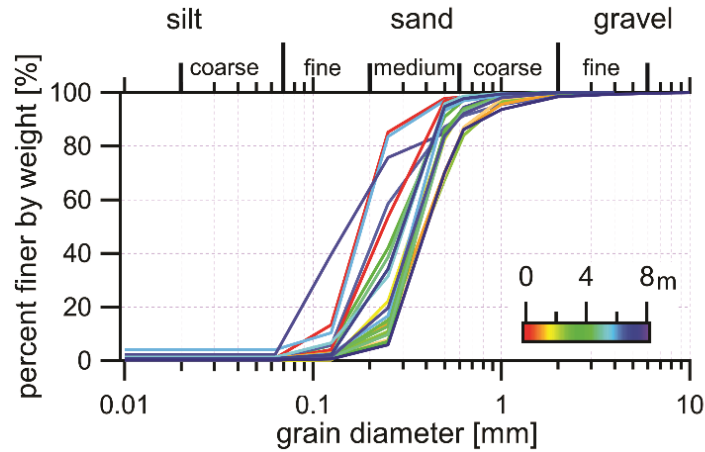


Fig.3.2. Grain size distribution of soil.

Three pairs of static and vibratory cone penetration tests were conducted at three locations spaced 4 m apart. The space between the static CPTu and Vibro-CPTu was 50 cm for P1 and 80 cm for P2 and P3 (Fig. 3.3). The used cone and the rod have a cross sectional area of 5 cm². In static mode, the cone is pushed at a rate of 2 cm/s. In case of vibratory mode, the sinusoidal vibration with different amplitudes is also added to an average velocity of 2 cm/s (Tab. 3.1, Fig. 3.4).

Table 3.1. Test scheme of Vibro-CPTu and static CPTu, where f = frequency; and ϵ_A = displacement amplitude

Type	f [Hz]	ϵ_A [mm]	Location
SCPT*			P1 P2 P3
VCPT*	15	±0.25	P1
VCPT*	10	±0.25	P2
VCPT	10	±0.5	P3

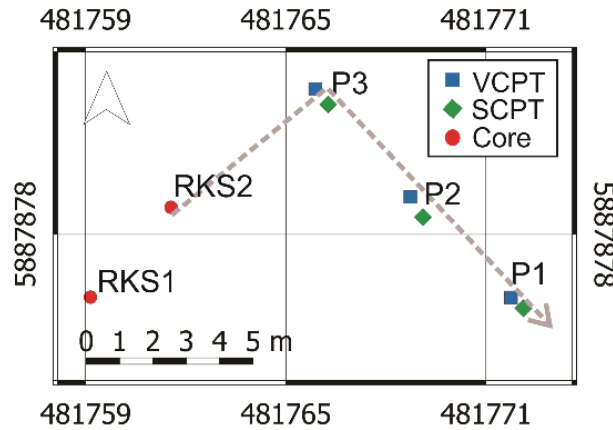


Fig. 3.3. Map of test field using UTM zone 32. The dotted line is the correlation section shown in figure 3.9.

3.2.2.1. Reduction ratio

The reduction ratio RR was calculated using equation (3.1). RR values, where the lateral correlations of two tests were unclear, are omitted. The reasoning is explained in more detail in the discussion.

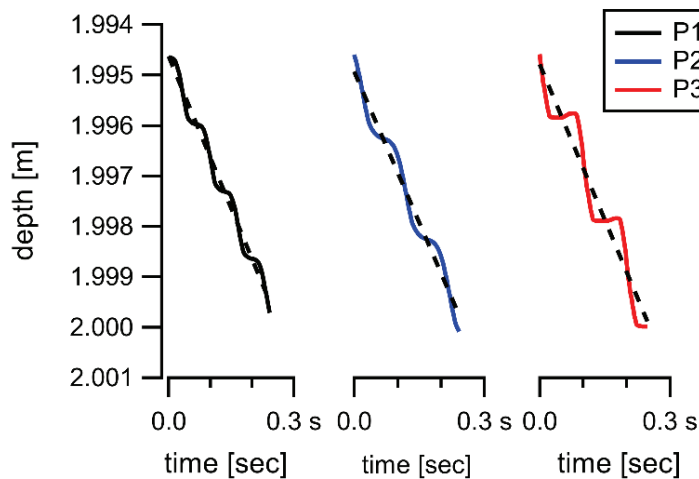


Fig. 3.4. Displacement for the three Vibro-CPTu runs.

3.2.3. In-situ displacement

The acceleration data is used to derive the in-situ displacement amplitude. The displacement amplitude is obtained by double integration of the acceleration. The noise of the raw acceleration data is too high to use it directly (Fig. 3.5). The data is refined by exploiting the

well-defined cyclic character of the vibratory push. The noise is reduced by averaging the result of multiple cycles over a certain depth interval. This requires that the cycles are measured at similar material that is only marginally changing during the rod penetration in this interval. The averaged points have all exactly the same phase in the vibration cycle. We call this “stacking”, following the naming of a similar processing step in reflection seismic.

The technique is also comparable to the working principle of lock-in amplifiers. This stacking is done for three cycles in row, with a stacking factor of 100, so each point in the red curve is the average of 100 raw data points from different depths (Fig. 3.5). The averaged cycles were gathered over a total depth of 0.4 m, and it was established that there is no significant change in the soil behavior over that depth. The refined data is then integrated to get the velocity and displacement. Knowing that the underlying movement is uniform, the average value of the stacked acceleration data was subtracted before integrating the data. The integration constants, initial velocity, and initial displacement were obtained from the differentiated displacement data and the actual displacement data, respectively. For the comparison of the cyclic displacement amplitude, the trend of the uniform movement was subtracted.

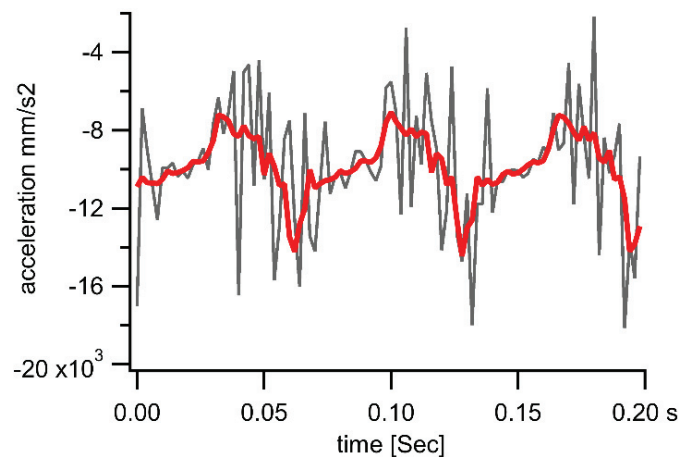


Fig. 3.5. Raw acceleration of the first three cycles in gray and refined acceleration for 100 x 100 stacked data points in red for depth of 2-2.4 m for location P1.

3.3. Results

3.3.1 Vibro cone performance

The Vibro-CPTu system is able to apply an amplitude of ± 0.25 mm until 6 m depth, and there is no significant influence of the penetration depth (Fig. 3.6). The resulted velocities from the acceleration and displacement sensor are shown in Figure 3.7. The velocity derived from the

displacement sensor was equal to 20 mm/s and the resulted velocity from integrating the acceleration sensor had an average value of 20 mm/s at all three tested depths.

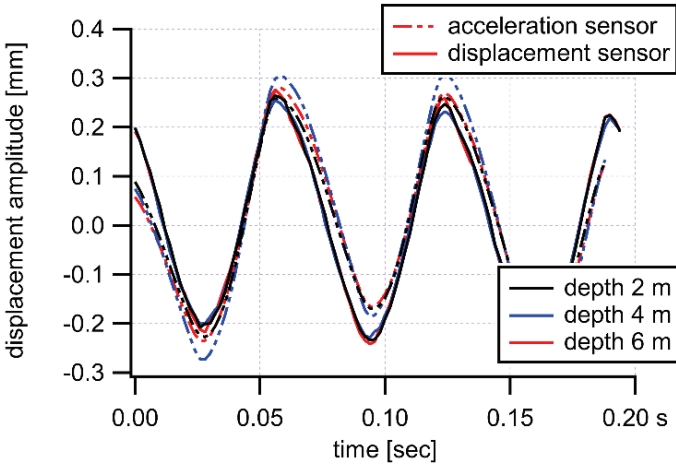


Fig.3.6. Amplitude of vibration at different depths derived from the displacement and acceleration sensors for P1.

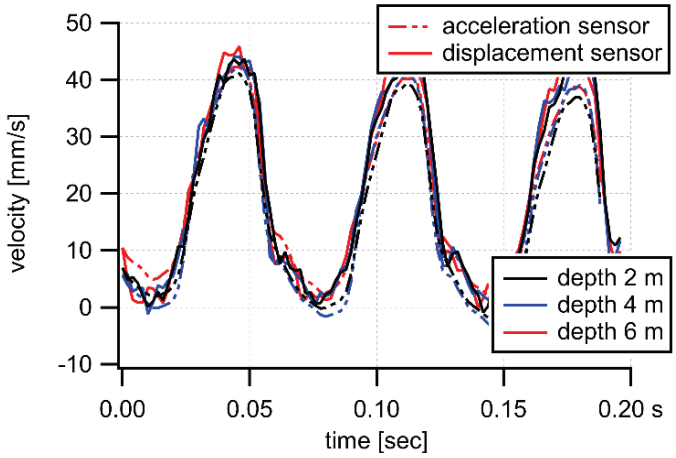


Fig. 3.7. Velocity of vibration at different depths derived from the displacement and acceleration sensors for P1.

3.3.2. Vibro-CPTu results

The soil behavior type SBT has been identified according to Lunne et al. (1997) (Fig. 3.8) and is used for correlating the three SBT profiles with core RKS2 (Fig. 3.9).

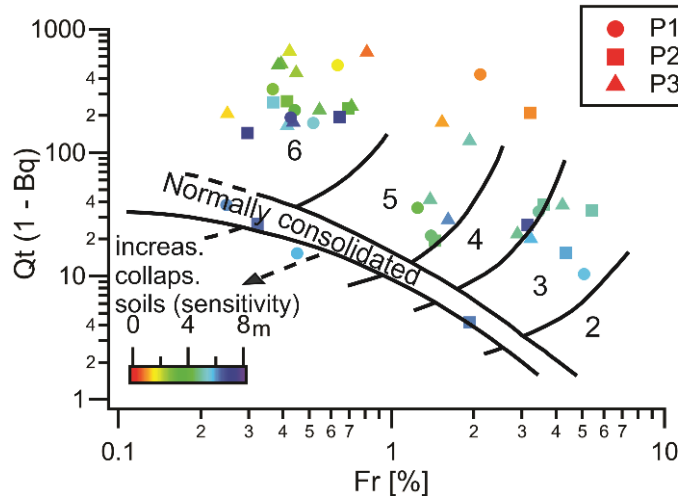


Fig. 3.8. Soil behavior type after Lunne et al. (1997).

In test location P1 there are two layers that suffer from relatively high reduction in the cone resistance. The zones are shadowed in Fig. 3.10 and named Zone 1 and Zone 2. The same zones are also evident for test location P2 in Fig. 3.11. Although the vibration frequency was lower than for P1, the reduction ratio RR values are higher in the soil layers at Zone 1 and 2 (Tab. 3.2). Zone 1 in location P3 has only small RR values although the vibration amplitude was the highest in the study (Fig. 3.12, Tab. 3.2).

At the test locations P2 and P3, there is a layer with high reduction ratios shadowed and named Zone 3, which is not present in location P1.

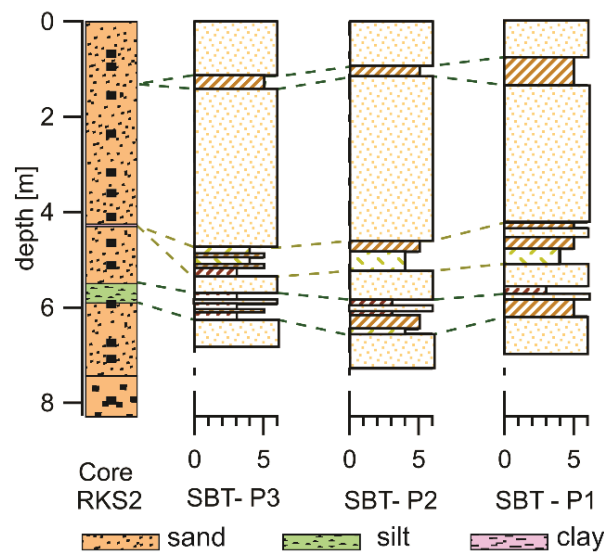


Figure 3.9. Correlation of soil behavior types SBTs after Lunne et al. (1997) with soil profile RKS2. Patterns of SBTs are for visualization purposes only.

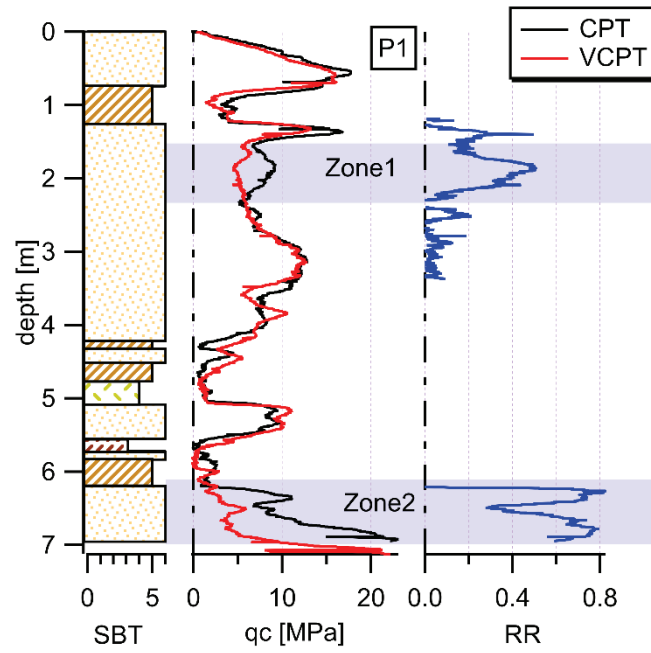


Fig. 3.10. Soil behavior type SBT after Lunne et al. 1997, Cone resistance q_c and reduction ratio RR over depth for location P1.

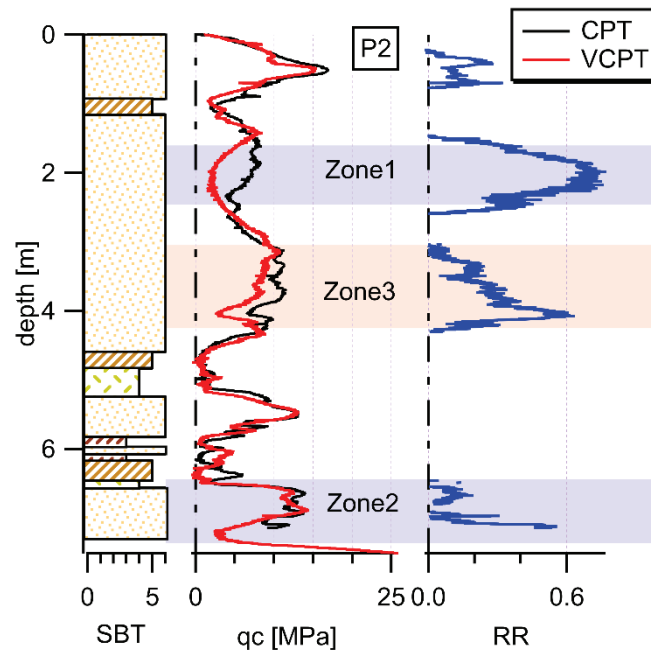


Fig. 3.11. Soil behavior type SBT after Lunne et al. 1997, Cone resistance q_c and reduction ratio RR over depth for location P2.

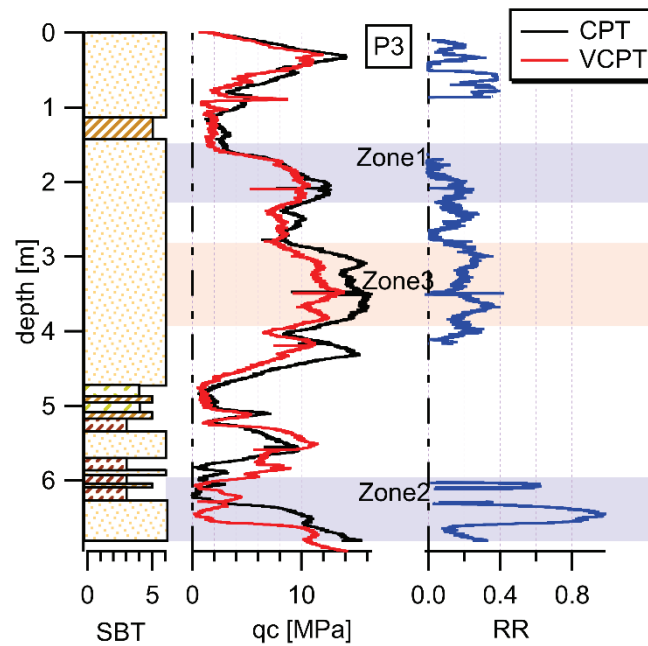


Fig. 3.12. Soil behavior type SBT after Lunne et al. 1997, Cone resistance q_c and reduction ratio RR over depth for location P3.

Table 3.2. Maximum reduction ratio values

<i>Reduction ratio RR</i>			
Location	Zone 1	Zone 2	Zone 3
P1	0.5	0.8	0.1
P2	0.7	0.59	0.6
P3	0.2	0.85	0.3

3.4. Discussion

3.4.1. Vibro cone

The observed results in Fig. 3.6 and 3.7 were unexpected, since it was presumed that the amplitude of the displacement cycles would decrease with increasing the depth of penetration (Kluger et al., 2016, Moore, 1987). This presumption relied on the expected increment of the axial deformation and buckling of the rod as it penetrates deeper in the ground. Therefore, the 6 m depth of penetration was not deep enough to cause big deformation in the rod and thus no

noticeable reduction was observed in the displacement amplitude. The total applied hydraulic force increases as the depth of penetration increases. The amplitude of cycles of the not shown hydraulic force remains surprisingly constant even though it is the displacement which is controlled. However, as the cone penetrates deeper in the soil a loss in the real resulted displacement amplitude is expected, due to rod deformation. The real time controller is designed to compensate for such an amplitude loss in the future and the in-situ acceleration is expected to be a sensitive tool to detect the onset of rod extensive buckling during cyclic loading.

3.4.2. Field tests

Accurate values of the RR rely on Vibro-CPTu and CPTu within the same sediment material. Two closely positioned CPTu profiles should therefore perfectly correlate. One main result of this study is that even a distance of 50 cm does not guarantee a good correlation. This is probably caused by the high energy in the environment during the sedimentation of the sand which led to short range local changes in material and stratigraphy. Those changes include variations in depth and thickness of the same soil layer over very small lateral distances (NGI, 2014). These variations may include inclined sand layers, local absence or presence of certain layers, and internal crossbedding of some layers which may additionally influence the correlation of CPTu and the determination of RR .

Local stratigraphic changes are recognized by similar patterns of two CPTu profiles at a shifted depth. Evidence of those changes is observed for the sand layer at Zone 2 at test locations P1 and P3 (Fig. 3.10 & 3.12). At P1 a local increase in the static cone resistance is observed at 6.3 m which becomes evident at 6.5 m for the Vibro-CPTu. At P3 similar observations are made below 5.9 m depth for the static and vibratory cone resistance. The high values for the reduction ratios observed for these zones are therefore not caused by cyclic loading during Vibro-CPTu, but rather due to miscorrelation of the CPTu data. Such observations are in contrast to Zone 2 in location P2 (Fig. 3.11) where static and Vibro-CPTu show similar patterns without any evidence of shift in depth. This indicates that the values of RR for Zone 2 in P2 are probably accurate, whereas the RR in P1 and P3 may be influenced by the effect of geological structure similar to the effect described in Boulanger et al. (2016).

Good correlations are also observed in Zone 3 at test location P2 and P3 (Fig. 3.11 & 3.12) where the same pattern of CPTu and Vibro-CPTu is evident at the same depth. The considerable reduction in the cone resistance is therefore very likely caused by the cyclic loading of Vibro-CPTu.

The uncertainty of testing the same material leads us to the point that one pair of static and vibratory CPT is in most cases insufficient for accurate conclusions on the soil's cyclic behavior in sands. Two or more pairs of CPTs should be conducted at small distances to allow the distinction between the cyclic soil behavior and local changes in soil state or composition. Small depth shifts in a scenario with high data density will probably allow for even better *RR* results, especially on test sides with inclined layers.

Two pairs of CPTs and Vibro-CPT profiles at P1 and P2 show the same pattern for Zone 1 (Fig. 3.10 & 3.11). A considerable reduction in the cone resistance seems to be apparent at Zone 1 for both P1 and P2. Therefore, it is concluded that the sand layer at Zone 1 is weak against cyclic loading during Vibro-CPTu and has experienced cyclic softening. Nevertheless, only very small reduction in the cone resistance was observed at Zone 1 for the third testing location P3 (Fig. 3.12), although the Vibro-CPTu at P3 used a higher amplitude. This is probably caused by a local change of the sediment material or state that lead to a lower susceptibility to cyclic soil softening of Zone 1 at P3.

3.5. Conclusion

In this study a new tool, the vibro crawler, has been developed to investigate the cyclic behavior of the soil. The new device proved to generate constant amplitudes until the final depth of penetration. Two sand layers reacted to the applied cyclic loads by showing high values of the reduction ratio. It was found that local stratigraphic changes have large effect on the response of CPTu and Vibro-CPTu. One suggested way to minimize their effect is to conduct two or more pairs of CPTu and Vibro-CPTu at small distances. This could help in differentiating between the cyclic soil behavior and local changes in soil composition or state.

Acknowledgment

This project was supported by the Federal Ministry for Economic Affairs and Energy (BMWi), project: Vibro Drucksondierungen, FKZ: 0325906. We thank Marc Huhndorf, Joann Schmid, Wolfgang Schunn and Joshua Albai for invaluable technical assistance during field work and construction of the Vibro-CPTu

CHAPTER 4

Vibratory cone penetration test A new experimental approach to investigate in situ cyclic soil behavior

D. Al-Sammarraie, S. Kreiter, M.O. Kluger, M. Goodarzi, T. Mörz

MARUM-Center for Marine Environmental Sciences, University of Bremen, Bremen, Germany

Submitted 2020 to Géotechnique

4. Abstract

Vibratory pile driving is a fast and gentle technique, and more developers want to use it to install piles for offshore wind projects. One of the main challenges with vibratory pile driving is that there is no accepted method for drivability analysis. This is because the current practices and soil investigation methods are unable to predict the soil's degradation processes along the pile shaft toe and the effect of amplitudes on the cyclic soil behavior during vibratory pile driving. In the present study, the vibratory cone penetration test (VCPT) is introduced as a new in-situ soil investigation method to assess the cyclic soil behavior during vibratory pile driving. VCPT penetrates the ground while inducing controlled vertical cyclic strains and measuring the cone resistance, sleeve friction, and pore water pressure. Nine static CPTs and 15 VCPTs were performed in a systematic grid. The vibratory CPTs were performed at a constant frequency of 20 Hz and at three different amplitudes of 3, 5, and 7 mm. It was found that the degradation of soil resistance to vibratory cone penetration increased with increasing cyclic displacement amplitudes. This degradation was not accompanied by any increase in pore water pressure. Cyclic cone resistance-displacement hysteresis loops indicated the formation of a cavity between the cone and soil during the upward movement of the cone. Furthermore, a distinct difference between the loading and the unloading stiffness during the vibratory penetration was observed. The results demonstrated that there is no unique relation between static and vibratory cone resistance, therefore, current practices that estimate the degradation in soil resistance due to vibratory pile driving from the static cone resistance are probably not sufficient.

4.1. Introduction

Vibratory pile driving is increasingly used in offshore projects as an alternative technique to impact pile driving, because it produces less noise, causes less pile fatigue, allows for easier pile handling, and has a higher installation speed (Holeyman and Whenham, 2017a). One of the main challenges with vibratory pile driving is that there is no acceptable method for the drivability analysis. Until now, the drivability analysis of vibratory pile driving is based on soil-pile interaction models developed for impact driven piles (Jonker, 1987, Wong et al., 1992, van Baars, 2004, Viking, 2006, Holeyman and Whenham, 2017a, Lee et al., 2012). These models are multiplied by degradation factors in order to account for the induced dynamic mobility of soil and the increase in pore water pressure during vibratory pile driving (Wong et al., 1992). These degradation factors are based on analyses of test piles that have been installed by vibratory pile driving technique. In cases where installation of test piles is not practical, degradation factors for vibratory pile driving are very uncertain (Jonker, 1987). In such cases, a soil-pile interaction model is likely unable to predict 1) degradation processes along the pile shaft and pile toe; 2) the effect of different amplitudes of vibratory pile driving on cyclic soil behavior (Jonker, 1987, Holeyman and Whenham, 2017b).

The vibratory cone penetration test (VCPT) is an in-situ soil investigation method which induces cyclic loads during the penetration process (Sasaki and Koga, 1983, Koga et al., 1987, Shibata and Teparaksa, 1988). VCPT was first developed to assess the liquefaction potential in earthquake prone areas in Japan (Sasaki and Koga, 1983). The device used in the studies cited above applied horizontal vibrations, whereas newer studies utilized VCPT with vertical down-hole vibrators (Wise et al., 1999a, McGillivray et al., 2000, Mayne, 2000). The vertical cyclic motion of VCPT resembles the motion of vibratory driven piles (Al-Sammorraie et al., 2018, Stähler et al., 2019, Viking, 2006). VCPT records displacements and cone resistance directly at the cone with high resolution (Al-Sammorraie et al., 2018), enabling the evaluation of cyclic soil parameters for every loading cycle. One important cyclic soil parameter for vibratory pile driving is the stiffness during each individual loading and unloading cycle (Wong et al., 1992, Lee et al., 2012). At high cyclic amplitudes a cavity is formed between pile toe and surrounding soil which influences the soil resistance during vibratory pile driving (Massarsch and Westerberg, 1996, Viking, 2006, Rodger and Littlejohn, 1980). The degree of cavitation during vibratory pile driving is defined as the length of upward and downward movement of the penetrating object without soil contact (Massarsch and Westerberg, 1996, Massarsch et al., 2017, Vogelsang et al., 2017). Until now, the VCPT method was not applied to study the

loading and unloading stiffness as well as the cavitation that may occur during vibratory pile driving. Early VCPT devices did not measure the variation of cyclic displacement amplitudes with depth, thus, the in-situ cyclic soil behavior during VCPT was unknown (Wise et al., 1999b, McGillivary et al., 2000, Mayne, 2000, Jorat et al., 2015, Kluger et al., 2016). Al-Sammarraie et al. (2018) developed a VCPT device that measures acceleration in the cone. The acceleration measurements in the cone allowed to determine the cyclic displacement amplitudes in-situ. However, the displacement amplitudes applied during VCPT were smaller than the ones usually applied during vibratory pile installation.

In the present study, the VCPT device of Al-Sammarraie et al. (2018) is modified to more realistically resemble vibratory pile driving in a very dense natural sand deposit. The testing site is located near Cuxhaven in Northern Germany, having been used for vibratory pile driving tests since 2014 (Gattermann et al., 2015, Quinteros et al., 2018, Goodarzi et al., 2019, Knudsen et al., 2019). VCPTs were performed at three different cyclic displacement amplitudes of 3, 5, and 7 mm, being in the range of the recommended values for vibratory pile driving in dense non-cohesive soils (Rodger and Littlejohn, 1980). The natural variations in soil properties effect the results of CPT and VCPT (Al-Sammarraie et al., under review, 2019). Therefore, repetition tests were performed to minimize the influence of natural soil variation and to increase the statistical significance of the VCPT results. The influence of displacement amplitudes on the degradation of cone resistance was investigated. It was explored to what extent the stiffness during loading and unloading cycles and the cavitation changed with displacement amplitudes. Finally, implications of the present study for civil engineering practice were discussed.

4.2. Materials and Methods

4.2.1 VCPT device

The VCPT device used in the present study consisted of two separate units: a hydraulic power unit and a VCPT unit (right sketch in Fig. 4.1). The hydraulic power unit provided a flow capacity of 300 l/min at a pressure of 200 bar which was required to supply the VCPT unit. The CPT unit was built on a metal frame and consisted, among others, of a 100 kN hydraulic cylinder, a clamp, a valve unit, a displacement sensor, and a real time controller (left sketch in Fig. 4.1). The hydraulic cylinder was operated by the valve unit which consisted of three parallelly connected control valves. The control valves received their control signals from the real time controller which operated at a frequency of 5 kHz.

The hydraulic cylinder was used to push the rods and the cone into the ground. The movement of the rod during CPT and VCPT was controlled by the real time controller which used an external displacement sensor as input variable. The displacement amplitude of VCPT measured from the displacement sensor is referred to as “VCPT amplitude” hereafter. The actual displacement of the cone was obtained from a three-axis acceleration sensor which was implemented in the cone. This acceleration sensor had a sampling rate of $f=500$ Hz (Tab.4.1).

The hydraulic system exhibited a time delay around eight milliseconds which corresponded to 40 calculation cycles. This time delay was caused by the response time between the setting of a value and the response in the displacement sensor. Therefore, a model-based real-time controller approach was adopted.

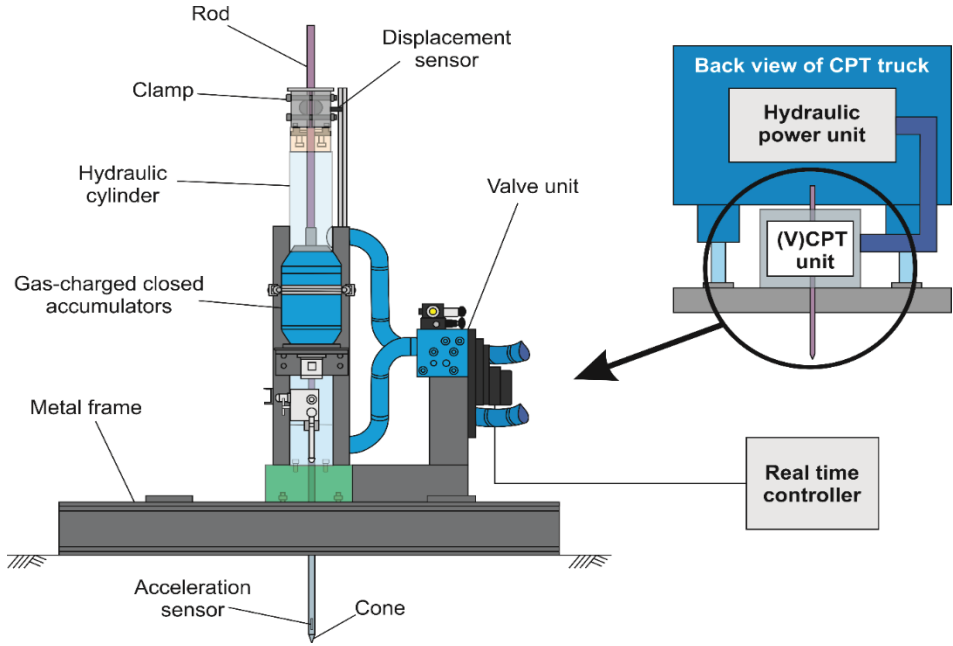


Fig. 4.1. Vibratory cone penetration test device.

Table 4.1. Specifications of the cone used in the present study.

Cone diameter [cm]	Cone area [cm ²]	Resolution [Hz]			
		Cone	Sleeve	Pressure	Acceleration
2.52	5	125	125	125	500

4.2.2 Geological and geotechnical setting

The study area is located in Cuxhaven, Northern Germany (Fig. 4.2). Three glacial periods, Elsterian, Saalian and Weichselian, formed the test field, being located in the “Altenwalder Geest” moraine (Sindowski, 1965, Ehlers et al., 1984, Goodarzi et al., 2019, Ehlers, 1990).

A drill core from the vicinity of the test field (Fig. 4.3) was used to determine stratigraphic units and physical properties of the upper twelve meters of the sand deposits. The stratigraphic characterization followed (Sindowski, 1965, Ehlers et al., 1984, Geo-Engineering, 2014) (Fig. 4.4), grain size analyses were carried out according to DIN 18123 (2011), and the unit weight was provided from Geo-Engineering (2014).

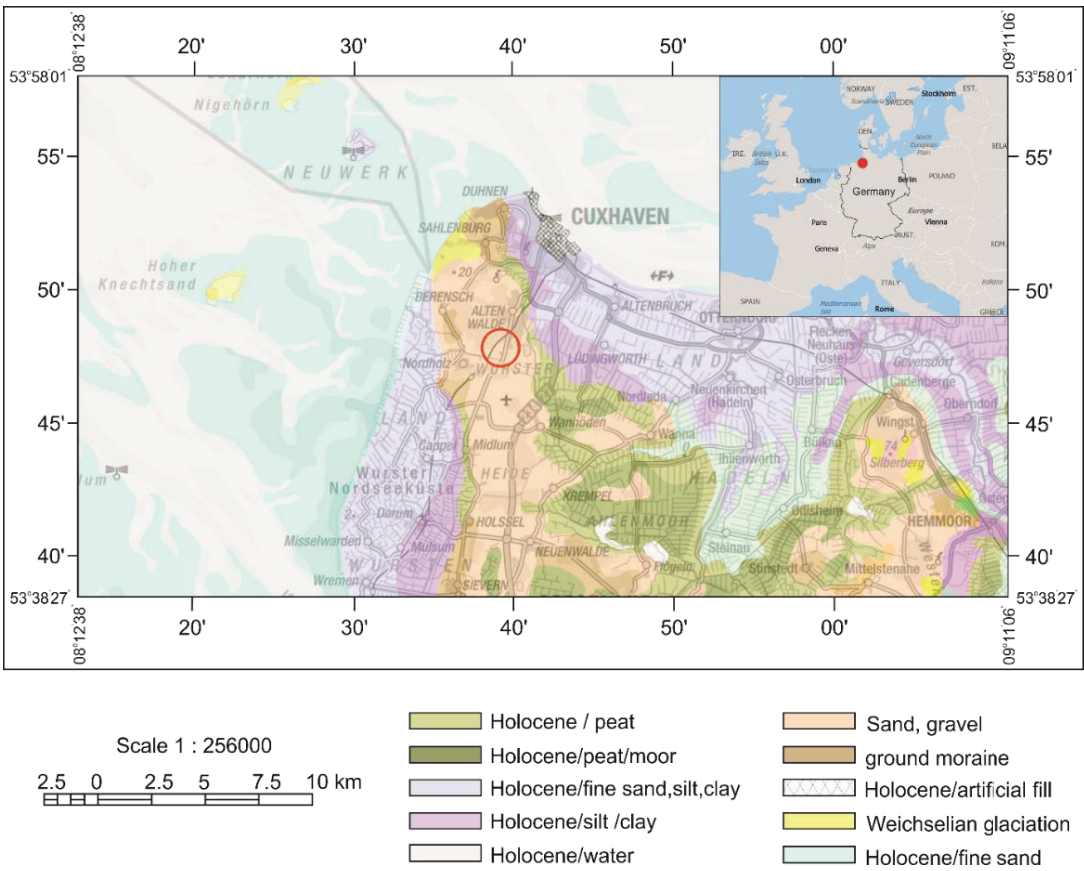


Fig. 4.2. Geological map of Cuxhaven, North Germany, indicating the location of the test site (NIBIS, 2014).

The deposits are of Pleistocene age and were subdivided into a 4-m-thick middle Saalian unit (U1 and U2) and an underlying 7-m-thick older Saalian unit (U3–U5) (Fig. 4.4). The first two units (U1 and U2) consist of fine- to medium-grained glacio-fluviatile sands that were probably deposited in a sandur environment. The third unit (U3) is a 60-cm-thick till layer, composed of grains from clay to gravel size. The till layer was probably formed during the Drenthe II ice

advance (Hepp pers. comm. 2020). The till layer is underlain by U4 and U5 which are composed of compacted heterogenic stratified sand deposits. The sand layers of U4 and U5 exhibit discontinuous thicknesses due to deposition and erosion in a proximal glacio-fluviatile environment (Ehlers et al., 1984, Quinteros et al., 2018, Ehlers, 1990). The soil behavior types were calculated following Robertson (2009) from CPT S7 (Fig. 4.3). Most of the sand deposits are soil behavior type 6 (sand like). Only the till layer (U3) is soil behavior type 3 and 4 (clay-like, silt-like). The sand deposits have relative densities between dense to very dense following the CPT correlation of Baldi et al. (1986).

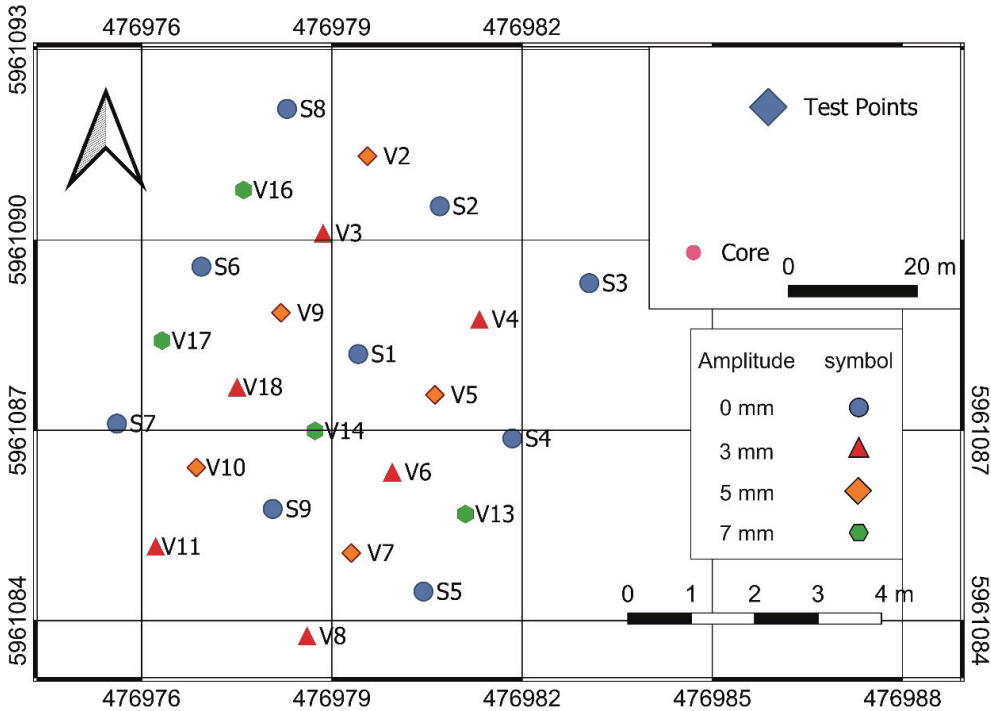


Fig. 4.3. Maps of the layout of test points and the location of the core. The coordinate system used to create the maps was UTM zone N32.

4.2.3 Experimental layout

A cone with an area of 5 cm² (Tab. 4.1) was used to perform nine static CPTs (SCPTs hereafter) and 15 vibratory CPTs (VCPTs hereafter) in a systematic grid (Tab. 4.2, Fig. 4.3). The spacing between tests was chosen to be 1.4 m, being equivalent to 55 times cone diameter. The spacing was chosen to be larger than the minimum recommended distance between CPTs (DIN EN ISO

22476-1, 2012, BS 1377-9, 1990, Al-Sammarraie et al., under review, 2019). The SCPTs were performed before the VCPTs. The VCPTs were performed at a constant frequency of $f=20$ Hz and at three different VCPT amplitudes of 3, 5, and 7 mm (Tab. 4.2, Fig. 4.3). The CPT locations were determined by a DGPS system with a horizontal resolution of ± 2 cm. A theodolite with an accuracy of ± 0.3 cm was used to ensure a common height reference at the start and the end of each CPT.

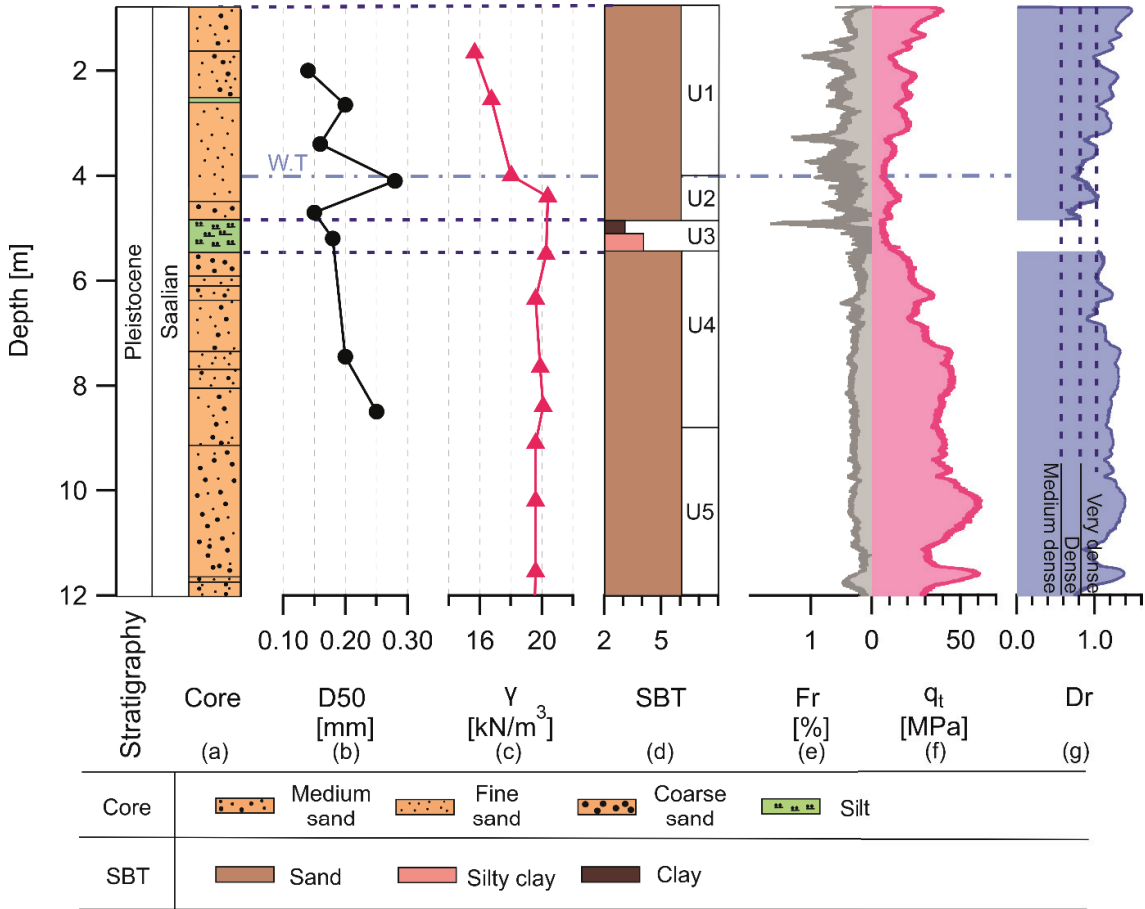


Fig. 4.4. Stratigraphy and soil properties of test site (a) core; (b) grain size distribution (Geo-Engineering, 2014); (c) bulk unit weight (Geo-Engineering, 2014); (d) soil behavior types (SBT); (e) friction ratio; (f) corrected tip resistance; and (g) relative density derived after Baldi et al. (1986).

Table 4.2. Location of test points and parameters considered for VCPT.

Test	Date	UTM WGS84		Amplitude mm	Frequency Hz
		X	Y		
S1	18.06.2019	476979.4155	5961088.203	0	0
S2	19.06.2019	476980.702	5961090.532	0	0
S3	19.06.2019	476983.0597	5961089.32	0	0
S4	19.06.2019	476981.8453	5961086.873	0	0
S5	24.06.2019	476980.444	5961084.459	0	0
S6	25.06.2019	476976.9426	5961089.58	0	0
S7	25.06.2019	476975.6109	5961087.105	0	0
S8	25.06.2019	476978.2926	5961092.067	0	0
S9	25.06.2019	476978.067	5961085.761	0	0
V1	26.06.2019	-	-	-	-
V2	26.06.2019	476979.5607	5961091.322	5	20
V3	26.06.2019	476978.8621	5961090.108	3	20
V4	01.07.2019	476981.3266	5961088.748	3	20
V5	01.07.2019	476980.6244	5961087.559	5	20
V6	02.07.2019	476979.9525	5961086.342	3	20
V7	02.07.2019	476979.3055	5961085.066	5	20
V8	02.07.2019	476978.6083	5961083.76	3	20
V9	02.07.2019	476978.1979	5961088.853	5	20
V10	02.07.2019	476976.8629	5961086.414	5	20
V11	03.07.2019	476976.2215	5961085.17	3	20
V12	03.07.2019	-	-	-	-
V13	03.07.2019	476981.1071	5961085.681	7	20
V14	04.07.2019	476978.7349	5961086.991	7	20
V15	04.07.2019	-	-	-	-
V16	04.07.2019	476977.6097	5961090.788	7	20
V17	04.07.2019	476976.3226	5961088.414	7	20
V18	04.07.2019	476977.5052	5961087.682	3	20

4.2.4 Evaluation of SCPT and VCPTs datasets

The evaluation procedure was divided into three main phases (Fig. 4.5):

1. Correlation;
2. Cyclic behavior analyses;
3. Statistics.

Numbers from 1 to 12 were added to the boxes in Fig. 4.5, which represent the steps of the evaluation process.

4.2.4.1 Correlation

Step 1: SCPT and VCPT datasets were pre-processed (Fig. 4.5, Tab. 4.3). The recorded acceleration data was delayed by 0.6 seconds to the displacement sensor on the hydraulic frame. Therefore, the time information of the VCPT datasets were shifted in order to match the recorded time of the displacement sensor. Afterwards, the SCPT and VCPT datasets were resampled using a moving average filter. The interval of data points used for the moving average filter were 13 and 5 for the SCPT and VCPT datasets, respectively.

Step 2: For the entire VCPT datasets, the peak values of each individual cycle were selected. The resulting VCPT datasets were defined as peak vibratory cone resistance, $vq_{c,p}$, peak sleeve friction, $vf_{s,p}$, and peak pore water pressure, vu_p . These three parameters are jointly referred to as peak VCPT datasets, hereafter. The vibratory cone resistance datasets that included the full information about each cycle is hereafter referred to as vibratory cone resistance cycles, $vq_{c,cy}$.

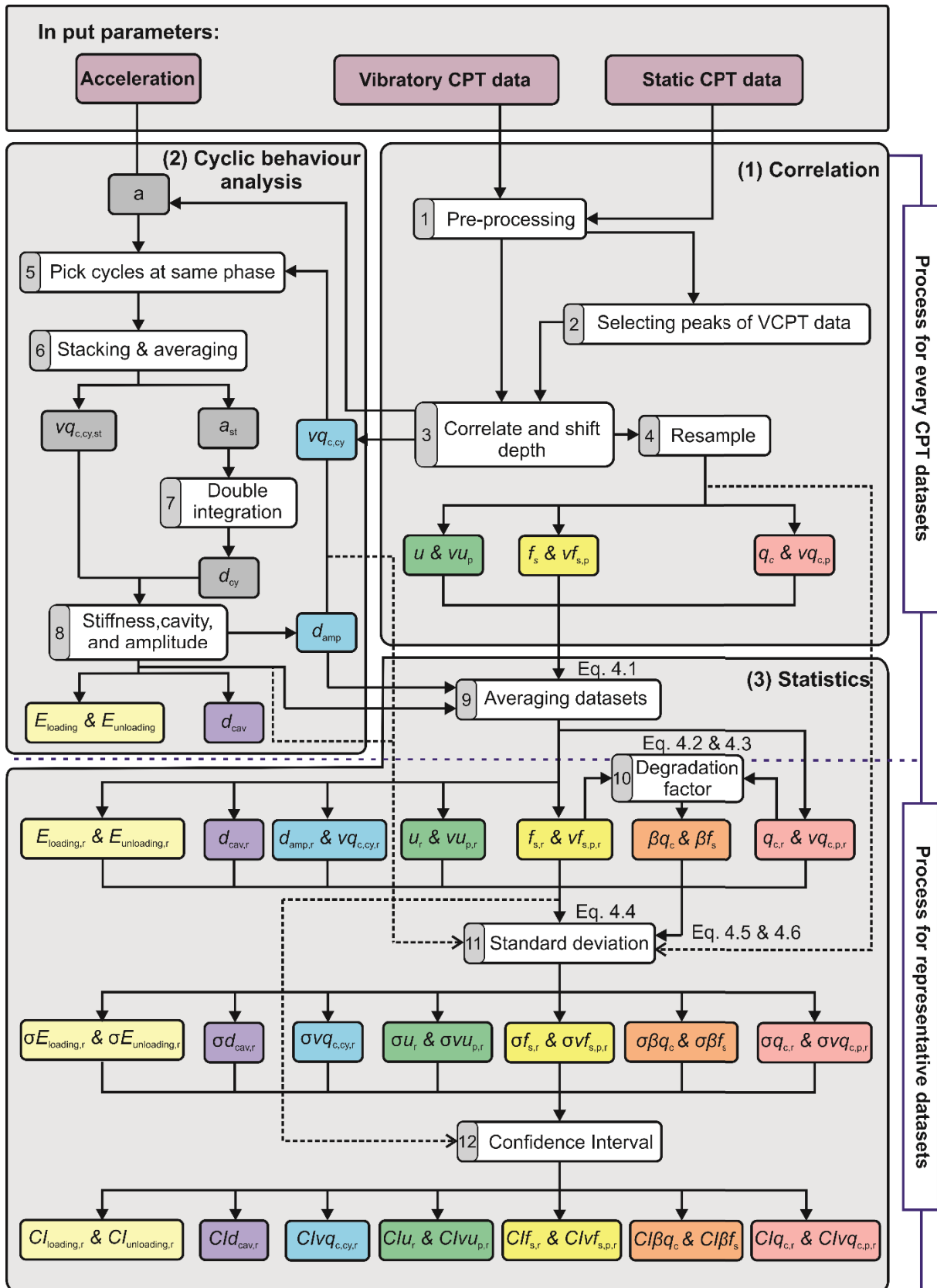


Fig. 4.5. Procedure of SCPT and VCPT data processing. See text for further explanations.

Table. 4.3. Datasets measured from SCPT and VCPT.

CPT	Datasets	
SCPT	Cone resistance	q_c
	Sleeve friction	f_s
	Pore water pressure	u
VCPT	Vibratory cone resistance	vq_c
	Vibratory sleeve friction	vf_s
	Vibratory pore water pressure	vu
	Acceleration	a

Step 3: Because of local heterogeneities in the sand deposits and the changes in depth of specific soil layers within small horizontal distances, all SCPT and VCPT datasets were correlated and shifted to a common depth. The SCPT S7 dataset was taken as “reference dataset” to which all other SCPT and VCPT datasets were correlated. The correlation process consisted of the following steps. (a) Stratigraphic units were defined for the reference SCPT by considering changes in soil behaviour types, relative density, and cone resistance. (b) Correlation tie points were selected between the nine static cone resistance datasets, q_c . The correlation tie points were defined based on distinctive stratigraphic boundaries and through local minima in the static cone resistance datasets. For VCPT datasets local minima were not always recognisable. Therefore, the correlation tie points of VCPT datasets and thus of vibratory cone resistance cycles were based on linear interpolation between neighbouring SCPT datasets. (c) The depths of tie points of all SCPTs and peak VCPT datasets were shifted to the depth of the reference SCPT. The depth increments between the tie points were increased or decreased using linear interpolation between the two adjacent tie points.

Step 4: After the depth shift, the depths of the SCPT and peak VCPT datasets were resampled to a common vertical depth scale with an increment of 0.5 mm. The depth of the vibratory cone resistance cycles, $vq_{c,cy}$ was not resampled, because the shape of each individual cycle was required for subsequent processing steps.

4.2.4.2 Cyclic behaviour analysis

The objective of the cyclic behaviour analysis phase is to quantify the loading stiffness $E_{loading}$, and unloading stiffness, $E_{unloading}$, as well as the upward displacement with cavitation, d_{cav} , for each individual VCPT cycle. The stiffnesses were calculated using both the cyclic displacement, d_{cy} , of the cone during VCPT as well as the cone resistance cycles, $vq_{c,cy}$. The cyclic displacement was calculated from acceleration data which was continuously recorded in the cone during VCPT. The raw acceleration, a , and the raw vibratory cone resistance cycles datasets, $vq_{c,cy}$, exhibited noise due to the large amplitudes and frequency used in the present study. Therefore, the quality of both datasets was improved during steps 5 and 6 as follows.

Step 5: The correlated and shifted datasets of vibratory cone resistance and raw acceleration were divided into sub-datasets. Each sub-dataset consisted of three consecutive cycles (“triple cycle” hereafter) with a total length of $3 \cdot 2\pi$ (Fig. 4.6(a) and 4.6(c)).

The starting and endpoints of the triple cycles were based on the control signal of the real-time controller of the VCPT device. The control signal that controlled the displacement of the rod had a sinusoidal shape. Therefore, the starting point of the triple cycles at a phase of 0π was where the control signal for cyclic displacement crossed zero. A triple cycle was selected for every centimetre depth (“selected triple cycle” hereafter).

Step 6: The selected triple cycles of cone resistance cycles, $vq_{c,cy}$, and raw acceleration, a , were stacked and averaged in order to reduce the noise level. The stacking process is schematized in Fig. 4.6(b). Each of the rectangles in the plot represent one triple cycle. The average vertical displacement of a triple cycle was 0.3 mm. Dark shaded rectangles indicate the selected triple cycles of cone resistance cycles, $vq_{c,cy}$, and acceleration, a , which were selected at every centimetre depth. The purple shaded rectangles represent neighbouring triple cycles in the cone resistance cycles, $vq_{c,cy}$, dataset. The pink shaded sections represent neighbouring triple cycles in the raw acceleration, a , dataset. All data points of the selected triple cycle were added to the equivalent points of the neighbouring cycles and divided by the number of triple cycles. This approach is similar to a moving average where the points are overlaid in

phase. For cone resistance cycles every point is the average of 5 points and for the raw acceleration triple cycles each point is the average of 41 points. The moving average windows corresponded to vertical displacements of 1.5 and 12.3 cm, for the cone resistance cycles and acceleration datasets respectively. The improvement in data quality is visualized in Figs. 4.6(a) and 4.6(c). The thick lines represent the selected triple cycle, which was stacked and averaged by neighbouring triple cycles (thin lines). The stacking and averaging process resulted in stacked cone resistance cycles, $vq_{c,cy,st}$, and stacked acceleration, a_{st} .

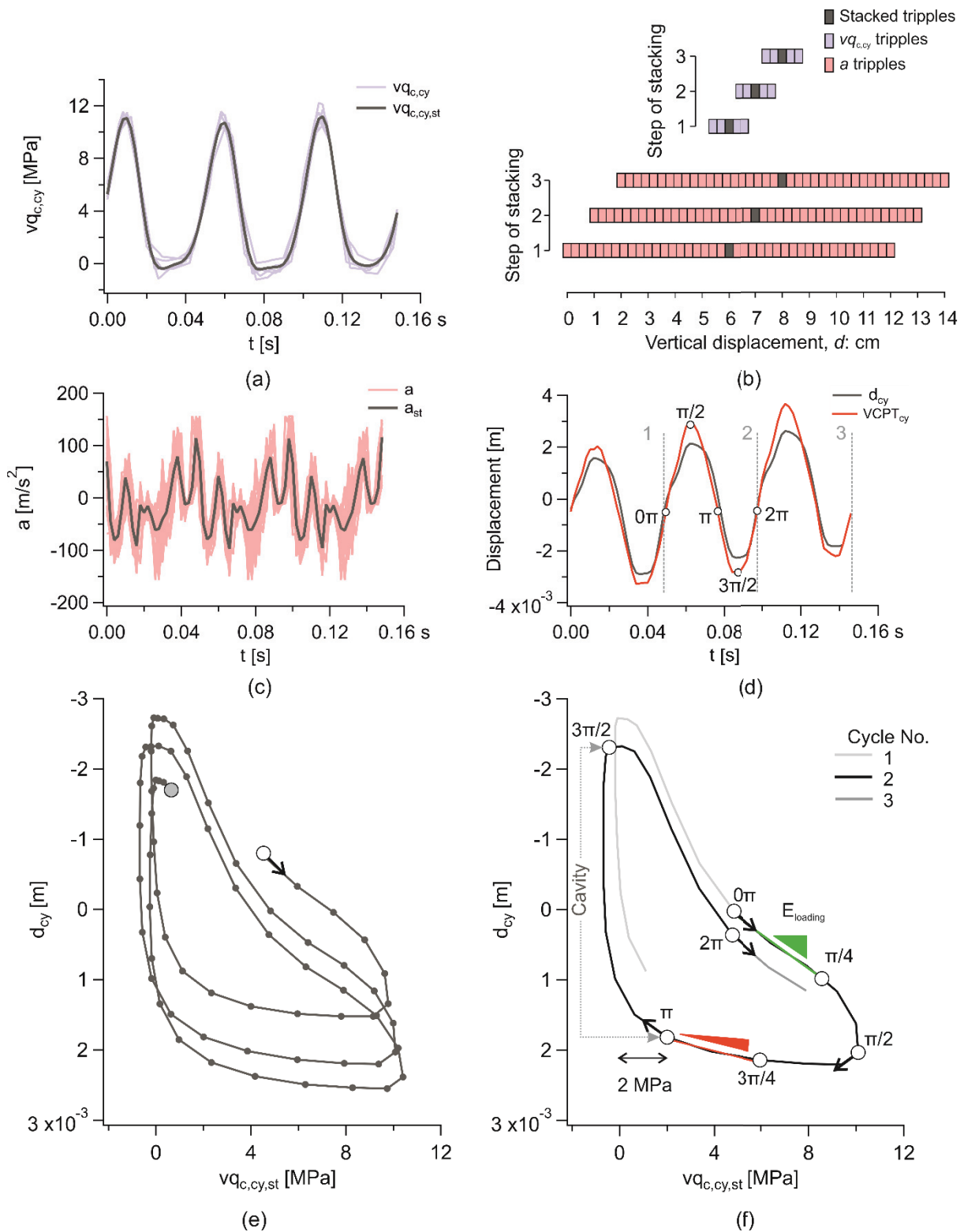


Fig. 4.6. Stacking and stiffness calculation procedure for test V4 depth of 7 m: (a) Stacked and neighboring cone resistance triple cycles; (b) stacking process of the triple cycles; (c) stacked and neighboring acceleration triple cycles; (d) cyclic displacement obtained from acceleration sensor and from displacement sensor, respectively; (e) example of stacked cone resistance – displacement hysteresis loops; (f) procedure to determine loading stiffness, unloading stiffness and upward displacement with cavitation

Step 7: The stacked acceleration data, a_{st} , was integrated twice to obtain the cyclic displacement, d_{cy} (Fig. 4.6(d)). The stacked cone resistance cycles, $vq_{c,cy,st}$, were then plotted against the cyclic displacement, d_{cy} , in order to obtain hysteresis loops (Fig. 4.6(e)).

Step 8: The hysteresis loop of the second cycle was selected for the determination of loading and unloading stiffnesses as well as the upward displacement with cavitation (Fig. 4.6(f)). The hysteresis loop of the second cycle begins at a sinus phase 0π and consists of a linear and nonlinear part until it reaches the highest cone resistance at $\frac{\pi}{2}$. The cone resistance decreases between $\frac{\pi}{2}$ and $\frac{3\pi}{2}$, commonly having a linear decrease between $\frac{3\pi}{4}$ and π and a nonlinear decrease between π and $\frac{3\pi}{2}$. The loading stiffness was calculated by fitting a line to the linear loading part between 0π and $\frac{\pi}{4}$ (Fig. 4.6(f)). The unloading stiffness was determined from the slope of the linear decrease in cone resistance between $\frac{3\pi}{4}$ and π (Fig. 4.6(f)). The upward displacement with cavitation, d_{cav} , was defined as the cyclic displacement between the point where the cone resistance decreased below 2 MPa and the end of the upward movement at $\frac{3\pi}{2}$. The displacement amplitude, d_{amp} , was determined as half the difference between the local maxima and local minima of displacement cycle, d_{cy} . The steps performed in the stiffness phase resulted in datasets of loading stiffness, $E_{loading}$, and unloading stiffness, $E_{unloading}$, upward displacement with cavitation, d_{cav} , and the displacement amplitude, d_{amp} , with a vertical resolution of one centimeter.

Table. 4.4. Individual and representative datasets for SCPT and VCPT

CPT	Datasets	Individual datasets X_i	Representative datasets X_r
SCPT	Cone resistance	q_c	$q_{c,r}$
	Sleeve friction	f_s	$f_{s,r}$
	Pore water pressure	u	u_r
VCPT	Peak vibratory cone resistance	$vq_{c,p}$	$vq_{c,p,r}$
	Peak vibratory sleeve friction	$vf_{s,p}$	$vf_{s,p,r}$

CPT	Datasets	Individual datasets X_i	Representative datasets X_r
	Peak vibratory pore water pressure	vu_p	$vu_{p,r}$
	Cone resistance cycles	$vq_{c,cyc}$	$vq_{c,cyc,r}$
	Displacement amplitude	d_{amp}	$d_{amp,r}$
	Loading stiffness	$E_{loading}$	$E_{loading,r}$
	Unloading stiffness	$E_{unloading}$	$E_{unloading,r}$
	Upward displacement with cavitation	d_{cav}	$d_{cav,r}$

4.2.4.3 Statistics

In the statistics phase, representative datasets were calculated by averaging the resulting datasets from different sites in the systematic grid (Fig. 4.3, Tab. 4.2).

Step 9: The datasets of the SCPT and VCPT that had the same VCPT amplitude, were averaged using Eq 4.1. It was made sure that cone resistance cycles datasets $vq_{c,cy}$ were averaged at the same phase of the penetration cycle.

$$X_r = \frac{\sum_{i=1}^n X_i}{n} \quad (4.1)$$

Where X_r is the representative dataset; X_i is an individual dataset of the datasets show in Tab. 4.4; n is the total number of CPTs, with $1 \leq i \leq n$. It is important to note that the cone resistance cycles datasets are used in the unstacked versions but with the displacement amplitudes from the acceleration data that were stacked and integrated twice (Tab. 4.4).

Step 10: The degradation factor of representative cone resistance was determined from the representative static cone resistances and the representative vibratory cone resistances (Eq. 4.2) in order to investigate whether or not the changes in VCPT amplitude affect the cone resistance.

$$\beta q_c = \frac{vq_{c,p,r}}{q_{c,r}} \quad (4.2)$$

Where βq_c is the degradation factor of representative cone resistance; $vq_{c,p,r}$ is the representative peak vibratory cone resistance; and $q_{c,r}$ is the representative static cone resistance. The degradation factor of representative sleeve friction was calculated (Eq. 4.3).

$$\beta f_s = \frac{vf_{s,p,r}}{f_{s,r}} \quad (4.3)$$

Where βf_s is the degradation factor of representative sleeve friction; $vf_{s,p,r}$ is the representative peak vibratory sleeve friction; and $f_{s,r}$ is the representative static sleeve friction. Degradation factors with values near zero represent high reduction, whereas values close to one represent small reduction in the representative cone resistances and sleeve frictions due to VCPT.

Step 11: The standard deviation was calculated for the representative datasets and the degradation factors. For the representative datasets in Tab. 4.4 the standard deviation was calculated using Eq. 4.4.

$$\sigma X_r = \sqrt{\frac{\sum_{i=1}^n (X_r - X_i)^2}{n-1}} \quad (4.4)$$

Where σX_r is standard deviation of the representative datasets X_r ; X_i is an individual dataset of the datasets show in Tab. 4.4; n is the total number of CPTs, with $1 \leq i \leq n$. The standard deviation for the degradation factor of representative cone resistance and sleeve friction was calculated using the propagation of uncertainty rule (Taylor, 1982, Morgan and Henrion, 1990) (Eq. 4.5).

$$\sigma \beta q_c = \sum \frac{\partial \beta q_c}{\partial vq_{c,p,r}} * (\sigma vq_{c,p,r})^2 + \sum \frac{\partial \beta q_c}{\partial q_{c,r}} * (\sigma q_{c,r})^2 \quad (4.5)$$

Where $\sigma\beta q_c$ is the standard deviation of degradation factor of representative cone resistance; $\sigma vq_{c,p,r}$ is the standard deviation of $vq_{c,p,r}$; $vq_{c,p,r}$ is the representative peak vibratory cone resistance; $\sigma q_{c,r}$ is the standard deviation of $q_{c,r}$; and $q_{c,r}$ is the representative static cone resistance. The standard deviation of the degradation factor of representative sleeve friction was also calculated:

$$\sigma\beta f_s = \sum \frac{\partial\beta f_s}{\partial v f_{s,p,r}} * (\sigma v f_{s,p,r})^2 + \sum \frac{\partial\beta f_s}{\partial f_{s,r}} * (\sigma f_{s,r})^2 \quad (4.6)$$

Where $\sigma\beta f_s$ is the standard deviation of degradation factor of representative sleeve friction; $\sigma v f_{s,p,r}$ is the standard deviation of $v f_{s,p,r}$; $v f_{s,p,r}$ is the representative peak vibratory sleeve friction; $\sigma f_{s,r}$ is the standard deviation of $f_{s,r}$; and $f_{s,r}$ is the representative static sleeve friction.

Step 12: To assess the effect of inherent variability of the soil on the characterization of the results in the field; the 95% confidence interval was calculated. The confidence interval represents the lower and upper limit of the mean, and the narrower the confidence interval, the more precise the estimation (Snedecor and Cochran, 1989) (Eq. 4.7).

$$CIX_r = X_r \mp t \cdot \frac{\sigma X_r}{\sqrt{n}} \quad (4.7)$$

Where CIX_r is the confidence interval for the representative datasets; X_r is the representative datasets in Tab. 4.4; t is the student coefficient which depends on the number test and confidence level; σX_r is the standard deviation for the representative datasets; and n is the number of tests. The confidence interval was normalized with the representative datasets in Eq. 4.8:

$$CIX_{r,norm} = \frac{CIX_r}{X_r} \quad (4.8)$$

Where $CIX_{r,norm}$ is the normalized confidence interval for the representative datasets; CIX_r is the confidence interval for the representative datasets; and X_r is the representative datasets in Tab. 4.4.

4.3. Results

The developments of representative SCPT and peak VCPT datasets with depth are depicted in Fig. 4.7. The peak vibratory cone resistances of the sand deposits were nearly always below the static cone resistance. The difference between vibratory and static cone resistance increased with VCPT amplitude. Some layers exhibited small reduction in cone resistance due to VCPT (see example I in Fig. 4.7(b)). Others had a pronounced reduction in vibratory cone resistance (see examples II and III in Fig. 4.7(b) and 4.7(c)). With increase in VCPT amplitude, the local maxima in the peak vibratory cone resistances were less pronounced. In some layers, the peak vibratory cone resistances were reduced to very low values when the highest VCPT amplitude was applied (see example II in Fig. 4.7(b)). In the silty till layer (U3), the difference between vibratory and static cone resistances was negligible. The behaviour of the representative static sleeve friction mimics the behaviour of the representative static cone resistance (Fig. 4.7(c)). During VCPT, the sleeve friction was also reduced. At medium VCPT amplitude of 5 mm, the vibratory sleeve friction was reduced to c. 0 MPa below the ground water table, indicating total loss in shear stress between the sleeve and soil. Gradual reduction in the sleeve friction was observed with increasing the amplitudes for the sand deposits of U1 above the groundwater table. The static pore water pressure was slightly negative above the water table, which was found to be at a depth of c. 4 m (Fig. 4.7(d)). From 4 m downwards, the static pore water pressure increased isostatically with depth. The pore water pressure seemed to be unaffected by the VCPT amplitude.

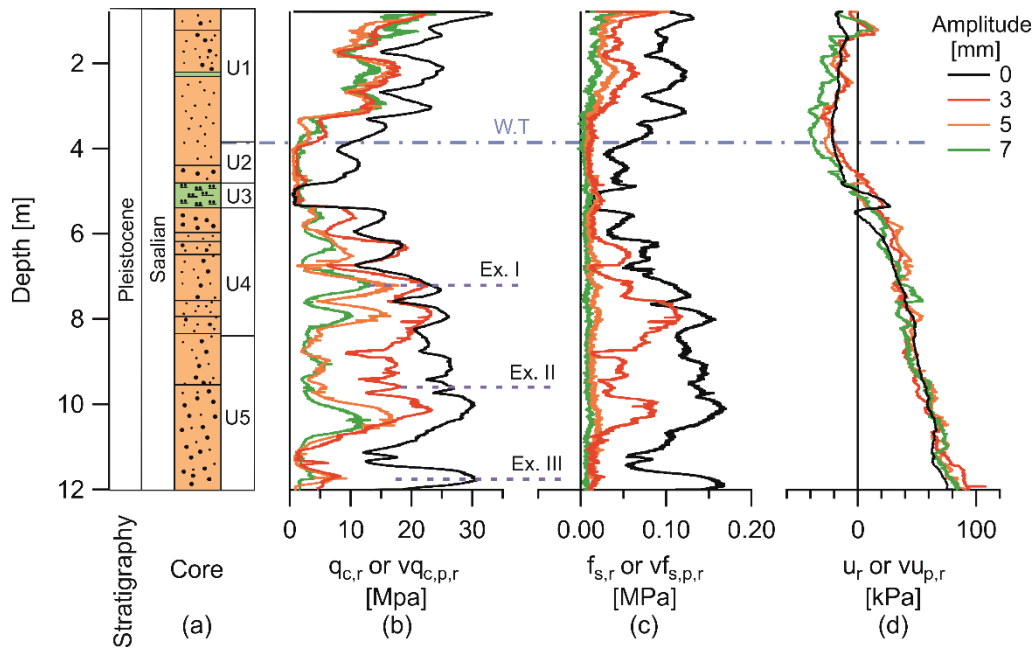


Fig. 4.7. Cone resistance, sleeve friction, and pore water pressure of SCPT and peak VCPT of different VCPT amplitudes

The reduction in the representative cone resistance and representative sleeve friction due to vibratory penetration was quantified by the degradation factors, βq_c and βf_s , of cone resistance and sleeve friction, respectively (Eqs. 4.2 and 4.3, Fig. 4.8). For the sand deposits (U1–U2, U4–U5), the degradation factors of cone resistance decreased with increasing VCPT amplitude (Fig. 4.8(c)). For the lowest VCPT amplitude of 3 mm, the degradation factor of cone resistance commonly ranged between 0.9 and 0.5, indicating degradations in cone resistance of 10 to 50 %. The degradation factors of cone resistance were considerably smaller for larger VCPT amplitudes of 5 and 7 mm, respectively. For example, at c. 8 to 10 m depth (sand layer U5), the cone resistance was degraded by 90 % during VCPT. However, in some sand layers, e.g. at around 6 to 8 m depth, the degradation in cone resistance was not as much influenced by the VCPT amplitude. In the silty till layer (U3), the degradation factors of cone resistance were close to one, indicating no effect of VCPT on its soil behaviour.

In the sand deposits, the degradation in sleeve friction was highly affected by the VCPT amplitude (Fig. 4.8(e)). At 3 mm VCPT amplitude, the degradation in sleeve friction was commonly between 20 and 70 % and exhibited a similar shape as the peak vibratory sleeve friction dataset with VCPT amplitude of 3 mm. At higher VCPT amplitudes of 5 and 7 mm, the sleeve friction was almost entirely degraded. The shape of degraded sleeve friction was very different than the static sleeve friction, as the sand deposits U2–U5 exhibited 100% degradation

for VCPT amplitudes 5 and 7 mm. The silty till layer (U3) exhibited no degradation in sleeve friction during VCPT.

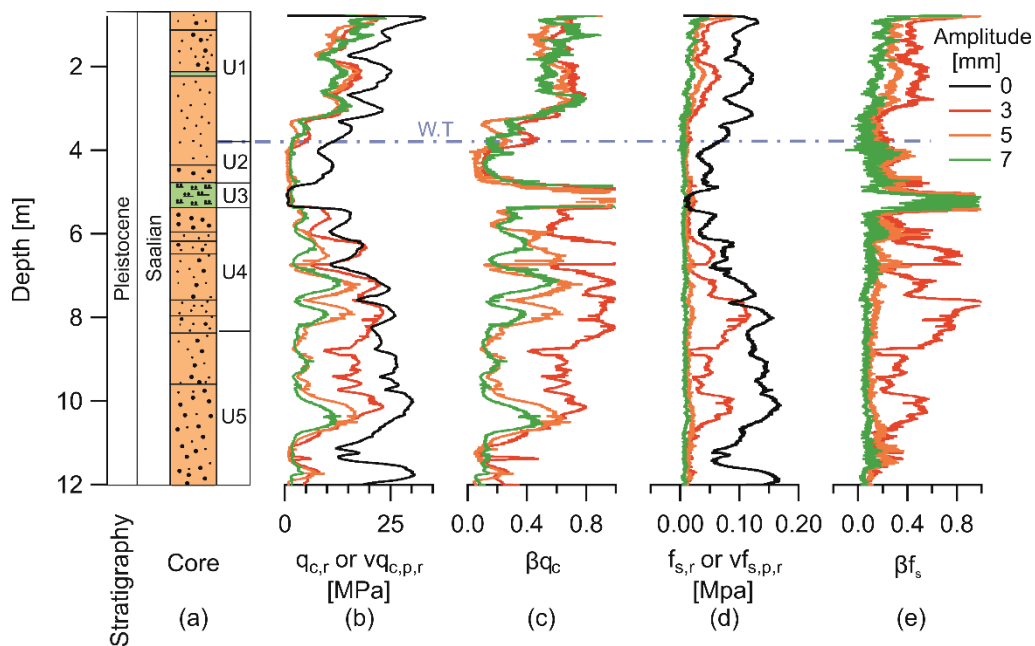


Fig. 4.8. Degradation factors of representative cone resistance and sleeve friction for different VCPT amplitudes

The degradation in cone resistance due to VCPT was further analysed by plotting representative static and peak vibratory cone resistances against the representative displacement amplitude, $d_{amp,r}$, obtained from the acceleration data in the cone (Fig. 4.9). Note that in Fig. 4.9, a representative displacement amplitude of $d_{amp,r} = 0 \text{ mm}$ refers to the representative static cone resistance values. Degradation curves were plotted for different depths that corresponded to the soil units U1 to U5. The majority of degradation curves significantly decreased in cone resistance with increasing displacement amplitude. Exceptions could be found in the sand layers at depths of, e.g. 3 m (U1), where large displacement amplitudes sometimes led to an increase in representative vibratory cone resistance compared with smaller displacement amplitudes. The silty till layer (U3) had very low representative static cone resistance. With displacement amplitude, the cone resistance slightly increased. It was further observed that the static representative cone resistance was not a reliable indicator for the degradation behaviour. When comparing degradation curves that started at similar static representative cone resistances (e.g., at depths of 10 m and 11.6 m, respectively), the degradation behaviour was very different. At the same displacement amplitude of $d_{amp,r} = 1.5 \text{ mm}$, the degradation curve at a depth of

11.6 m exhibited reductions in cone resistance of 70 %, whereas the degradation curve at a depth of 10 m was only reduced by 10 %.

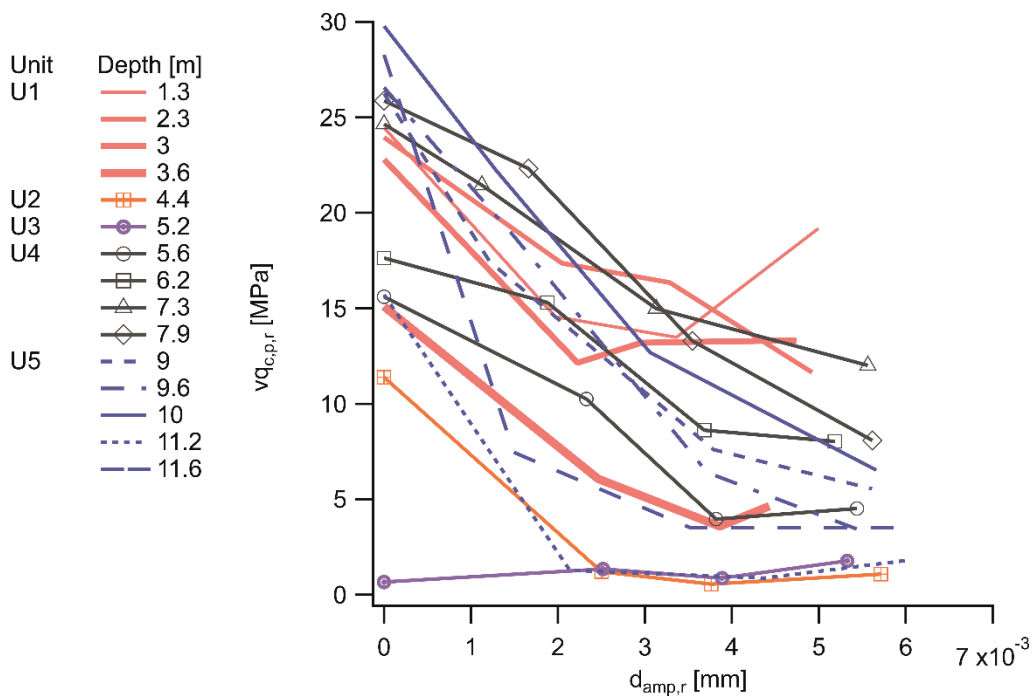


Fig. 4.9. Representative peak vibratory cone resistances for different soil units plotted against the displacement amplitudes

The representative loading and unloading stiffness values and the upward displacement with cavitation were plotted along the depth (Fig. 4.10). In general, both loading and unloading stiffness values decreased with VCPT amplitude (Figs. 4.10(c) and 4.10(d)). All stiffness values exhibited very low values towards the silty till layer (U2 and U3). The shapes of loading stiffness curves mimicked the shapes of their representative peak vibratory cone resistance counterparts (Figs. 4.10(b) and 4.10(c)). The shapes of the unloading stiffness curves were very different compared with the peak vibratory cone resistance curves, although a general decrease in unloading stiffness with increasing VCPT amplitudes was observed, too.

The upward displacement with cavitation generally increased with VCPT amplitude (Fig. 4.10(e)). All curves exhibited less cavitation above and in the till layer (U2 and U3). At sand layers U4–U5, the upward displacement with cavitation for VCPT 3 mm exhibited an approximately linear reduction with depth. This linear reduction was not observed in the upward displacement curves of VCPT 3 and 5 mm.

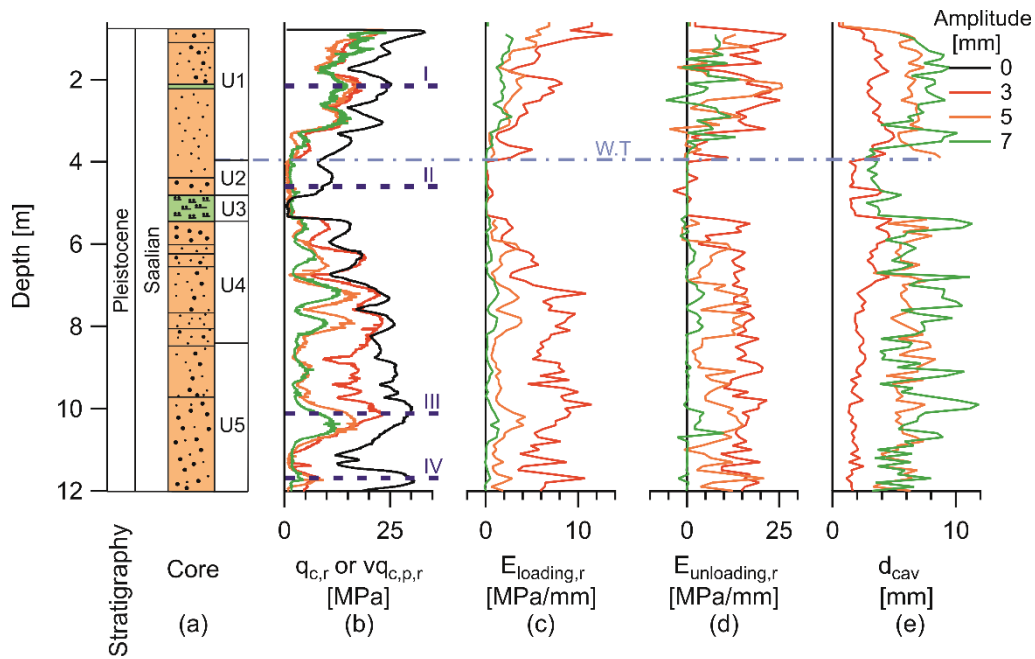


Fig. 4.10. Loading and unloading stiffnesses and the upward displacement with cavitation plotted along the depth of penetration.

The degradation behavior was further studied by comparing Individual cone resistance – displacement hysteresis loops measured by VCPT at different depths (Fig. 4.11). In the four panels of Fig. 4.11, hysteresis loops are given for different VCPT amplitudes in respect to the static cone resistance shown as black vertical lines. Loading and unloading stiffness values as well as upwards displacement of cavitation were added to the panels, as blue lines and grey bars, respectively. Dotted lines represent preceding hysteresis loops.

For initially stiff sand above the ground water level with high static cone resistance (U1), loading and unloading stiffness values were steadily reduced with increasing VCPT amplitude (Fig. 4.11(a)). The upward displacement with cavitation increased with VCPT amplitude. In a loose sand layer at U2 below the water table, the cone resistance was degraded to values around zero for all applied VCPT amplitudes (Fig. 4.11(b)). The hysteresis loops became very narrow, indicating not only a total loss in cone resistance but also in loading and unloading stiffness. The upward displacement with cavitation extended along the entire upward movement of hysteresis loops. In sand layers of unit U5 with high static cone resistance, very different cyclic soil responses were observed (Fig. 4.11(c) and 4.11(d)). In the sand layer at 10 m depth, a small VCPT amplitude of 3 mm did not lead to high degradation in cone resistance compared with

the sand layer at 11.6 m depth. Furthermore, the loading and unloading stiffness values were higher for the sand deposit at 10 m depth than for sand deposit at 11.6 m depth.

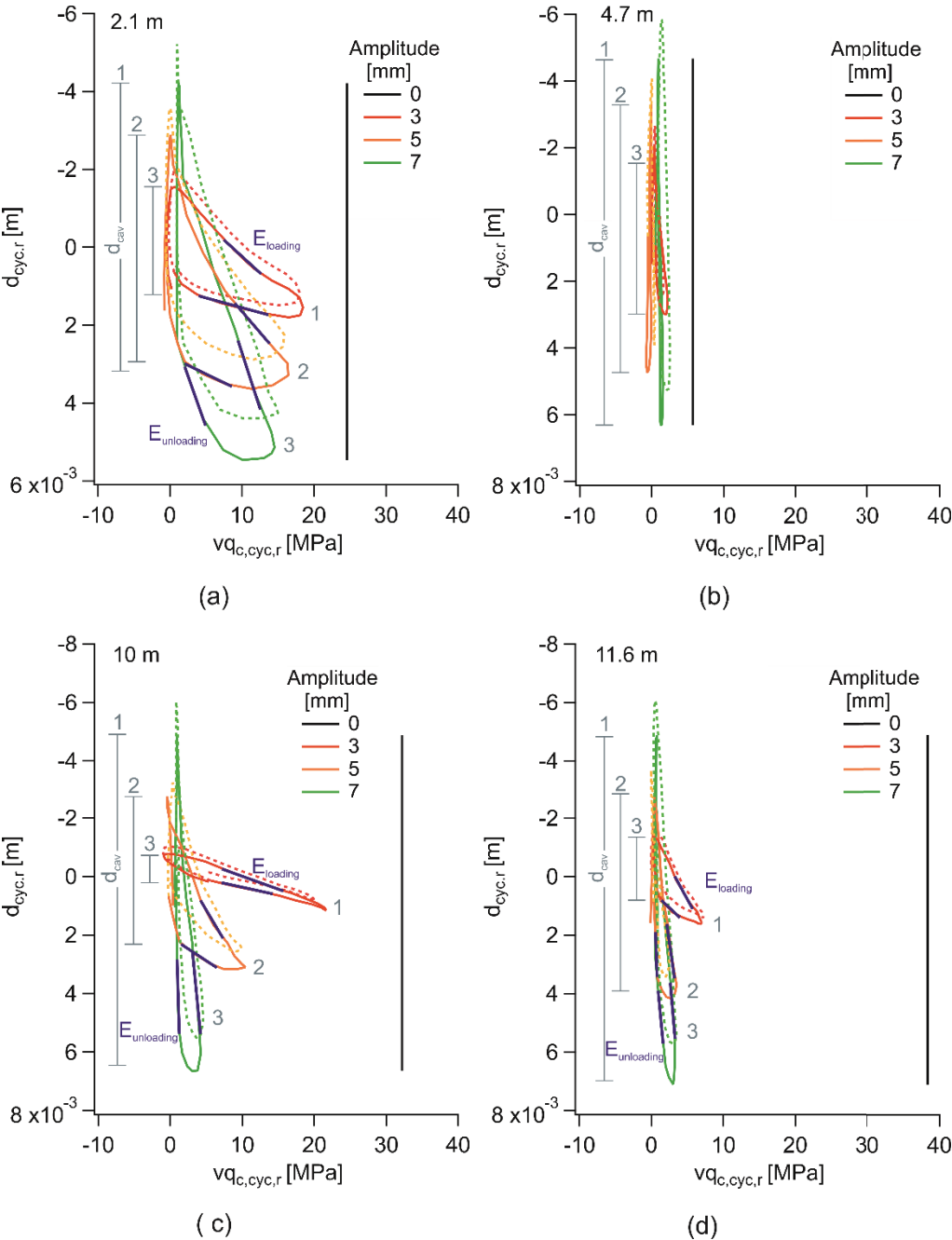


Fig. 4.11. Representative cyclic cone resistance – displacement behavior for the three applied VCPT amplitudes at depths of (a) 2.1 m; (b) 4.7 m; (c) 10 m; and (d) 11.6 m. See text for further explanation

The statistical significance of the results presented in this study were analyzed by the width of the 95 % confidence interval. The confidence intervals for static and vibratory cone resistances and loading and unloading stiffness were normalized to their corresponding representative datasets for better comparability (Eq. 4.8, Fig. 4.12(b)–4.12(d)). The normalized confidence intervals of the vibratory cone resistances were commonly larger than those of the static cone resistance for all soil layers. For a better comparison between the normalized confidence intervals, mean values were calculated for every normalized confidence interval dataset and were summarized in Tab. 4.5. The mean values of normalized confidence interval increased with VCPT amplitude. The normalized confidence interval for the loading stiffness and its mean value show similar increase with VCPT amplitude compared with that of cone resistance (Fig. 4.12(c), Tab. 4.5). The normalized confidence interval for the unloading stiffness does not show a clear trend with increasing the VCPT amplitude (Fig. 4.12(d)). However, its mean values show gradual increase with increasing VCPT amplitude (Tab. 4.5). The confidence intervals for the representative cone resistance cycles at depth of 2.6 m are depicted in Fig. 4.12 (e)–4.12(g). No pronounced increase was observed in the confidence interval with increasing VCPT amplitudes. The confidence intervals for the representative datasets in Tab. 4.4, are summarized in the appendix (Fig. 7.1.2 – Fig. 7.1.9).

Table. 4.5. Mean values of normalized confidence intervals of cone resistance and loading and unloading stiffnesses for the different VCPT amplitudes

Amplitude [mm]	Mean normalized confidence interval		
	Cone resistance	Loading stiffness	Unloading stiffness
0	0.22	-	-
3	0.54	1.47	1.57
5	0.79	2.07	1.79
7	0.82	2.45	2.18

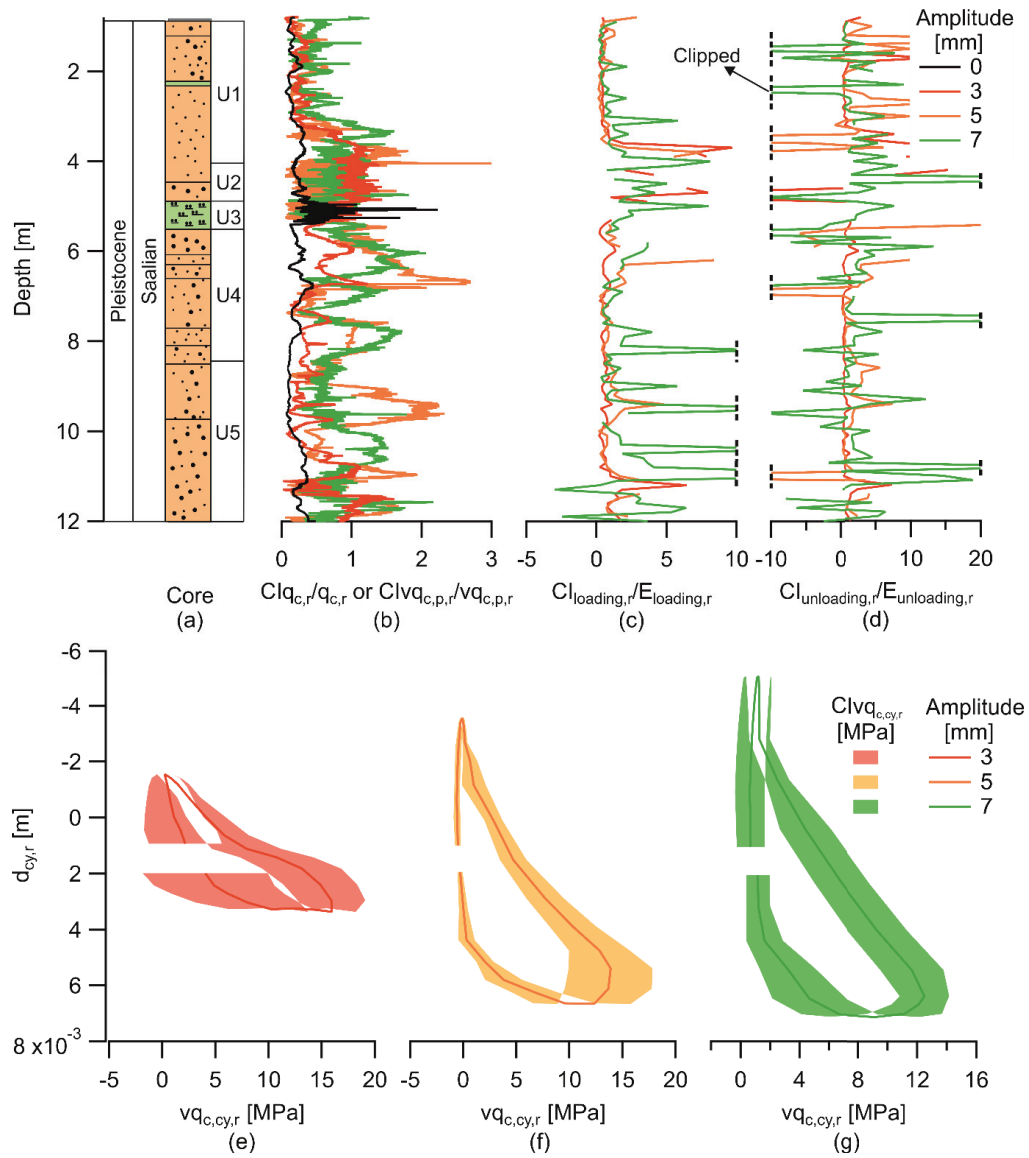


Fig. 4.12. Normalized confidence interval for: (b) cone resistance; (c) loading stiffness; (d) unloading stiffness; and the confidence interval for the cone resistance cycles at depth of 2.2 m for VCPT amplitudes: (e) 3 mm; (f) 5 mm; and (g) 7 mm

4.4. Discussion

In the present study, an increase in degradation of cone resistance and sleeve friction with VCPT amplitudes was observed (Figs. 4.7 and 4.8), which provided practical evidence that the degradation in soil resistance during vibratory pile driving depends on the amplitude of vibration. This conclusion is in agreement with previous studies about assessments of vibro-drivability in sand, in which it was assumed that one of the important factors affecting degradation factor for piles, β , is vibration amplitude (Jonker, 1987, van Baars, 2004).

The degradation in cone resistance during VCPT observed in the present study could be related to the cavitation that commonly occurs between the cone and soil during the upward movement

of the cone, in cases where the amplitude is large enough. Similar observations had been described in the Karlsruhe model for slow vibratory pile driving (Dierssens, 1994). During the upward movement of the cone, the unloaded soil loses its strength, collapses and starts to flow into the cavity, but because of the short interval time until the reversal to the downward movement, the cavity remains partially empty (Dierssens, 1994). This process results in remolding and/or loosening of the soil below the cone (Massarsch et al., 2017). Therefore, a reduction in cone resistance occurs when the cone gets again in contact with the soil during the downward movement.

Degradation factors have been studied for submerged and cohesionless soils (Bernhard, 1967, Nogami et al., 1997, Rodger and Littlejohn, 1980). These studies relate degradations in cyclic resistance during vibratory pile driving to induced pore water pressure and to the occurrence of liquefaction. Empirical liquefaction factors were also introduced to model the degradation in static soil resistance due to vibratory pile driving (Holeyman and Whenham, 2017a, Viking, 2006). In the present study, no influence of VCPT on pore water pressure was observed for all soil layers and all applied VCPT amplitudes. Therefore, it is concluded that classic liquefaction is not likely an important factor for cone resistance degradation in dense sand and silt deposits. This conclusion was also reached by O'Neill and Vipulanandan (1989). The authors performed a large-scale laboratory study to understand the behavior of piles that were installed by vibratory pile driving. The authors found that the measured total stress always exceeded the pore water pressure by considerable amount. This resulted in positive effective stresses between the pile shaft and surrounding soil, hampering the occurrence of classical liquefaction. Other studies related the degradation in soil resistance to large cyclic strains, which may have caused by a mechanism known of “cyclic mobility” (Rao, 1993, Bonita, 2000).

The degradation in cone resistance and sleeve friction was also observed for the dry sand layer (Fig. 4.8(e)), which agrees with results obtained from laboratory tests of vibratory pile driving in air-dried sand (Wong et al., 1992, O'Neill and Vipulanandan, 1989). The authors mentioned above related the degradation in shaft resistance during vibratory pile driving to decreases in effective stress caused by the induced dynamic motion of sand grains. This dynamic motion of sand grains occurs due to the drop in normal forces at inter-granular contacts and shear forces between grains when the acceleration amplitude exceeds specific threshold values related to the overburden pressure for certain soil volume in the field (Viking, 2006). This could explain the

gradual reduction in the sleeve friction with increasing the amplitude observed in the present study (Fig. 4.7(c)).

The present study highlighted that soils, having approximately similar relative densities, grain size, and static cone resistances can exhibit very different degradation behaviours (Figs. 4.9, 4.11(c), 4.11(d)). This observation is probably related to the different cyclic behaviour exhibited by these soils. The difference in cyclic soil behaviour could be related to the stiffness of sand, which commonly decreases with increasing strain. The stiffness modulus depends on the stress ratio and the stress history. Those effects could change from sand to sand depending on the presence of crushable materials (Yamashita et al., 2000). The loading and unloading stiffnesses also depend on the soil fabric and relative density. The changes in soil fabric by the cavitation depends on the VCPT amplitudes and affects the difference in the loading and unloading stiffnesses (Massarsch et al., 2017). The complexity of the observed cyclic behaviour and its dependency on the cyclic amplitude, raises questions regarding the fruitfulness of the efforts of current soil-pile interaction models to try to estimate soil cyclic resistance from the static cone resistance without assessing the complexity of the soil's cyclic behavior (Schneider and Harmon, 2010, Holeyman and Whenham, 2017a, Qin et al., 2017). Nevertheless, there have been some studies that assessed the cyclic soil behaviour by modifying the Ramberg-Osgood's static soil-pile load transfer model to include (1) cyclic degradation of the pile-soil interface, (2) residual stresses, and (3) loading and unloading phases during vibratory driving (Wong et al., 1992, Lee et al., 2012). However, these modifications were implemented empirically for very specific soil-pile systems, by multiplying the static load transfer model by a fitting factor, which represents a ratio of the maximum value of dynamic unit load transfer to the maximum value of the static unit load transfer, with no regards to the effect of the cyclic amplitude (Wong et al., 1992, Lee et al., 2012). Although the present study clearly demonstrated the important effect of the cyclic amplitude, future work should account for this effect. This is especially important since the cyclic amplitude of the pile toe in the soil will gradually reduce just before the pile gets stuck. The present study may overestimate the differences in degradation behavior, because local lateral changes in the soil layers may have affected the results. However, since four to six repetition tests were included in every point, there remains a statistical significance.

The cyclic behaviour, assessed by the loading and unloading stiffness, showed increases in degradation of loading and unloading stiffness with increasing amplitudes (Fig. 4.10 (c)–4.10(d)), which agrees with findings of the secant Young's modulus, exhibiting very

pronounced degradation with increasing strain (Yamashita et al., 2000). The direct proportional behavior of the representative vibratory cone resistances and their respective loading stiffness is in accordance to studies, where unique correlations between cone resistance and deformation modulus was obtained from calibration chamber experiments (Sadrekarimi, 2016). Stiffness decreases were observed when upward displacement with cavitation was increased (Fig. 4.11) This observation can be explained from the increased disturbance and remolding of soil with increasing the amplitudes of vibration (Massarsch and Westerberg, 1996). This reduction is due to the loss of strength due to high degree of remoulding, which in turns affected the cyclic cone resistance-displacement behaviour.

The present study further showed that the inherit variation in soil properties, which are caused by the sedimentation regime and diagenetic history of the test site, affected the VCPT results (Fig. 4.12) (Nichols, 2009, Phoon and Kulhawy, 1999). The increase in normalized confidence intervals with increasing the VCPT amplitudes as observed in the present study (Fig. 4.12(b)–4.12(d)) indicates that the uncertainties of test results corresponded to an increase in vibrational amplitudes. These uncertainties could be caused by the different cyclic soil response to VCPT due to the different degree of soil remoulding during cavitation accompanied by the inherit variability in the test site further vary the response of the soil to cyclic loads.

4.5. Conclusions

A systematic grid of static and vibratory cone penetration tests was performed in a natural sand deposit of a test site in Northern Germany in order to investigate the cyclic soil behaviour in-situ during vibratory pile driving. It was found that:

- 1- Degradation in vibratory cone resistance and sleeve friction increased with VCPT amplitudes.
- 2- No influence of VCPT on pore water pressure was observed for all soil layers and all VCPT amplitudes considered in this study. Therefore, liquefaction is probably not an important factor for cone resistance degradation.
- 3- The degradation in vibratory cone resistance is believed to be related to the increase in the displacement with cavitation.

- 4- The degradation in vibratory sleeve friction could be related to the drop in normal forces at inter-granular contacts and shear forces between the grains when the acceleration amplitude exceeded specific threshold values.
- 5- The degradation in the loading and unloading stiffness, increased with increasing VCPT amplitudes.
- 6- The general practices in pile engineering that estimates the degradation in soil due to vibratory pile driving from the static cone resistance is probably not sufficient, because soils with similar static cone resistance exhibited different responses to vibration.

Acknowledgements

This project was funded by the Federal Ministry for Economic Affairs and Energy (BMWi), project: Vibro Drucksondierungen, FKZ: 0325906. We thank, Joann Schmid, Wolfgang Schunn, and Marc Huhndorf, for invaluable technical assistance during field work and construction of the VCPT device.

CHAPTER 5

5. Conclusion

In this doctoral thesis, 45 static cone penetration tests and 18 vibratory cone penetration tests were performed in the two tests areas, Bremen and Cuxhaven, to investigate the research hypotheses. Findings and conclusions of Chapter 1, together with the research hypotheses, are presented below:

Hypotheses 1: “Decreasing the spacing between CPTs locations and increasing the number of tests give a sufficient confidence interval and improve the characterization of cone resistance, if the distance falls not below minimum acceptable distance.”

The study shows that there is a spacing threshold equal to 24 cone diameters at which an artificial reduction in cone resistance occurs in medium dense sand. For silt and clay spacing threshold was not observed in our study and is probably below 7 cone diameters. Increasing the number of CPT datasets and decreasing the spacing between the test site leads to a narrower confidence interval and helps to obtain depth-dependent characteristic values of cone resistance. CPTs spacing and natural variations in soil properties are deciding factors for the number of the SCPTs in the field to give a sufficient confidence interval.

Hypotheses 2: “VCPT could be used to investigate the cyclic soil behavior in-situ until the final depth of penetration”

The new device proved to generate constant amplitudes until the final depth of penetration. Two sand layers reacted to the applied cyclic loads by showing high values of the reduction ratio. It was also found that even a distance of 50 cm does not guarantee a good correlation between SCPT and VCPT. Therefore, two or more pairs of CPT and VCPT should be conducted in order to minimize misinterpretations of the data.

Hypotheses 3: “Degradation in cyclic soil resistance and stiffness increase with cyclic displacement amplitudes”

Degradation in cyclic soil resistance and in the loading and unloading stiffness increased with VCPT amplitudes. This degradation was not accompanied by any increase in pore water pressure. Therefore, liquefaction is probably not an important factor for degradation. The

degradation is believed to be related to the cavitation which increases with displacement amplitude.

The conclusions from the three hypotheses motivate us to believe that the current civil engineering practice is not sufficient to predict the cyclic soil behavior during vibratory pile installation. This conclusion comes from the fact that the practice depends on degradation factors that do not consider the effect of cyclic displacement amplitude on soil resistance. Furthermore, the results in this thesis demonstrate that there is no unique relation between static and vibratory cone resistance, therefore, the current practice that estimates the degradation in soil resistance due to vibratory pile driving from the static cone resistance is probably not sufficient. VCPT could be used to assess the cyclic soil behavior, however, several tests should be performed in order to have statistical significance and consider the effect of the local variation in soil properties.

CHAPTER 6

6. References cited

- AADNOY, B., S, 1991. Effects of Reservoir Depletion on Borehole Stability. *Journal of Petroleum Science and Engineering*, 6, 57-61.
- AHMADI, M. M. & ROBERTSON, P. K. 2008. A Numerical Study of Chamber Size and Boundary Effects on CPT Tip Resistance in NC Sand. *Scientia Iranica*, 15, 541-553.
- AL-SAMMARRAIE, D., KREITER, S., STÄHLER, F. T., GOODARZI, M. & MÖRZ, T. New Vibratory Cone Penetration Device for in-Situ Measurement of Cyclic Softening. *International Symposium on Cone Penetration Testing*, 2018.
- BALDI, G., BELLOTTI, R., GHIONNA, V., JAMIOLKOWSKI, M. & PASQUALINI, E. Interpretation of CPT's and CPTU's. 2nd Part: Drained Penetration” *Proceeding 4th International Geotechnical Seminar*, 1986 Singapore. 143-15.
- BEEN, K. & JEFFERIES, M. G. 1985. A state parameter for sands. *Géotechnique*, 35, 99-112.
- BERNHARD, R. K. 1967. FLUIDIZATION PHENOMENA IN SOILS DURING VIBRO-COMPACTION AND VIBRO-PILE-DRIVING AND-PULLING. COLD REGIONS RESEARCH AND ENGINEERING LAB HANOVER NH.
- BOND, A., J., SCHUPPENER, B., SCARPELLI, G. & ORR, T., L.,L., 2013. Eurocode 7: Geotechnical Design Worked examples. In: DIMOVA, S., NIKOLOVA, B. & PINTO, A., V., (eds.) Report EUR 26227 EN. Dublin: Institute for the Protection and Security of the Citizen.
- BONITA, J. A. 2000. The effects of vibration on the penetration resistance and pore water pressure in sands. Virginia Tech.
- BOULANGER, R. W., MOUG, D. M., MUNTER, S. K., PRICE, A. B. & DEJONG, J. T. 2016. Evaluating Liquefaction and Lateral Spreading In Interbedded Sand, Silt, and Clay Deposits Using The Cone Penetrometer. *Australian Geomechanics Society*
- BS 1377-9 1990. Methods for test for soils for civil engineering purposes. In-situ tests
- CASTO, G. 1975. Liquefaction and cyclic mobility of saturated sands. *Journal of Geotechnical and Geoenvironmental Engineering*, 101.
- DIERSSENS, G. 1994. Ein bodenmechanisches Modell zur Beschreibung des Vibrationsrammens in körnigen Böden. Doctoral Thesis, University of Karlsruhe.
- DIN 18123 2011. Soil, investigation and testing–determination of grain-size distribution.
- DIN EN ISO 14688-1 2003. Geotechnische Erkundung und Untersuchung-Benennung, Beschreibung und Klassifizierung von Boden-Teil 1: Benennung und Beschreibung. Burmeier Ingenieurgesellschaft mbH.
- DIN EN ISO 22476-1 2012. Geotechnical investigation and testing - Field testing Part 1: Electrical cone and piezocone penetration test.
- EHLERS, J. 1990. Reconstructing the dynamics of the north-west European Pleistocene ice sheets. *Quaternary Science Reviews*, 9, 71-83.
- EHLERS, J., MEYER, K.-D. & STEPHAN, H.-J. 1984. The pre-Weichselian glaciations of north-west Europe. *Quaternary Science Reviews*, 3, 1-40.
- FRANK, R., BAUDUIN, C., DRISCOLL, R., KAVVADAS, M., KREBS, O., N., , ORR, L. & SCHUPPENER., B. 2004. *Designers’ Guide to EN 1997-1 Eurocode 7*, London, Thomas Telford.
- GEO-ENGINEERING 2014. Geotechnical site investigation report VIBRO-project Altenwalde.

- GOODARZI, M., OSSIG, B., BRANDT, L., BUSCH, A., GHASEMI, P. & MÖRZ, T. 2019. Axial capacity of impact-driven monopiles: the case study at Cuxhaven, Germany.
- GUPTA, D. & ZAMAN, M. 1999. Stability of Boreholes in A Geologic Medium Including The Effects of Anisotropy. *Applied Mathematics and Mechanics*, 20.
- HASHEMI, S., MOMENI, A. & MELKOUMIAN, N. 2014. Investigation of borehole stability in poorly cemented granular formations by discrete element method. *Journal of Petroleum Science and Engineering*, 113, 23-35.
- HOLEYMAN, A. & WHENHAM, V. 2017a. Critical Review of the Hypervib1 Model to Assess Pile Vibro-Drivability. *Geotech Geol Eng*, 35, 1933–1951.
- HOLEYMAN, A. & WHENHAM, V. 2017b. Critical review of the Hypervib1 model to assess pile vibro-drivability. *Geotechnical and Geological Engineering*, 35, 1933-1951.
- HSU, H., H., & HUANG, A., B., 1998. Development of an Axisymmetric Field Simulator for Cone Penetration Tests in Sand. *Geotechnical Testing Journal*, 21, 348 - 355.
- JONKER, G. Vibratory pile driving hammers for pile installations and soil improvement projects. *Offshore Technology Conference*, 1987. *Offshore Technology Conference*.
- JORAT, M. E., MÖRZ, T., MOON, V. G., KREITER, S. & DE LANGE, W. P. 2015. Utilizing piezovibrocone in marine soils at Tauranga Harbor, New Zealand. *Journal of Geomechanics and Engineering*, 9, 1-14.
- KLUGER, M. O., KREITER, S., L'HEUREUX, J.-S., STEGMANN, S., MOON, V. & MÖRZ, T. 2016. In situ cyclic softening of marine silts by vibratory CPTU at Orkdalsfjord test site, mid Norway. *Submarine Mass Movements and their Consequences*. Springer.
- LABIOUSE, V. & VIETOR, T. 2014. Laboratory and in situ simulation tests of the Excavation Damaged Zone around galleries in Opalinus Clay. *Rock Mechanics and Rock Engineering*, 47, 57-70.
- LAUFER, I. 2013a. Statistical analysis of CPT tip resistances. *Periodica Polytechnica Civil Engineering*, 57, 45-61.
- LAUFER, I. 2013b. Statistical analysis of CPT tip resistances. *Civil Engineering*, 57, 45–61.
- LEE, S.-H., KIM, B.-I. & HAN, J.-T. 2012. Prediction of penetration rate of sheet pile installed in sand by vibratory pile driver. *KSCE Journal of Civil Engineering*, 16, 316-324.
- LINGWANDA, M. I., LARSSON, S. & NYAORO, D. L. 2015. Correlations of SPT, CPT and DPL Data for Sandy Soil in Tanzania. *Geotechnical and Geological Engineering*, 33, 1221-1233.
- LINGWANDA, M. I., PRÄSTINGS, A., LARSSON, S. & NYAORO, D. L. 2017. Comparison of geotechnical uncertainties linked to different soil characterization methods. *Geomechanics and Geoengineering*, 12, 137-151.
- LUNNE, T., ROBERTSON, P. K. & POWELL, J. J. M. 1997. *Cone Penetration Testing in Geotechnical Practice*
- MASSARSCH, K. R., FELLENIUS, B. H. & BODARE, A. 2017. Fundamentals of the vibratory driving of piles and sheet piles. *geotechnik*, 40, 126-141.
- MASSARSCH, K. R. & WESTERBERG, E. 1996. FREQUENCY-VARIABLE VIBRATORS AND THEIR APPLICATION TO FOUNDATION ENGINEERING. 한국지반공학회 학술발표 및 세미나 자료집, 1996, 25-40.
- MAYNE, P. W. 2000. Evaluating ground liquefaction potential by piezovibrocone. Georgia Institute of Technology.
- MCGILLIVRAY, A., CASEY, T., MAYNE, P. W. & SCHNEIDER, J. A. 2000. An electro-vibrocone for site-specific evaluation of soil liquefaction potential. *Innovations and Applications in Geotechnical Site Characterization*.

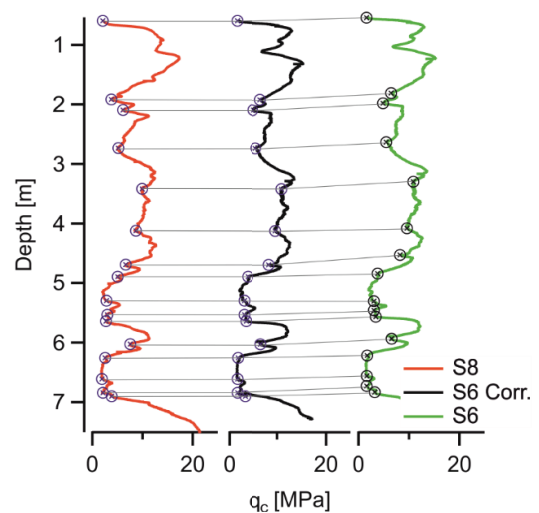
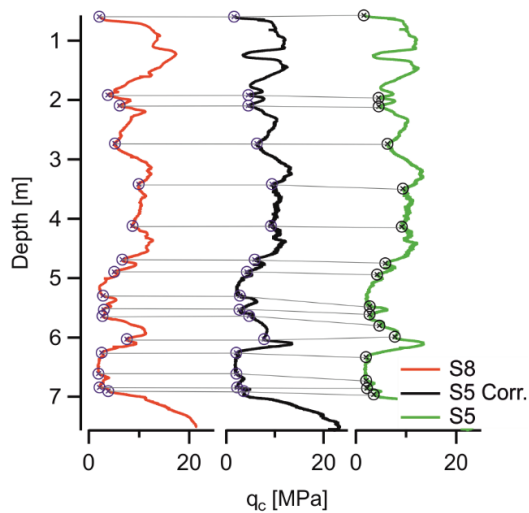
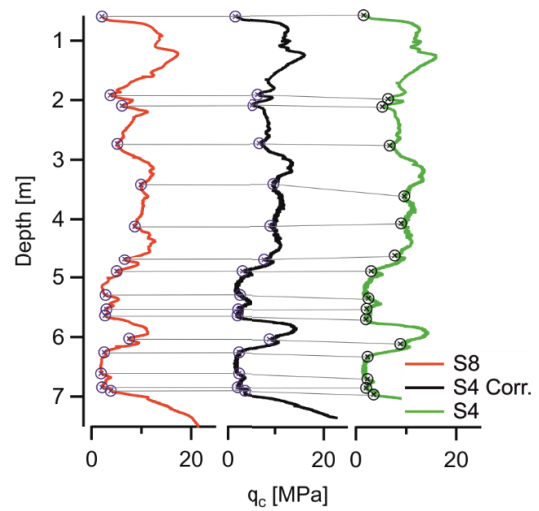
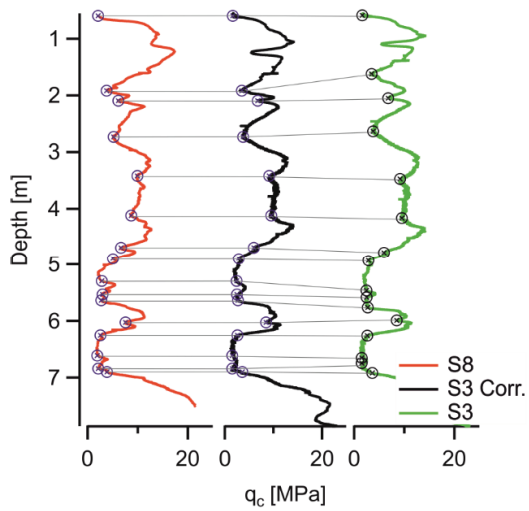
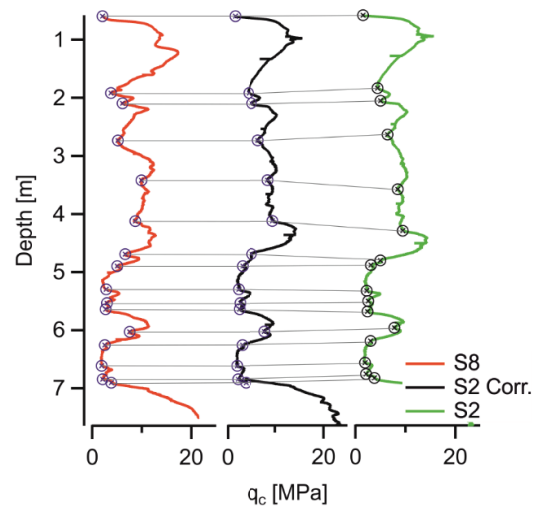
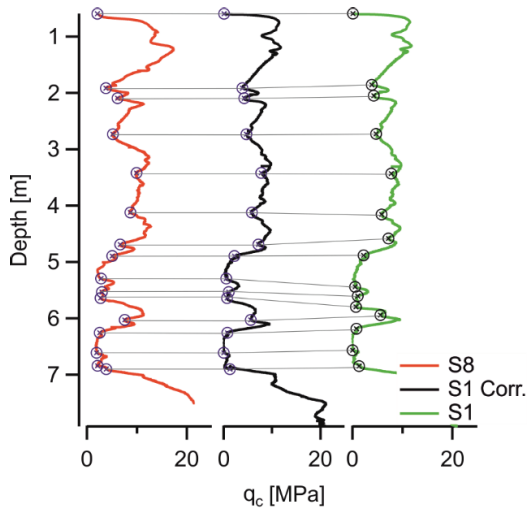
- MITCHELL, J. New developments in penetration tests and equipment. International Symposium on penetration testing; ISOPT-1. 1, 1988. 245-261.
- MOORE, D. 1987. Evaluation of the cone penetrometer & its effect on cone bearing and pore pressure.
- MORGAN, M. G. & HENRION, M. 1990. Uncertainty: a Guide to dealing with uncertainty in quantitative risk and policy analysis Cambridge University Press. New York, New York, USA.
- NGI 2014. Time effects on pile capacity. Summary and evaluation of test results. Norway.
- NIBIS 2014. Topic of imbedded map. - Landesamt für Bergbau, Energie und Geologie (LBEG). Hannover.
- NICHOLS, G. 2009. Sedimentology and Stratigraphy, The Atrium, Southern Gate, Chichester, West Sussex, PO19 8SQ, UK, John Wiley & Sons Ltd.
- NOGAMI, T., REN, F., CHEN, J.-W. & MASON, A. B. 1997. Vertical vibration of pile in vibration-induced excess pore pressure field. Journal of Geotechnical and Geoenvironmental Engineering, 123, 422-429.
- O'NEILL, M. W. & VIPULANANDAN, C. 1989. Laboratory evaluation of piles installed with vibratory drivers.
- ORR, T., L., L., 2000. Selection of characteristic values and partial factors in geotechnical designs to Eurocode 7. Computers and Geotechnics, 26, 263-279.
- ORTLAM, D. & SCHNIER, H. 1980. Erläuterungen zur Baugrunderkarte Bremen, Sen. fd Bauwesen, Kataster-u. Vermessungsverwaltung.
- PANIAGUA, P., ANDO, E., SILVA, M., EMDAL, A., NORDAL, S. & VIGGIANI, G. 2013. Soil deformation around a penetrating cone in silt. Geotechnique Letters, 3, 185–191.
- PHOON, K. K. & KULHAWY, F. H. 1999. Characterization of Geotechnical Variability. Can. Geotech. J., 36, 612-624.
- POULOS, S. J., CASTRO, G. & FRANCE, J. W. 1985. Liquefaction evaluation procedure. Journal of Geotechnical Engineering, 111, 772-792.
- QIN, Z., CHEN, L., SONG, C. & SUN, L. 2017. Field tests to investigate the penetration rate of piles driven by vibratory installation. Shock and Vibration, 2017.
- QUINTEROS, S., LUNNE, T., KROGH, L., BØGELUND-PEDERSEN, R. & BRINK CLAUSEN, J. Shallow depth characterisation and stress history assessment of an over-consolidated sand in Cuxhaven, Germany. Cone Penetration Testing IV: Proceedings of the 4th International Symposium on Cone Penetration Testing (CPT 2018), June 21-22, 2018, Delft, The Netherlands, 2018.
- RAO, P. M. 1993. Effect of pile geometry and soil saturation on the behavior of nondisplacement piles installed by vibration. University of Houston.
- ROBERTSON, P., K., 2009. Interpretation of Cone Penetration Tests - A Unified Approach. Can. Geotech. J., 46, 1337 - 1355.
- RODGER, A. & LITTLEJOHN, G. 1980. A study of vibratory driving in granular soils. Geotechnique, 30, 269-293.
- ROGERS, J. D. 2006. Subsurface exploration using the standard penetration test and the cone penetrometer test. Environmental & Engineering Geoscience, 12, 161-179.
- SADREKARIMI, A. 2016. Evaluation of CPT-based characterization methods for loose to medium-dense sands. Soils and Foundations, 56, 460-472.
- SALGADO, R., PREZZI, M. & GANJU, E. 2015. Assessment of Site Variability from Analysis of Cone Penetration Test Data. (Joint Transportation Research Program Publication No. FHWA/IN/JTRP-2015/04). West Lafayette: Purdue University.
- SASAKI, Y. & KOGA, Y. Vibratory cone penetrometer to assess the liquefaction potential of the ground. Proceedings, 1982. 541-555.

- SCHNEIDER, J. A. & HARMON, I. A. 2010. Analyzing drivability of open ended piles in very dense sands. *DFI Journal-The Journal of the Deep Foundations Institute*, 4, 32-44.
- SEED, B. & LEE, K. L. 1966. Liquefaction of saturated sands during cyclic loading. *Journal of Soil Mechanics & Foundations Div*, 92.
- SEED, H. B. & IDRISSE, I. M. 1971. Simplified procedure for evaluating soil liquefaction potential. *Journal of Soil Mechanics & Foundations Div*.
- SHU, B. & MA, B. 2015. Study of ground collapse induced by large-diameter horizontal directional drilling in a sand layer using numerical modeling. *Canadian Geotechnical Journal*, 52, 1562-1574.
- SINDOWSKI, K.-H. 1965. Die drenthestadiale Altenwalder Stauchmoräne südlich Cuxhaven. *Zeitschrift der Deutschen Gesellschaft für Geowissenschaften (ZDGG)*, 158-162.
- SNEDECOR, G., W., & COCHRAN, W., G., 1989. *Statistical Methods*. Iowa State University Press.
- STÄHLER, F., T., , KREITER, S., GOODARZI, M., AL-SAMMARRAIE, D. & MÖRZ, T. Liquefaction Resistance by Static and Vibratory Cone Penetration Tests. In: HICKS, M., A., PISANÒ, F. & PEUCHEN, J., eds. *Proceedings of the 4th International Symposium on Cone Penetration*, 2018 Delft.
- SZE, H. & YANG, J. 2013. Failure modes of sand in undrained cyclic loading: impact of sample preparation. *Journal of geotechnical and geoenvironmental engineering*, 140, 152-169.
- TAYLOR, J. R. 1982. *An introduction to error analysis: Mill Valley*. California, University Science Books.
- TOKIMATSU, K. 1988. Penetration tests for dynamic problems. *Proc. Penetration Testing ISOPT-1*, 117-136.
- VAN BAARS, S. 2004. Design of sheet pile installation by vibration. *Geotechnical & Geological Engineering*, 22, 391-400.
- VAN DER STOEL, A., E.,C.,. 2001. *Grouting for Pile Foundation Improvement*. Doctoral, Technische Universiteit Delft.
- VIKING, K. The vibratory pile installation technique. *Proceedings of the International Conference on Vibratory Pile Driving and Deep Soil Compaction*, 2006. 65-82.
- WHENHAM, V. & HOLEYMAN, A. 2012. Load transfers during vibratory driving. *Geotechnical and Geological Engineering*, 30, 1119-1135.
- WHITE, D., J., & BOLTON, M., D., 2004. Displacement and Strain Paths During Plane-Strain Model Pile Installation in Sand. *Geotechnique*, 54, 375-397.
- WISE, C., MAYNE, P. & SCHNEIDER, J. Prototype piezovibrocone for evaluating soil liquefaction susceptibility. *Earthquake geotechnical engineering*, 1999. 537-542.
- WONG, D., O'NEILL, M. W. & VIPULANANDAN, C. 1992. Modelling of vibratory pile driving in sand. *International Journal for numerical and analytical methods in geomechanics*, 16, 189-210.
- YAMASHITA, S., JAMIOLKOWSKI, M. & PRESTI, D. C. L. 2000. Stiffness nonlinearity of three sands. *Journal of Geotechnical and Geoenvironmental Engineering*, 126, 929-938.
- YASUFUKU, N. & HYDE, A. 1995. Pile end-bearing capacity in crushable sands. *Geotechnique*, 45, 663-676.
- YIMSIRI, S. & SOGA, K. 2010. DEM analysis of soil fabric effects on behaviour of sand. *Geotechnique*, 60, 483.
- YU, H. & MITCHELL, J. 1998. Analysis of cone resistance: review of methods. *Journal of geotechnical and geoenvironmental engineering*, 124, 140-149.

CHAPTER 7

7. Appendix

7.1 Figures



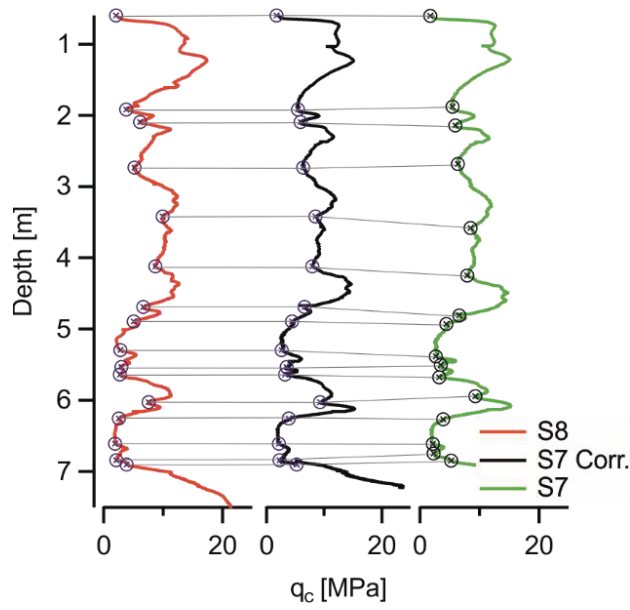


Fig. 7.1.1. Correlated and shifted cone resistance datasets of SCPTs S1 – S7. The SCPT S8 is the reference dataset.

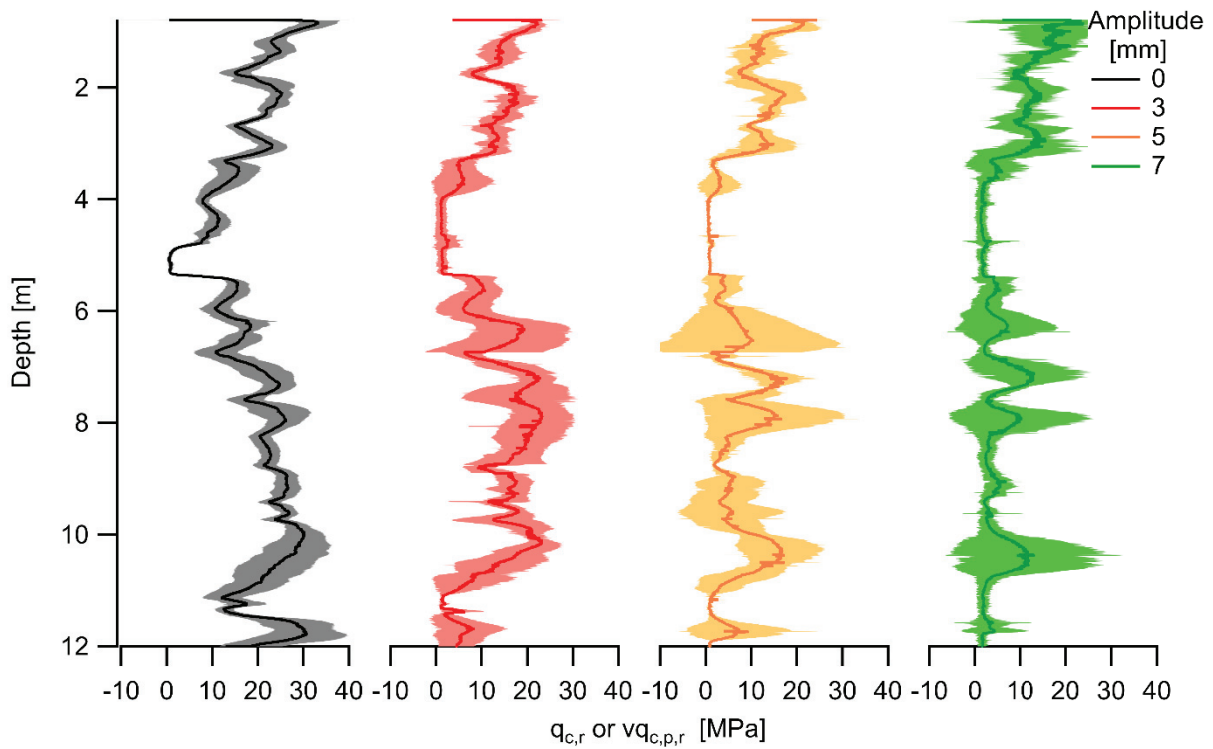


Fig. 7.1.2 Static and vibratory peak cone resistance for the three VCPT amplitudes. The shading represents the confidence interval

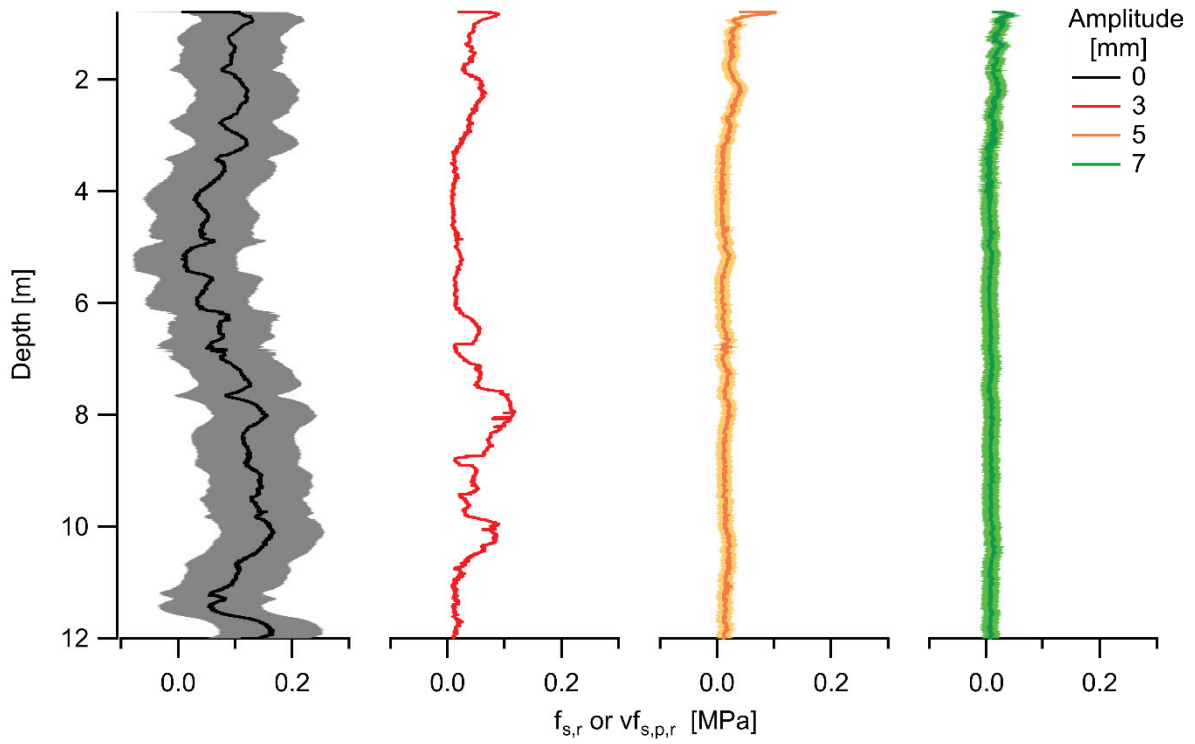


Fig. 7.1.3. Static and vibratory peak sleeve friction for the three VCPT amplitudes. The shading represents the confidence interval

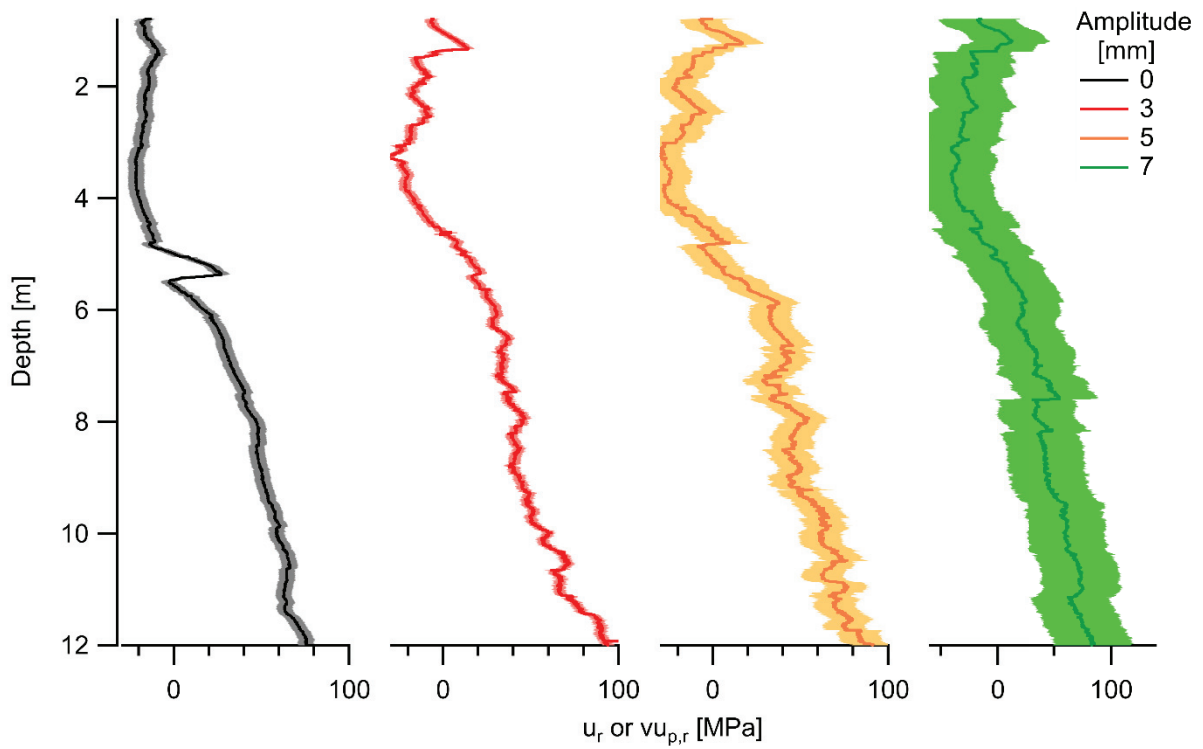


Fig. 7.1.4. Static and vibratory peak pore water pressure for the three VCPT amplitudes. The shading represents the confidence interval

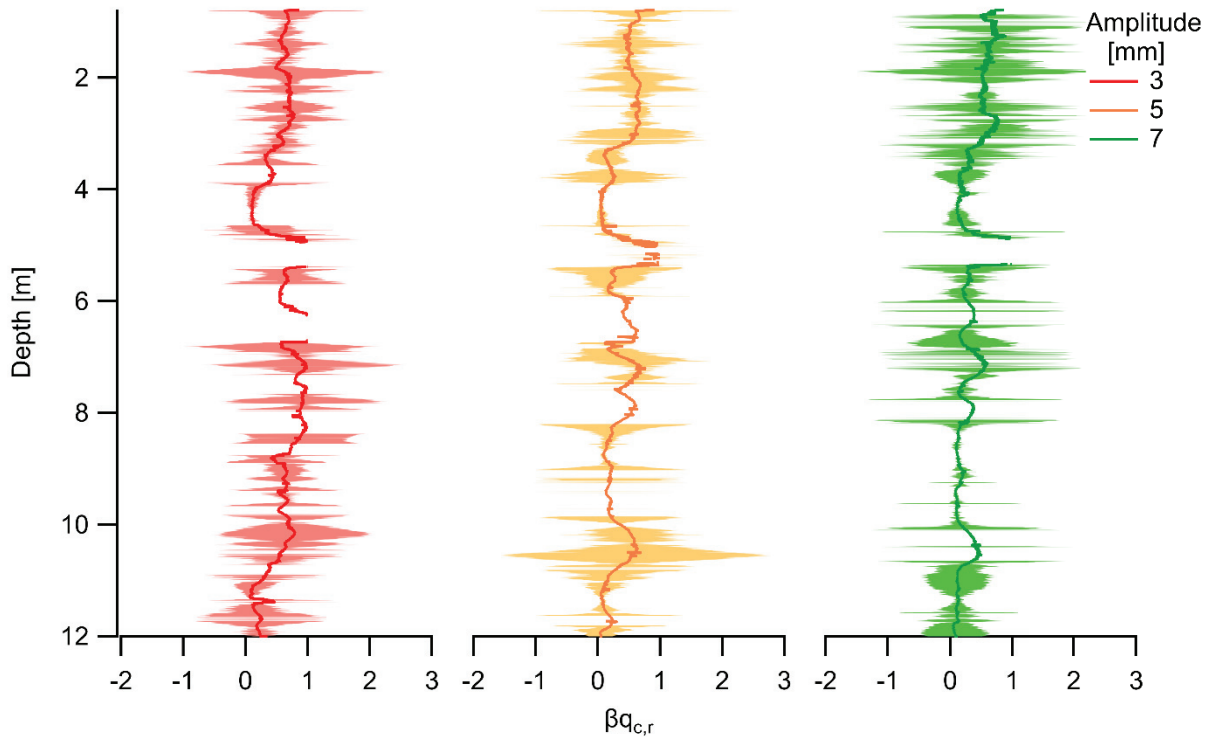


Fig. 7.1.5. Degradation factory of cone resistance for the three VCPT amplitudes. The shading represents the confidence interval

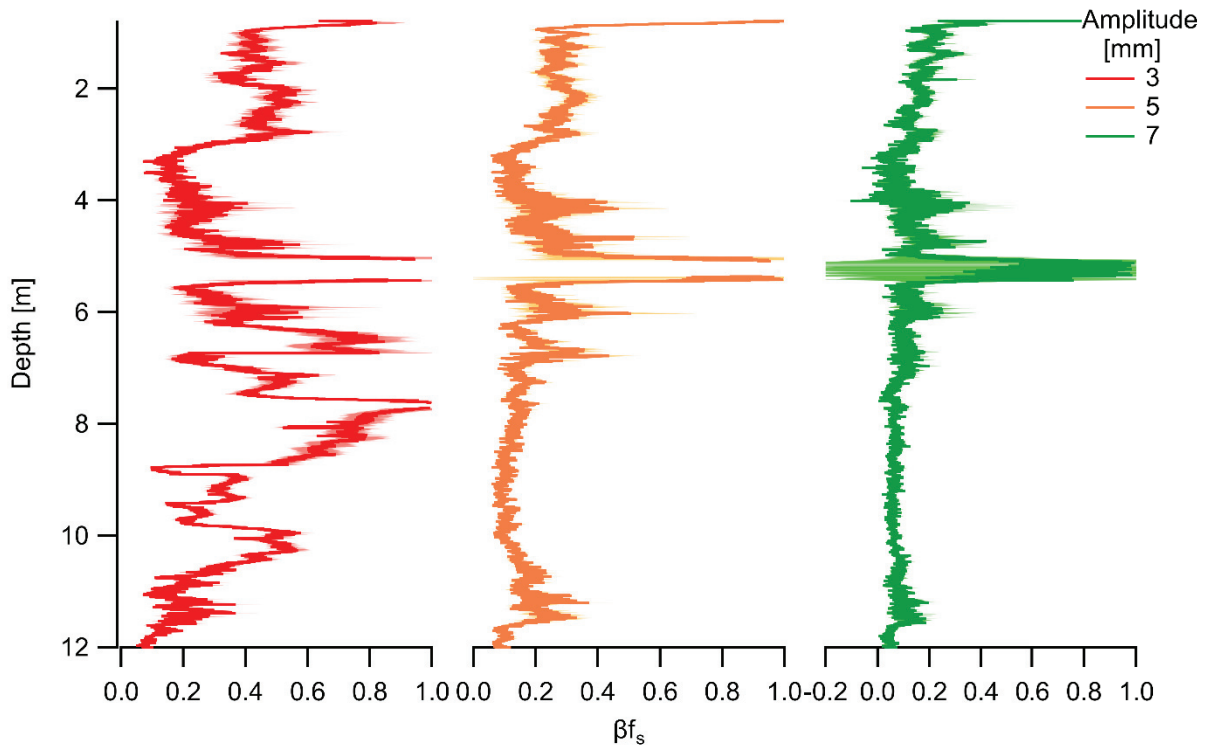


Fig. 7.1.6. Degradation factory of sleeve friction for the three VCPT amplitudes. The shading represents the confidence interval

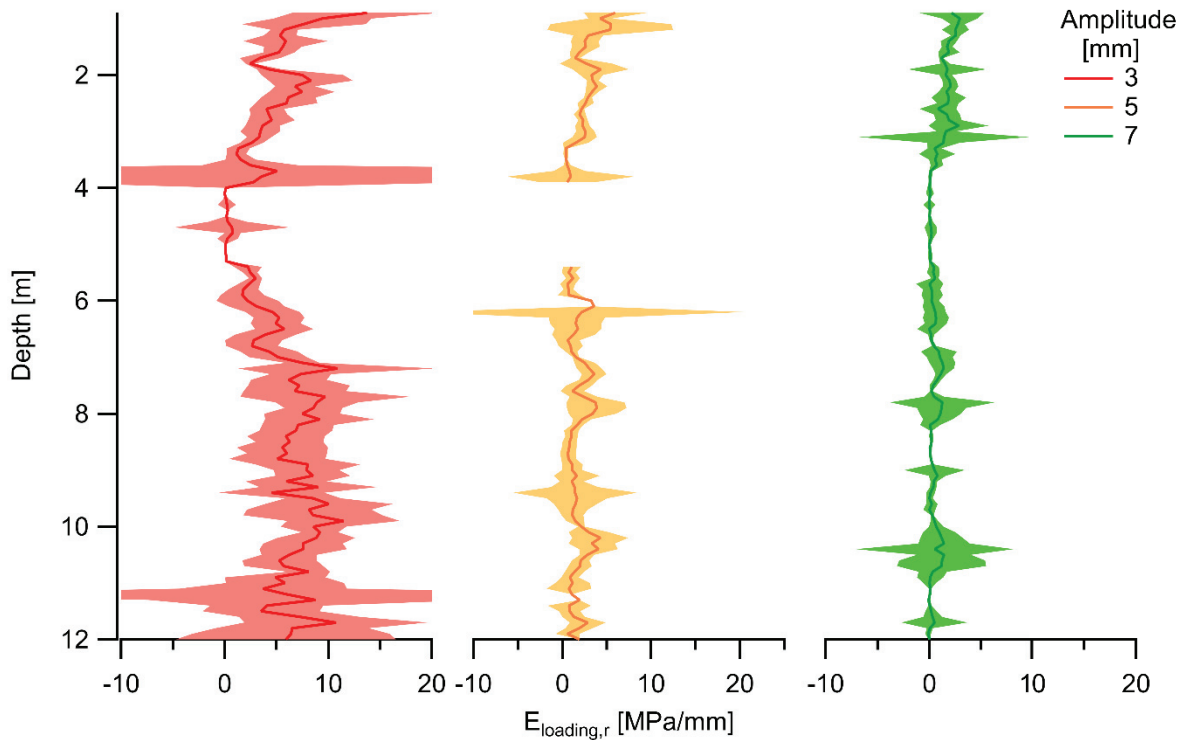


Fig. 7.1.7. Loading stiffness for the three VCPT amplitudes. The shading represents the confidence interval

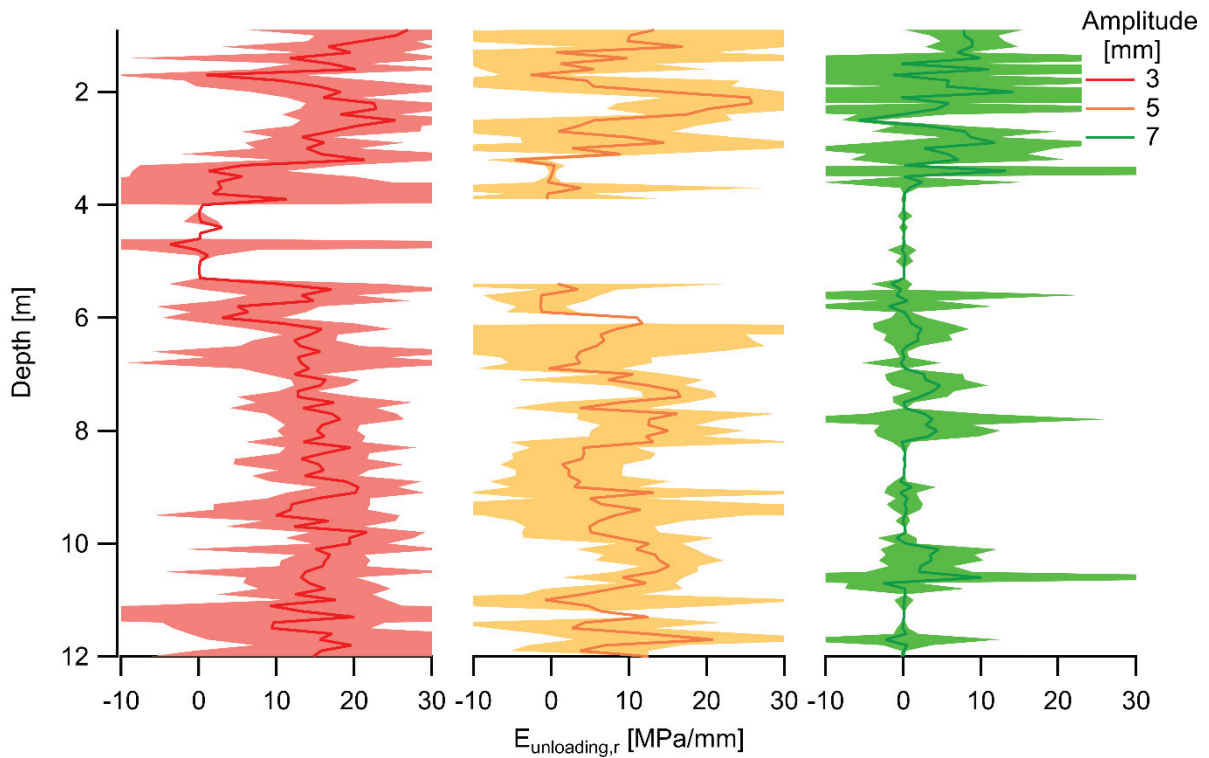


Fig. 7.1.8. Unloading stiffness for the three VCPT amplitudes. The shading represents the confidence interval

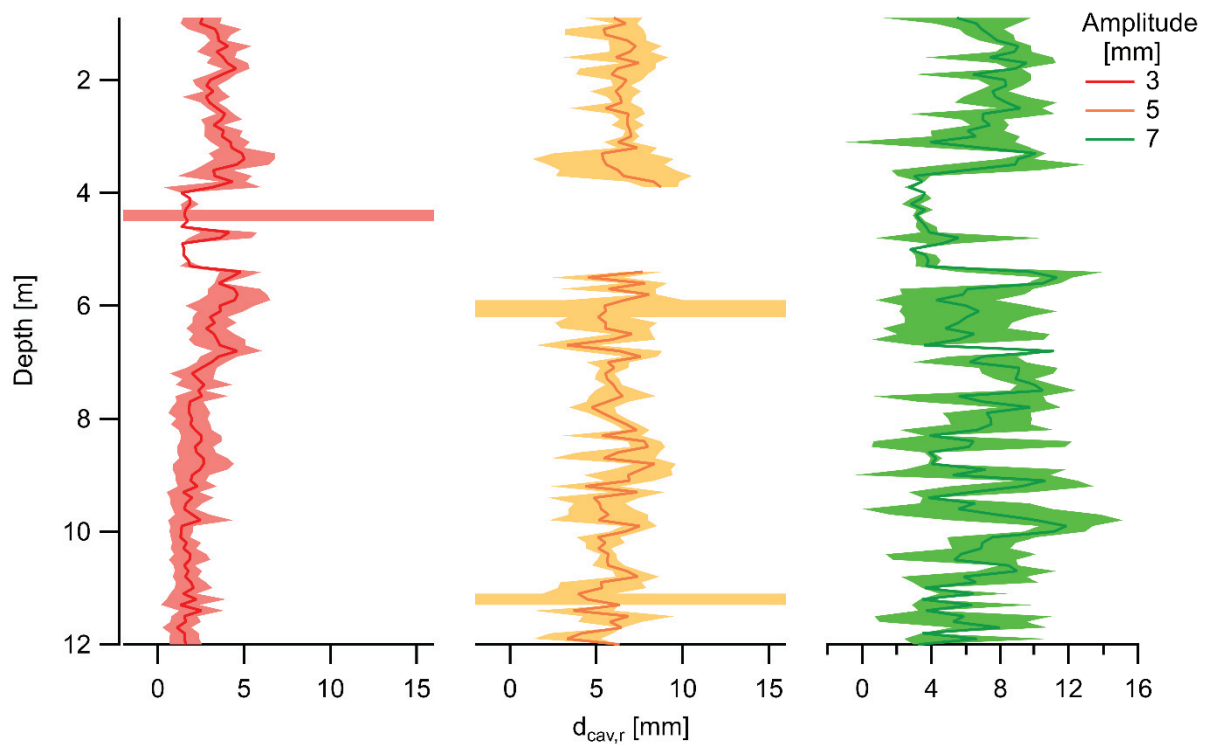


Fig. 7.1.9. Upward displacement with cavitation for the three VCPT amplitudes. The shading represents the confidence interval

7.2 Abstracts of Co-Author papers

7.2.1 A small volume calibration chamber for cone penetration tests under simulated field conditions

F.T. Stähler¹, M. Goodarzi^{1,2}, S. Kreiter¹, D. Al-Sammarraie¹, M. Fleischer¹, T. Stanski¹, B.Ossig², T. Mörz^{1,2}

*1MARUM - Center for Marine Environmental Sciences, University of Bremen, Germany
2Geo-Engineering.org GmbH, Bremen, Germany*

Published 2018 in Mitteilungen des Instituts für Grundbau und Bodenmechanik Technische Universität Braunschweig, 104: 171-182

Abstract: A small volume calibration chamber has been developed to better constrain the interpretation of cone penetration tests (CPT). Three different boundary conditions (BC) are technically feasible in the MARUM calibration chamber (MARCC), with either applying a constant lateral stress (BC1), a constant lateral strain (BC3) or a quasi-constant lateral stiffness (BC5) on the sample boundary. The quasi-constant stiffness of BC5 simulates an infinite surrounding soil to replicate field conditions. The boundary conditions are validated by CPTs in well-studied Ticino sand. Correction factors between BC1 and BC5 are proposed and a numerical model is established for the prediction of CPT-profiles. Good agreement between numerical and experimental CPT-results proved the reliability of BC5 in the MARCC and the applicability of correction factors for calibration chamber testing.

7.2.2 Liquefaction resistance by static and vibratory cone penetration tests

F.T. Stähler¹, S. Kreiter¹, M. Goodarzi^{1,2}, D. Al-Sammarraie¹, T. Mörz^{1,2}

1MARUM - Center for Marine Environmental Sciences, University of Bremen, Germany

2Geo-Engineering.org GmbH, Bremen, Germany

Published 2018 in Hicks, Pisanò & Peuchen (eds.) Cone penetration testing 2018, CRC

Press/Balkema, pp. 591 – 597

ISBN: 978-0-429-50598-0 (eBook)

Abstract: Soil liquefaction is an important hazard and one of the causes of earthquake-related disasters. The prediction of soil liquefaction is a major issue in geotechnical engineering and the soil liquefaction resistance is often determined in-situ by static cone penetration tests (CPT). The determination of the soil liquefaction resistance relies on empirical correlations and one way to increase accuracy might be the use of vibratory CPT. We report on displacement controlled vibratory and static CPT performed in a calibration chamber under a simulated field boundary condition, known as BC5. Vibratory CPT led to a reduction in cone resistance for medium- to very-dense Ticino sand. The reduction ratio increased at high vibrational frequencies and was independent of the relative density for the specific stress state and type of soil. A correlation between the liquefaction resistance and static or vibratory CPT is proposed.

